Fall 12-14-2018

# An Engineered Fit-For-Purpose Polymer Nanocomposite Seal Repair Material for Wellbores

Moneeb Genedy

Follow this and additional works at: https://digitalrepository.unm.edu/ce_etds
Part of the Civil Engineering Commons

**Moneeb Genedy**

*Candidate*

**Civil, Construction & Environmental Engineering**

*Department*

This dissertation is approved, and it is acceptable in quality
and form for publication:

*Approved by the Dissertation Committee:*

Mahmoud Reda Taha _____, Chairperson

John Stormont _____

Edward Matteo _____

Yu-Lin Shen _____

Harvey Goodman _____

_____

_____

_____

_____

_____

_____

i

**An Engineered Fit-For-Purpose Polymer Nanocomposite Seal Repair Material for Wellbores**

**BY**

**Moneeb Genedy**

**B.S. Civil Engineering, Alexandria University, Egypt, 2008**

**M.S. Civil Engineering, University of New Mexico, USA, 2014**

DISSERTATION

Submitted in Partial Fulfillment of the
Requirements for the Degree of

**Doctor of Philosophy**

**Engineering**

The University of New Mexico
Albuquerque, New Mexico

**December, 2018**

# DEDICATION

I would like to dedicate this work to my parents, Gamal Genedy and Samyah Genedy, and my wife, Rania Ghallab, who have provided me with everything that I have needed to succeed.

# ACKNOWLEDGMENTS

**An Engineered Fit-For-Purpose Polymer Nanocomposite Seal Repair Material for Wellbores**

**BY**

**Moneeb Genedy**

**B.S. Civil Engineering, Alexandria University, Egypt, 2008**
**M.S. Civil Engineering, University of New Mexico, USA, 2014**
**Ph.D. Engineering, University of New Mexico, USA, 2018**

**ABSTRACT**

Seal integrity of wellbores has become of significant interest due to repeated leakage and spill incidents occurring worldwide that jeopardize both human health and the environment in addition to causing significant economic burden. This is attributed to the fact that wellbores intersecting geographical formations contain potential leakage pathways. The cement-steel and cement-rock formation interfaces are recognized as two critical leakage pathways.

A seal repair material that has good bond strength with both steel and rock formations in addition to the ability to completely fill thin microcracks is needed to restore the seal integrity of wellbores. In this research, engineered polymer nanocomposites are proposed for use as seal repair materials for wellbores. Novolac epoxy polymer nanocomposites (PNCs) show more than 200% and 250% higher bond strength with steel and shale, respectively, when compared with microfine cement. In addition, it was found that Novolac epoxy PNCs have up to 545% and 761% higher displacement at peak load and toughness than microfine cement respectively. Moreover, Novolac epoxy PNCs was able to completely fill 800 μm microcracks that microfine cement were not able to

completely fill. Microstructural investigations using Fourier-Transform Infrared spectroscopy (FTIR) and Dynamic Mechanical Analysis (DMA) showed that incorporating aluminum nanoparticles (ANPs) in Novolac epoxy PNCs interrupted the polymerization process, which allowed free epoxy groups to improve the bond strength of PNCs with both shale and steel surfaces.

On the other hand, penetrability calculations based on contact angle and surface tension of seal repair materials showed that nanomodified methyl methacrylate (NM-MMA) incorporating 0.5 wt.% ANPs has higher potential to penetrate thin microannuli than microfine cement and Novolac epoxy PNCs. NM-MMA was able to seal thin microcracks as small as 30 μm while microfine cement has very limited penetration in such small microcracks. Furthermore, NM-MMA showed more than 1000%, 460%, and 8000% higher apparent bond strength, displacement at failure, and toughness than microfine cement respectively. Microstructural investigation using XRD analysis showed that incorporating ANPs in MMA increased the degree of polymer crystallization enabling significant improvement in polymer ductility, toughness, and reduced creep compliance.

A performance study of seal repair materials was evaluated based on their efficiency to seal the cement-steel interface, their ability to withstand cyclic casing pressure, and their ability to withstand harsh environmental conditions. The results showed that microfine cement efficiency was limited to 24%. On the other hand, NM-MMA was able to achieve seal efficiency as high as 103%. Moreover, NM-MMA was able to withstand casing pressure cycles two orders of magnitude higher than microfine cement. Finally, a durability investigation using a weight loss study showed that all PNC seal repair materials have higher resistance to harsh environmental conditions than microfine cement.

**Preface**

During the course of this PhD (2014-Now) the following papers have been published:

Genedy, M, Stenko, M, Stormont, J, Matteo, E.N., Dewers, T, Reda Taha, M.M. (2017). Fit-for-purpose Methyl Methacrylate (MMA) polymer nanocomposite for wellbore seal repair. *Patent Filed*, April 2018.

Genedy, M., Matteo, E., Stenko, M., Stormont, J., Reda Taha, M. M. Nanomodified Methyl Methacrylate Polymer for Repair of Microscale Defects in Wellbore Systems, *Journal of Materials in Civil Engineering*, Under Review.

Garner, A., Genedy, M., Kandil, U., & Taha, M. R. (2018). Controlling off-axis stiffness and stress-relaxation of carbon fiber-reinforced polymer using alumina nanoparticles. *Journal of Composite Materials*, *52*(18), 2483-2491.

Genedy, M., & Taha, M. M. R. (2018). Examining Alternative Strengthening Method for RC T-Beams Using CFRP and UHPC. *Special Publication*, 322, 10.1-10.14.

Genedy, M., Kandil, U. F., Matteo, E. N., Stormont, J., & Taha, M. M. R. (2017). A new polymer nanocomposite repair material for restoring wellbore seal integrity. *International Journal of Greenhouse Gas Control*, *58*, 290-298.

Genedy, M., Chennareddy, R., Soliman, E. M., Kandil, U. F., & Taha, M. M. R. (2017). Improving shear strength of bolted joints in pultruded glass fiber reinforced polymer composites using carbon nanotubes. *Journal of Reinforced Plastics and Composites*, *36*(13), 958-971.

Douba, A. E. M., Genedy, M. G., Tarefder, R., & Taha, M. R. (2016) Improving Fracture Toughness of Polymer Concrete Using MWCNTs. *Proceedings of the 9th International Conference on Fracture Mechanics of Concrete and Concrete Structures.*

Chennareddy, R., Genedy, M., Reda Taha, M. M., Tuwair, H., Elgawady, M. (2016). Improving UV Radiation Resistance of FRP Using Carbon Nanotubes.

*Proceedings of 7th International Conference on Advanced Composite Materials in Bridges and Structures*, Vancouver, Canada.

Douba, A., Genedy, M., Matteo, E., Stormont, J., & Taha, M. R. (2015). Apparent Vs. True Bond Strength of Steel and PC with Nanoalumina. *Advanced Materials Research*, *1129*.

Soliman, E., Genedy, M., Reda Taha, M. M. (2015). Short FRP Lap Splices Made Possible Using Nanomaterials. *Proceedings of 13th International Structural Engineering Conference*, Ain Shams University, Cairo, Egypt.

Genedy, M., Daghash, S., Soliman, E., & Taha, M. M. R. (2015). Improving Fatigue Performance of GFRP Composite Using Carbon Nanotubes. *Fibers*, 3(1), 13-29.

Garner, A., Genedy, M., Tarefder, R., & Taha, M. R. (2015, May). Monitoring Fatigue Damage in PC using Carbon Nanotubes. *In Advanced Materials Research* (Vol. 1129, pp. 94-101). Trans Tech Publications.

Genedy, M., Stormont, J., Matteo, E., & Taha, M. R. (2014). Examining epoxy-based nanocomposites in wellbore seal repair for effective CO2 sequestration. *Energy Procedia*, *63*, 5798-5807.

Genedy, M., Daghash, S., Soliman, E., & Reda Taha, M. (2014). Improving Tensile Strength of GFRP Using Carbon Nanotubes. in *The 7th International Conference on FRP Composites in Civil Engineering*. 2014: Vancouver, Canada.

Reda Taha, M. M., Taha, E., Genedy, M. (2014). Monitoring Fatigue Damage Propagation in GFRP Using Carbon Nanotubes. in *The 7th International Conference on FRP Composites in Civil Engineering*. 2014: Vancouver, Canada.

Genedy, M., Begaye, M. Reda Taha, M. M. (2014). Upgrading GFRP Bolted Lap Joint Capacity Using Carbon Nanotubes. *Proceedings of American Society for Composites 29th Technical Conference, 16th US-Japan Conference on Composite Materials*, San Diego, USA.

Genedy, M., Kim, J. J., Reda Taha, M. M., (2014). Innovative Strengthening of RC beams using CFRP-UHPC composite. *Proceedings of 7th International Conference on FRP Composites in Civil Engineering (CICE 2014)*, Vancouver, Canada.

# Table of Contents

# List of Figures

# List of Tables

# Chapter 1.  Introduction

## 1.1   Motivation and problem statement

There are millions of wellbores across the globe used for oil and gas production and storage or abandoned wells used in $CO_2$ sequestration process. Microscale defects (microcracks) that develop at the cement-steel and cement-rock formation, often referred to as microannuli, could jeopardize the seal integrity of wellbores. Loss in the seal integrity of wellbores could result in major leakage or spill incidents. Such incidents would have significant effects on both human health and the environment in addition to causing significant economic burden. Previous studies show that a microannulus as small as 30 μm is sufficient to jeopardize wellbore seal integrity. To restore wellbore seal integrity, the sealing technique usually used attempts to force seal repair material into the microcracks at the cement-steel or cement-rock interfaces through perforation in the steel casing or at the steel casing shoe.

It is well accepted in the oil and gas community that wellbore integrity is strongly dependent on the quality of the cementing material in the annulus, and the quality of bond between the cement sheath and the rock formation on one side and between the cement sheath and the steel casing on the other side. Thus, seal repair material with good durability and bond strength with both steel and rock formations is needed to ensure acceptable seal integrity of cement-steel and cement-rock interfaces.  In addition, the seal integrity of cement-steel and cement-rock interfaces depends on the ability of the seal repair material to completely fill microcracks at the interfaces, the impermeability of the seal repair material, its chemical resistance, and its ability to survive harsh wellbore conditions.

## 1.2   Objective and contribution

Wellbore seal integrity was the focus of several research studies during the past two decades. The vast majority of recent research discusses methods and techniques for integrity monitoring and evaluation (Crow et al. 2010, De Simone, Pereira, and Roehl 2017, Haagsma et al. 2017, Li et al. 2017, Xue and Hashimoto 2017, Alberty and Yao 2018, Chen et al. 2018, Davis 2018, Fan, Li, and Liu 2018, Phillips et al. 2018). Other studies investigated new cementitious materials for newly constructed wellbores to improve the wellbore integrity or have the ability of self-healing (Benge 2009, Guthrie et al. 2018, Guo et al. 2018). Very few research studies were initiated to study the ability of restoring the seal integrity of existing wellbores (Phillips et al. 2018, Tavassoli et al. 2018). However, no comprehensive study of restoring wellbore seal integrity has been conducted.

In this study, a comprehensive investigation of the fundamental science and engineering methods to develop an engineered fit-for-purpose polymer nanocomposite seal repair material to restore wellbore seal integrity is developed to answer three main scientific questions:

1- What are the desired properties of wellbore seal repair material?

2- What is the current state-of-the-art (performance and limitations of common seal repair material)?

3- What is the performance of engineered seal repair materials compared with common seal repair material?

The desired properties of wellbore seal repair material are summarized in Figure 1.1. High bond strength and ductility are required to allow the seal repair material to

withstand mechanical loading and prevent debonding of seal repair material from the steel casing or cement sheath. Moreover, viscosity, surface tension, and contact angle of the seal repair material controls its ability to penetrate and uniformly fill thin microcracks. Furthermore, for the seal repair material to be efficient in restoring and preserving wellbore seal efficiency, it should be able to block fluid flow and withstand pressure cycles. Finally, exposure to harsh environmental conditions that exist in the wellbore should not result in degradation of the seal repair material.
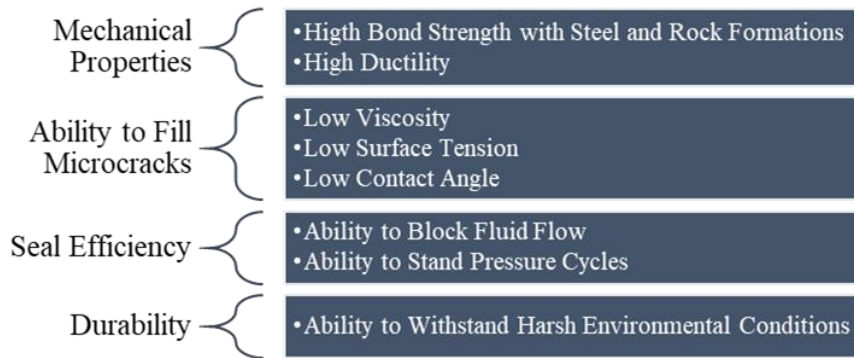


Figure 1.1: Summary of the desired properties of wellbore seal repair material.

The design process of the seal repair material (selection of polymer and incorporated nano particles) follows an elimination process of four phases summarized in Figure 1.2. First, the bond strength with steel, and flowability of the proposed polymer cement nanocomposites (PCNC) were investigated. Next, in Phase II the bond strength with shale of the selected polymer nanocomposites in Phase I was investigated. In Phase III, the ability of selected polymer nanocomposites to fill thin microcracks (30 µm) was then investigated. Finally, a performance study that includes examining the efficiency of seal repair material to the seal cement-steel interface, and the ability to withstand the wellbores' extreme environmental conditions was conducted in Phase IV. In all the

investigation steps, the proposed seal repair material was compared to microfine cement as it is the most common seal repair material used in wellbores (Harris et al. 1992).
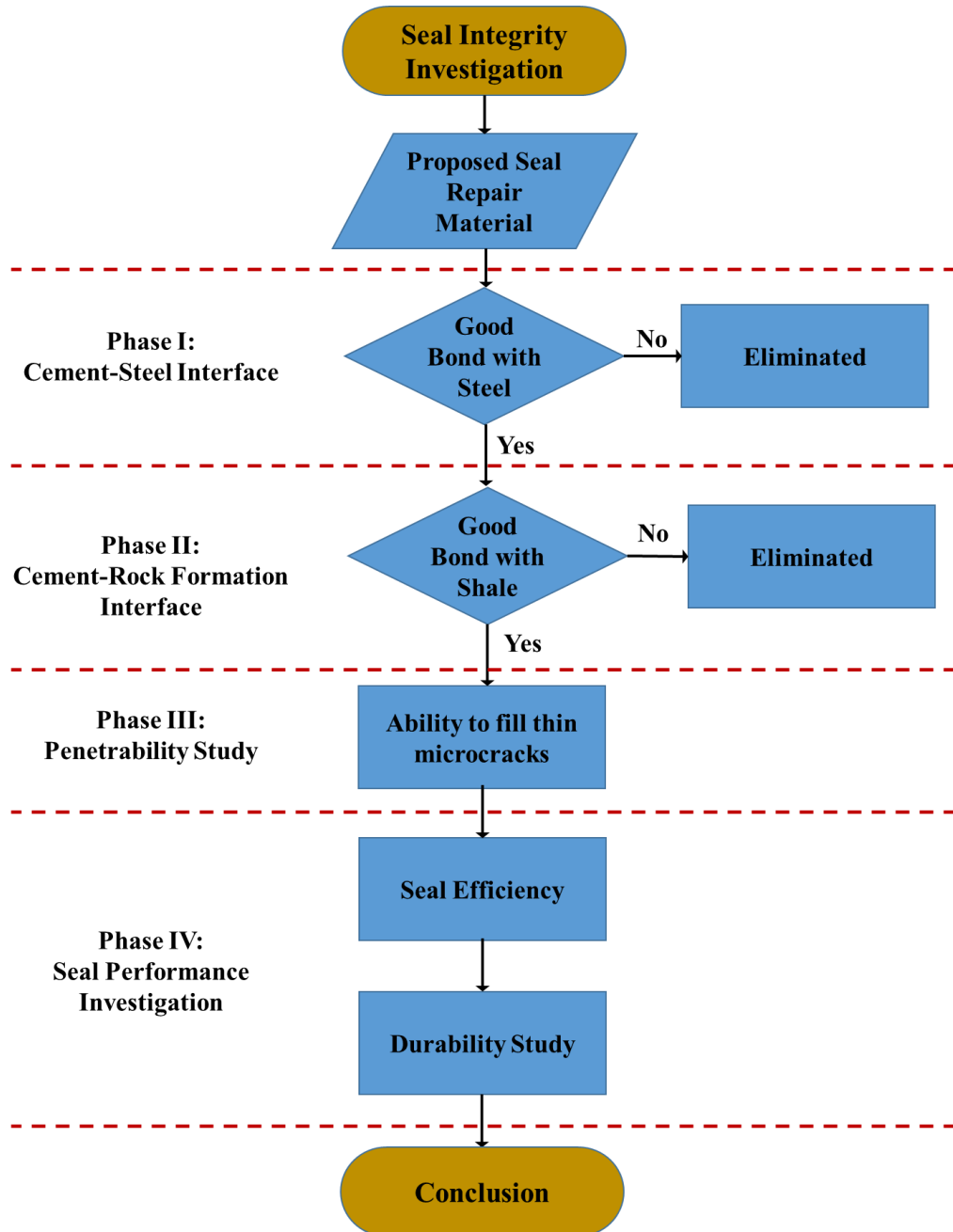
Figure 1.2: Flowchart summarizes the elimination process adopted in the investigation.

Slant shear test shows that Novolac epoxy always has higher bond strength with steel surfaces than Polysulfide siloxane epoxy. In addition, incorporating Aluminum

4

nanoparticles (ANPs) results in the highest improvement in bond strength of Novolac epoxy with steel surfaces (Genedy et al. 2017, Douba et al. 2017). Flowability test shows that incorporating nanoparticles results in loss in flowability of seal repair material (Genedy et al. 2017). However, incorporating 2.0 wt.% ANPs reduces the flowability of Novolac epoxy PCNC by only 8%. Moreover, push-out test shows that Novolac epoxy incorporating ANPs has 350% higher bond strength with shale than microfine cement (Genedy et al. 2014). Fourier Transform Infrared (FTIR) analysis and Dynamic Mechanical Analyses (DMA) investigations show that incorporating ANPs in Novolac epoxy decreases the degree of crosslinking, which improves the bond strength of the seal repair material with shale. Microscopic investigation shows that Novolac epoxy polymer nanocomposites were able to completely fill relatively large (800 μm) microcracks.

Although Novolac epoxy showed superior performance in sealing relatively large microcracks, it failed to fill thin microcracks (as small as 30 μm). On the other hand, viscosity, surface tension, and contact angle investigations show that methyl methacrylate (MMA) and nanomodified MMA (NM-MMA) have higher potential to fill such small microcracks, which was verified using microscopic investigation. Push-out test shows that incorporating ANPs in MMA has no significant effect on the bond strength. However, it shows more than 120% improvement in ductility. X-ray Diffraction (XRD) analysis shows that incorporating ANPs increases the degree of polymer crystallization of MMA resulting in more ductile polymer (Genedy et al. 2017).

Integrated testing shows that polymer nanocomposites are more efficient in sealing microannuli at the cement-steel interface. Incorporating ANPs improves the performance of polymer seal repair material. Polymer nanocomposite seal repair material was able to

withstand higher numbers of casing pressure cycles than microfine cement. In addition, the durability study shows that polymer nanocomposites have more resistance to extreme environmental conditions than microfine cement.

## 1.3   Dissertation layout

The dissertation has a total of 4 chapters. Literature review of wellbores and wellbores seal integrity is presented in Chapter 2. Chapter 2 also includes a brief literature review on the use of polymers and polymer nanocomposites in various applications. Experimental methods and results are presented in Chapter 3. The dissertation has deviated from the traditional layout that separates experimental methods from results due to the sequential structure of the research that adopted an elimination process of investigated seal repair materials.  Chapter 3 begins with a detailed description of the materials used in the research in addition to the preparation methods and techniques of polymer nanocomposites and polymer-cement nanocomposites. This is followed by the four phases of the seal repair material investigation. Phase I discusses the bond strength with steel surfaces and the flowability of proposed seal repair materials. Bond strength of the proposed seal repair material with shale in addition to microscopic and microstructures investigations are discussed in Phase II. The ability of the seal repair material to fill thin (30 μm) microcracks using push-out test, and a microscopic investigation are presented in Phase III. Phase IV presents a performance study of selected seal repair materials. This study includes an integrated seal test to investigate the efficiency of seal repair materials to seal the cement-steel interface in addition to a durability study to investigate the ability of seal repair materials to withstand harsh environmental conditions. Research conclusions and recommendations are presented in Chapter 4.

# Chapter 2.  Literature Review

## 2.1   Wellbore integrity

There are millions of wellbores across the globe (1.5 million wellbores are estimated in the State of Texas alone (Condor and Asghari 2009)) with several purposes from oil and gas production wells and storage caverns wells to abandoned wells that lie within the aerial extent of a $CO_2$ storage operation (Davies et al. 2014). These wellbores contain several potential leakage pathways (Figure 2.1 (Celia et al. 2005)) that might exist due to several factors including incomplete drilling mud removal prior to cementing, cement shrinkage, cement degradation, casing corrosion, and changes in pressure and temperature within the casing during operation (Goodwin and Crook 1992, Thiercelin et al. 1998, Zhang and Bachu 2011, Carey and Gardner 2012, De Simone, Pereira, and Roehl 2017, Fan, Li, and Liu 2018, Roy et al. 2018). Among possible leakage pathways described in Figure 2.1, cement-steel and cement-rock formations interfaces are known to be the most critical ones (Carey et al. 2007). Microscale defects (microcracks) develop at the cement-steel and cement-rock formation, often referred to as microannuli, could jeopardize the seal integrity of wellbores.
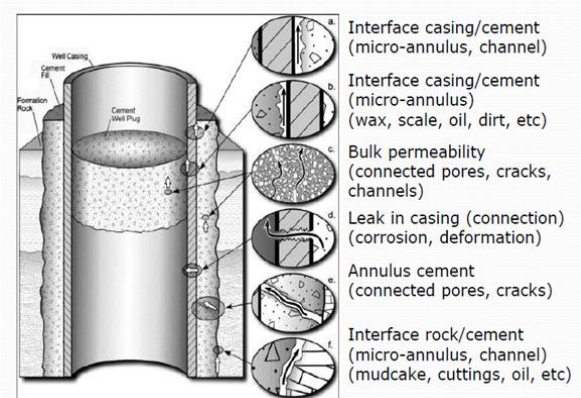


Figure 2.1: Schematic representation of zonal isolation and potential leakage pathways (Celia et al. 2005).

Loss in the seal integrity of wellbores could result in major leakages or spills incidents like the Deepwater Horizon event that released about 6500 million liters of liquid oil in the Gulf of Mexico (Reddy et al. 2012) and the Aliso Canyon event that released about 100,000 metric tons of methane into the atmosphere near Los Angeles, California (Michanowicz et al. 2017). Such incidents would have significant effect both human health and the environment in addition to significant economic burden (Smith, Smith, and Ashcroft 2011).

Stormont et al. showed that a 50 μm microcrack at the cement-steel interface would result in four orders of magnitude increase in effective permeability of a 0.23 diameter wellbore (Stormont et al. 2018). In a study involved 238 wellbores, Checkai et al. showed that 85% of the investigated wells that incorporating gas leakage or pressure buildup have 5 to 100 micron cracks (Checkai, Bryant, and Tao 2013). Moreover, Seidel and Greene showed that microcracks as small as 25 microns can be problematic for gas flow (Seidel and Greene 1985).

## 2.2   Evaluation of wellbores seal integrity

Due to the economic and environmental significance of wellbores seal integrity, regulations in many cases require evaluation of wellbores seal integrity using Mechanical Integrity Test (MIT) at least once every 5 years (Thornhill and Benefield 1990, Browning and Smith 1993, Kansas 2003). Using temperature, pressure, and motion in the Brine-Nitrogen interface measurements, loss of seal integrity can be detected. Although MIT is very effective in detecting loss of seal integrity, it requires very extensive work and can take weeks to have a complete test (Kansas 2011). Thus, several studies were conducted to

investigate alternative faster and more economic systems and techniques to evaluate and monitor wellbore integrity.

Cooke developed an apparatus that uses temperature measurements along the steel casing to detect leakage in wellbores (1994). Li et al. suggested the use of coaxial cable with imaging system to monitor steel casing deformations and presented the ability to use such deformations to evaluate wellbore integrity (Li et al. 2017, Li and Nygaard 2018). Moreover, distributed fiber optic sensing technique was able to monitor casing deformations with high resolution which was found to be sufficient to evaluate the seal integrity (Xue and Hashimoto 2017). Moreover, acoustic systems can be used for wellbores integrity diagnostics and assessment (Duguid and Tombari 2007, Chen et al. 2018, Davis 2018).

## 2.3   Restoring wellbore seal integrity

In several cases, once loss in wellbore seal integrity is detected, seal integrity should be restored to prevent any potential leakage incident. One of the common traditional method to restore the seal integrity of a wellbore is to install an additional casing inside the original one as shown in Figure 2.2 (Metcalf, Purvis, and Stilwell 2009). In this technique, the old wellbore is re-drilled then the new steel casing is inserted inside the old one. Once the new casing is installed, a new cement sheath is cast between the new and the old casings. Irregularity of original casing due to thermal stresses, operational stresses, or creep of rock formations complicates the installation of the new casing and can result in failure of the mitigation process (US DOE 2016).
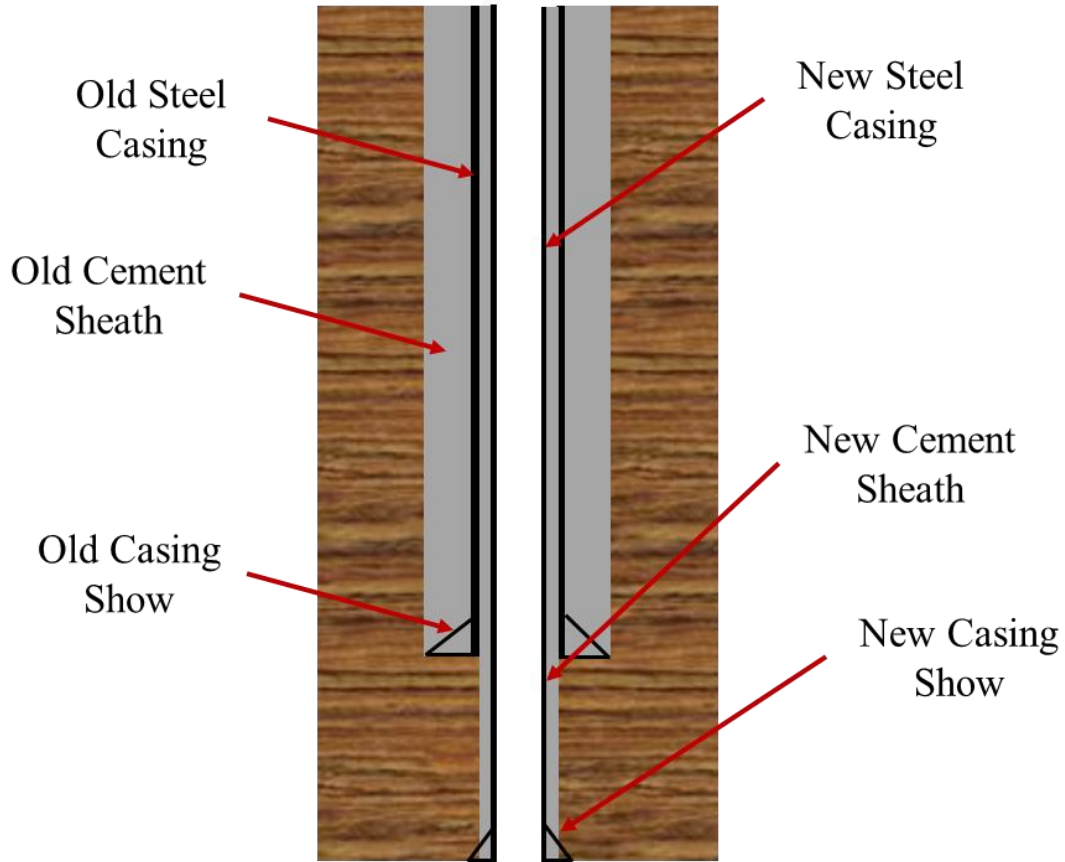
Figure 2.2: Restoring wellbore integrity by installing an additional casing.

To avoid such expensive and complicated process, several studies that aim to eliminate or delay the need to seal wellbores were carried out. Modifying Portland cement to improve its resistance to $CO_2$ attaches was suggested (Barlet-Gouedard et al. 2006, Barlet-Gouédard et al. 2007, Griffin et al. 2013). Moreover, cement systems with self-healing abilities that can seal microannuli without external actions were suggested to be used for cement sheath construction (Childers et al. 2017, Fernandez et al. 2018, Guthrie et al. 2018). In addition, it was found that incorporating polymers in cement sheath can improve its ductility and bond strength which improves the seal integrity of wellbores (Chatterji et al. 2001, Guo et al. 2018). Other studies suggest the use of swell packers that can be designed expands when exposed to specific fluid and seal leakage pathways (Freyer,

10

Fejerskov, and Huse 2002, Kennedy et al. 2005, Antonio, Barrios, and Martinez Rodriguez 2007, Rogers, Allison, and Webb 2008). These techniques showed the ability to improve the seal integrity of new constructed wellbores. However, they cannot be used to restore the seal integrity of existing ones. Thus, an effective sealing to restore the seal integrity of existing wellbores system is needed.

Another standard sealing technique attempts to force the seal repair material into the microcracks at the cement-steel or cement-rock interfaces through perforation in the steel casing or at the show of the steel casing is usually used to seal existing wellbores. An example of the sealing process through perforation in the steel casing is shown in Figure 2.3. Typically, microfine cement slurry with water to cement ratio between 0.7 and 2.0 is used as the seal repair material due to its higher flowability compared with Type G cement (Harris et al. 1992). However, experimental investigation showed that microfine cement was unable to completely fill relatively large ($> 400$ μm) microcracks (Genedy, et al. 2017, Tavassoli et al. 2018). Thus, the main challenge in this technique is whether the seal repair material can fill small microannuli or not.

Despite that it is widely accepted in the integrity research community that microfine cement is not an effective seal repair material (Bagal et al. 2016), limited number of studies were conducted to investigate an alternative seal repair material. Jones et al. showed that gels and epoxies can be effective seal repair material (Jones et al. 2014). In addition, Tavassoli et al. proposed using pH-triggered polymer as seal repair material (Tavassoli et al. 2018). Moreover, Phillips et al. proposed microbially induced calcite precipitation to restore wellbores seal repair integrity (Phillips et al. 2018). Furthermore, Rusch et al. presented pressure activated sealant that can be used to instead of conventional rig

workover (2004). These studies show that polymers and other seal repair material can be more effective than traditional microfine cement.
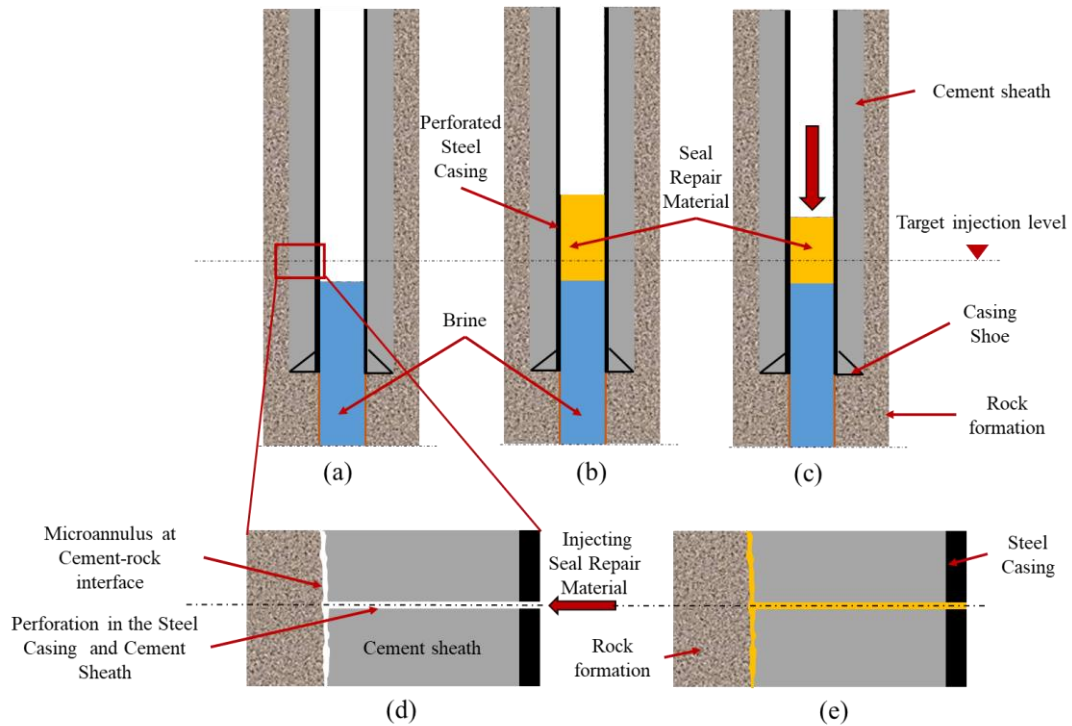


Figure 2.3: Injection process of seal repair material: (a) fill bottom hole with high density brine up to 2-3 m below the injection level, (b) fill 5-10 m of casing with seal repair material, (c) apply pressure to push seal repair material into the microcracks, (d) Microannulus at Cement-rock interface before injecting seal repair material, and (e) Sealed Microannulus at Cement-rock interface.

## 2.4   Cement-steel interface

The shear bond between the steel casing and cement sheath is strongly influenced by the physical interface properties of the casing (e.g. frictional characteristics). It has been reported that shear bonds are stronger when the casing is wire brushed or sand blasted and weaker when smooth finish or coatings are applied to the outside of the casing (Zhai et al. 2006). Casing expansion and contraction in response to pressure fluctuations within the casing can cause microcracking and debonding at the cement sheath-casing interface (Lacuve et al. 2015). Moreover, cement shrinkage during cement hydration has an

influence on the bond. Experiments on cement-steel interface bond showed that cement shrinkage leading to shrinkage microcracks is one reason for bond reduction with time (Nakayama and Beaudoin 1987). Bond quality may also be affected by the continuous growth of the calcium hydroxide (CH) crystals at the interface with time, resulting in a weak bond (Nakayama and Beaudoin 1987). While the bond strength decreases with time, the stresses due to processes in the wellbore may increase with time leading to lateral tension or shear applied to the cement-steel interface which can result in microcracking. Moreover, Shi and Ming show that the existence of microcracks at the cement-steel interface reduces the corrosion resistance of steel casing (Shi and Ming 2017). Corroded steel casing would result in lower bond and increase the permeability at the interface.

Studies have shown that microsilica (silica fume) enhances the cement paste-steel bond (Chung 2000). The increased bond strength of the interface was attributed to the pozzolanic nature of microsilica which allows microsilica to convert the CH crystals that govern the cement-steel interface to the mechanically stronger calcium-silicate-hydrate (CSH) phase. Nanosilica has been shown capable of producing a similar enhancement of bond strength between cement paste and aggregate with smaller quantities compared with microsilica due to its higher surface area (Mondal, Shah, and Marks 2007). Surface treatment of steel using ozone and silane has been shown to significantly improve the bond between cement paste and steel (Xu and Chung 1999). The improvement in bond strength from surface treatments may be attributed to the enhancement of surface wettability (Chung 2000) or to the availability of other functional groups (e.g. nitrogen, oxygen) with electron pairs that enhance the hydrophilic polymer-metallic bond (Berry and Namkanisorn 2005). Sand blasting under pressure has also been shown to improve cement-steel bond

due to an increase in the steel surface roughness. It was also found that early cement hydration would results in improved bond strength at the cement-steel interface (Wilson, Eustes, and Fleckenstein 2018).

## 2.5   Cement-rock formation interface

While considerable attention has been given to the cement-steel interface, little effort has been focused on studying the cement-rock interface while it represents a potential leakage pathway (Ravi, Bosma, and Gastebled 2002, Newell and Carey 2012). Chemical investigations showed that the process of cement hydration in contact with different types of soils and rock formations results in change in chemical compositions in the transition zone that can extend up to 2.5 mm on both sides of the interface (Hodgkinson and Hughes 1999, Read et al. 2001, Tinseau et al. 2006, Devol-Brown et al. 2007). Such changes can have significant effect on the integrity of the interface.

Prior investigations have shown that the cement-shale bond is affected by both cement and shale. As in cement-steel interface, cement shrinkage and growth of the calcium hydroxide crystals can weaken cement bond at cement-shale interface (Nakayama and Beaudoin 1987, Mehta and Monteiro 1976, Torsæter, Todorovic, and Lavrov 2015). Moreover, the swelling coefficient of the shale formation has a significant impact on interfacial bond between the cement sheath and shale. The higher the swelling coefficient, the weaker the bond-strength is between the cement sheath and shale (Ladva et al. 2005). Moreover, Silva and Milestone show that adding silica affects the size and complexity of interfacial transition zone (ITZ) at the cement-rock interface (Silva and Milestone 2018). Furthermore, thermo-elastic properties of cement sheath and formations were found to have significant effect on the sheath-formation interface. In addition, mechanical response

analysis showed that more ductile cement results in higher quality interface than brittle cement even with higher compressive strength (Thiercelin et al. 1998).

## 2.6 Polymer nanocomposites

Hydrophilic polymers have been shown to be capable of providing an excellent bond to existing metal surface (Baldan 2004)**.** Polymer adhesion to ceramic and metallic surfaces can be improved by surface treatment (Mansur, Santos, and Mansur 2007, Grujicic et al. 2008) which shifts the failure mode from adhesion failure to cohesion failure of the thin (10-50 μm thick) layer at the interface and thus improves the interfacial bond strength. Thermosetting polymers such as epoxy, unsaturated polyesters (UP), and vinyl ester (VE), and Novolac-epoxy co-polymers have been widely used for providing good bond with different surfaces. Moreover, considerable progress has been made in reinforcing the polymer/metal joint with organofunctional groups to improve covalent bond throughout the interface (Abel, Watts, and Digby 2004, Namkanisorn et al. 2001).

Nanomaterials have been suggested as potential reinforcements for polymers with the ability to improve their bond strength to metallic and ceramic substrates (Zhai et al. 2006). It has been widely suggested that nanoparticles, specifically carbon nanotubes (CNTs) and nanoclay, can be used to improve the mechanical characteristics of polymers (Gojny et al. 2004). Of special interest is the use of CNTs to improve the shear and tensile strength of epoxy (Ren et al. 2004) and failure strains of polymethyl-methacrylate (PMMA) (Zeng et al. 2004). Moreover, mechanical properties of polymer nanocomposites incorporating nanoclay were shown to depend on the clay loading and the degree of exfoliation of clay platelets (Ngo et al. 2007, Aboubakr, Kandil, and Taha 2014) . The presence of exfoliated clay substantially increases both the tensile strength and modulus of

elasticity (Park and Jana 2003), the shear strength and impact strength of polymers (Bakar et al. 2010). Furthermore, it was found that incorporating ANPs can significantly improve the mechanical properties of polymer nanocomposites such as ductility, fracture toughness, and strength (Wetzel et al. 2006, Pocius 2012, Emiroglu et al. 2017).

# Chapter 3.  Experimental Methods and Results

## 3.1   Material

### 3.1.1   Polymers

The first polymer used is polysulfide epoxy including silane.  This epoxy is usually used as an overlay material for repair of bridge decks.   The epoxy consists of two components, epoxy resin and epoxy hardener. The resin is mixture of Bisphenol A/Epichlorohydrin Epoxy Resin including silane. The hardener is Diethylenetriamine (DETA), Phenol, 4,4'-(1-methylethylidene)bis-, and Tetraethyllenepentamine.  The second polymer used is Novolac epoxy. Novolac epoxy resins are specifically designed to provide high thermal stability and chemical resistance.  This is accomplished by switching from Bisphenol A to Novolac backbones. The third polymer is Methyl Methacrylate (MMA) is a low viscosity methyl ester of methacrylic acid provided by Transpo Industry, Inc. Benzoyl peroxide powder was used as hardener for the MMA resin.

### 3.1.2   Cement

Type G (API Class G) oil well cement (OWC), provided by Grupo Cementos de Chihuahua (GCC) USA, was used as the reference cement material. This material was acquired from the manufacturer and is obtained by grinding clinker, consisting essentially of hydraulic calcium silicates, usually containing one or more forms of calcium sulfate as additive. Class G OWC is intended for use as a basic well cement and is available in moderate sulfate-resistant (MSR) and high sulfate-resistant (HSR) grades. Type G OWC is known for its flowability and high fineness. It is well known that type G cement is very comparable to ASTM Class II and Class V cements. The water/cement ratio for mixing Type G cement is 0.45. Microfine cement, generally used to seal cracks in oil wells,

provided by the manufacturer was used. The microfine cement has a composition that is

comparable to high sulfate-resistant cements and grain size ($d_{95}$) of 9.5 μm. The mix used

for the microfine cement has water to cement ratio (w/c) of 0.7 and 2.0% of the dry cement

weight super plasticizer (recommended by the manufacturer).

### 3.1.3   Shale

The shale used in this investigation is Mancos Shale, sourced from TerraTek shown

in Figure (3.1).



(a)                                  (b)
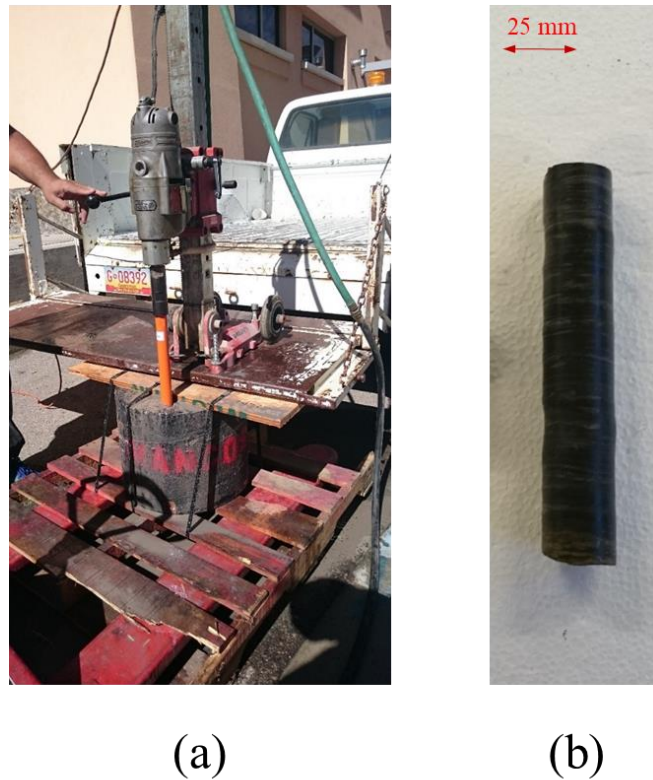
Figure 3.1: (a) Coring process of Mancos shale and (b) Mancos shale core.

### 3.1.4   Steel

The Steel used in this investigation is stainless steel obtained from a local provider.

Stainless was selected to eliminate the effect of steel corrosion on the results of the

investigation.

### 3.1.5 Filler

In all polymer-cement nanocomposites mixes, crystalline silica (quartz) and ceramic microspheres powder was used as mixing filler to produce the slurry to be cast and harden.

### 3.1.6 Nanomaterials

A group of four nanomaterials was used for this investigation. This includes functionalized Multi-Walled Carbon Nanotubes (MWCNTs), Nanoclay, Nanosilica and Alumina Nano Particles (ANPs).

#### 3.1.6.1 Multi-walled Carbon Nanotubes (MWCNTs)

Functionalized Multi-Walled Carbon Nano-Tubes (MWCNTs) were added to produce the nanocomposite. The MWCNTs have an outer diameter (OD) of 20–30 nm, inner diameter (ID) of 5–10 nm and length of 10–30 μm. The bulk density of the MWCNTs is 0.21 g/cm$^3$ and the specific surface area is 110 m$^2$/g. The functionalization of MWCNTs was performed by the manufacturer. A typical functionalization process is carried out in two steps as reported by Zhu et al. and Osorio et al. (Zhu et al. 2003, Osorio et al. 2008). First, a mixture of nonorganic acids such as sulfuric, nitric, and/or hydrochloric acids is added and stirred with the nanotubes under elevated temperature. The role of the aggressive mixture of acids is to create a defect on the surface of the nanotubes. The acids addition is followed by base such as ammonium hydroxide. The base is expected to neutralize the acidity and impregnate the carboxylic functional group on the nanotubes. Figure 3.2 shows Transmission electron microscope (TEM) images of MWCNTs.

Figure 3.2: Transmission electron microscope (TEM) images of MWCNTs.

### 3.1.6.2 Nanosilica

The nanosilica used is AEREOSIL® 380 from manufacturer Evonik Degussa Products, which is hydrophilic fumed silica with an average BET surface area of 380 m²/g and an average particle diameter of 7 nm. AEROSIL® 380 is a chemically prepared silicon dioxide powder that is white in color and odorless, and has a melting point of 1700 ℃ and a density of 2.2 g/cm$^3$.

### 3.1.6.3 Nanoclay

The nanoclay used in this research is Cloisite®30B supplied by Southern Clay Products, Inc. It is an off white material consists of natural montmorillonite modified with a quaternary ammonium salt. The nanoclay consists of dry particle sizes with 10%, 50%, and 90% by volume less than 2μ, 6μ, and 13 μ, respectively. Generally, clay minerals are composed of various combinations of: tetrahedral silica $SiO_4^{4-}$ and octahedral alumina

Al(OH)$_3^{6-}$ sheets (McLaren and Cameron 1996) as shown in Figure 3.3. In montmorillonite (2:1 type phyllosilicates), each layer is composed of one octahedral alumina sheet sandwiched between two tetrahedral silica sheets (Uddin 2008).
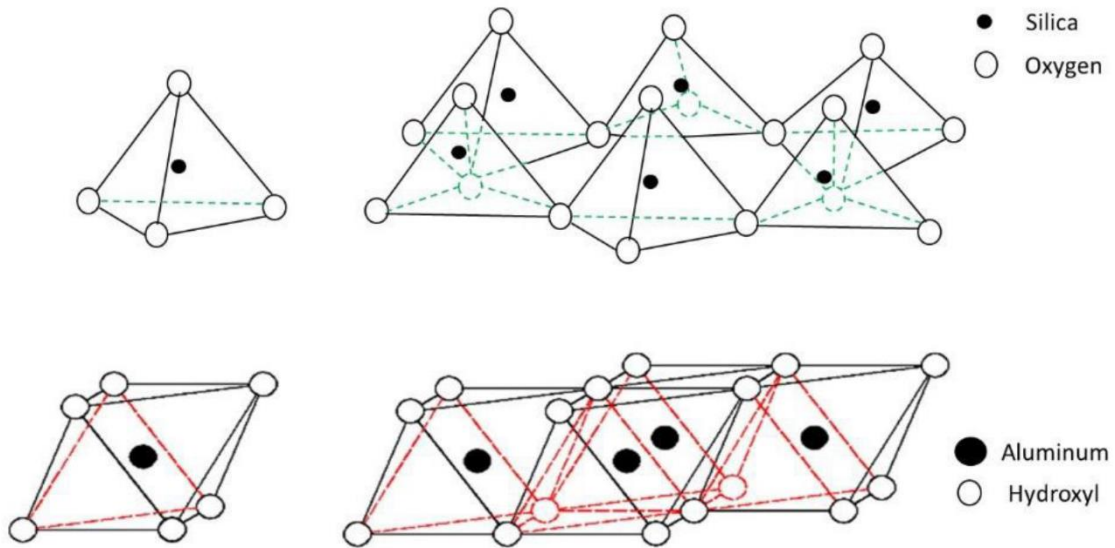


Figure 3.3: Structure of a silica tetrahedral sheet (up), and an alumina octahedral sheet (down) (McLaren and Cameron 1996).

### 3.1.6.4 *Alumina Nano Particles (ANPs)*

The nanoalumina used is aluminum oxide (Al$_2$O$_3$) nano- particles manufactured by Sigma Aldrich, Inc. and has a maximum particle size of 50 nm. Figure 3.4 shows Transmission electron microscope (TEM) images of ANPs.
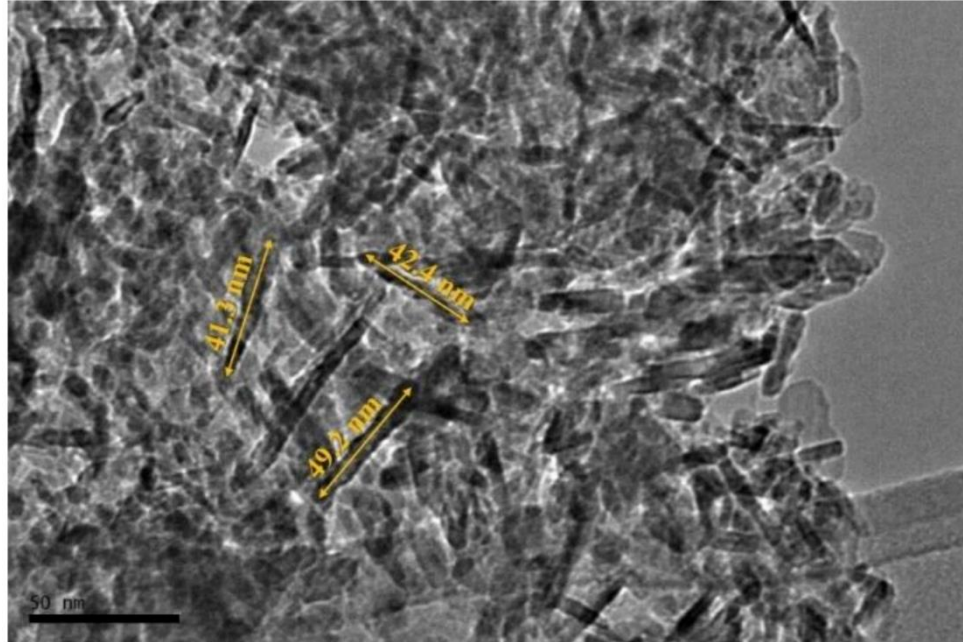
Figure 3.4: Transmission electron microscope (TEM) images of ANPs.

### 3.1.7    Polymer nanocomposite preparation

To prepare Novolac epoxy and polymer nanocomposite, the nanomaterial was added to the required amount of the resin, and the mix was stirred for 2 hours at 110 ℃ using. This relatively high mixing temperature was used to reduce the resin viscosity and improve the dispersion of nanomaterial. The mix was then sonicated for 2 additional hours at 65 ℃ using an ultrasonic homogenizer. For MMA PNCs, the magnetic stirring temperature was reduced to 80 ℃ due to its low evaporation temperature. The polymer resin nanocomposite was left to cool and reach room temperature. After the polymer resin nanocomposites reach the room temperature, it was mixed with the required amount of hardener. Figure 3.5 summarizes the polymer nanocomposites preparation process.
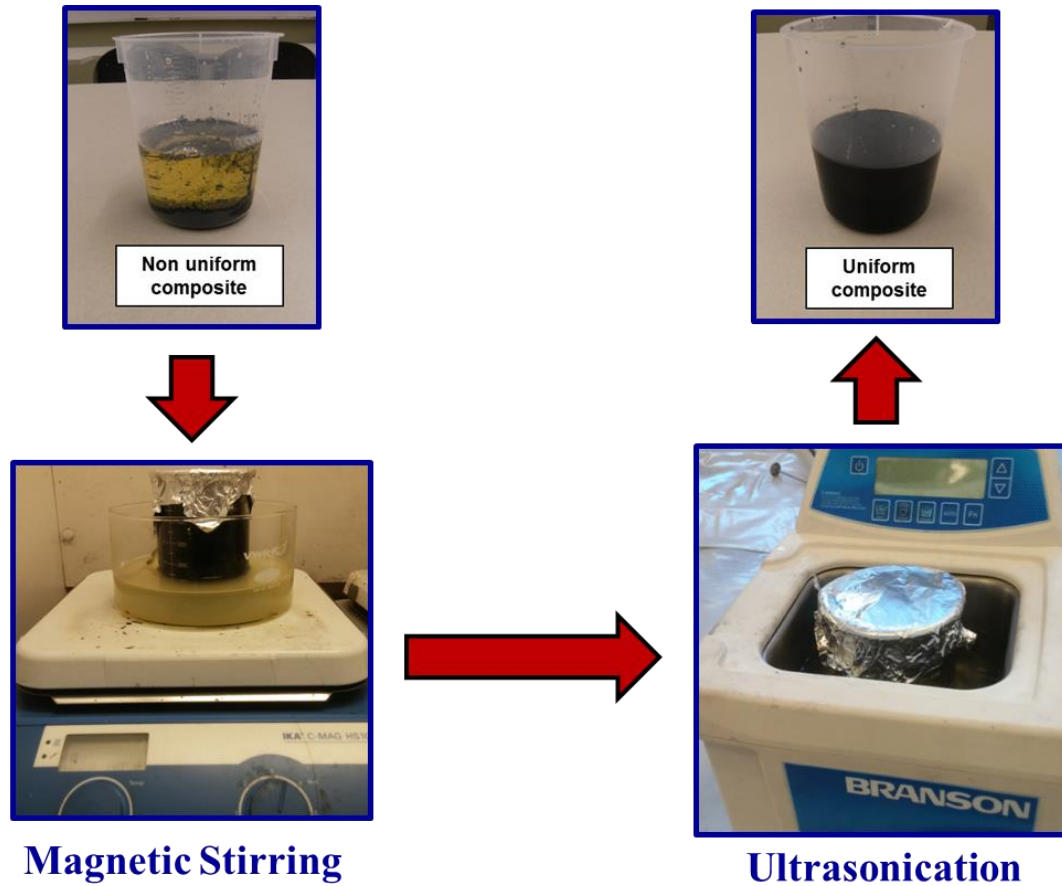
Figure 3.5: Schematic showing the steps to prepare polymer nanocomposites.

### 3.1.8  *Polymer cement nanocomposite preparation (PCNC)*

In order to prepare polymer cement nanocomposite (PCNC) of Novolac epoxy and polysulfide siloxane epoxy, the polymer resin nanocomposites were mixed with the required amount of hardener for 2-3 minutes using a low speed mixer, after which silica filling powder were added. Mixing continued for 2-3 minutes until the mixture was uniform. Schematic of mixing procedure is shown in Figure 3.6. Table (3.1) shows the list of PCNCs used in this study. The mix proportions for all Polysulfide siloxane epoxy and Novolac epoxy PCNC are presented in Tables 3.2 and 3.3 respectively.
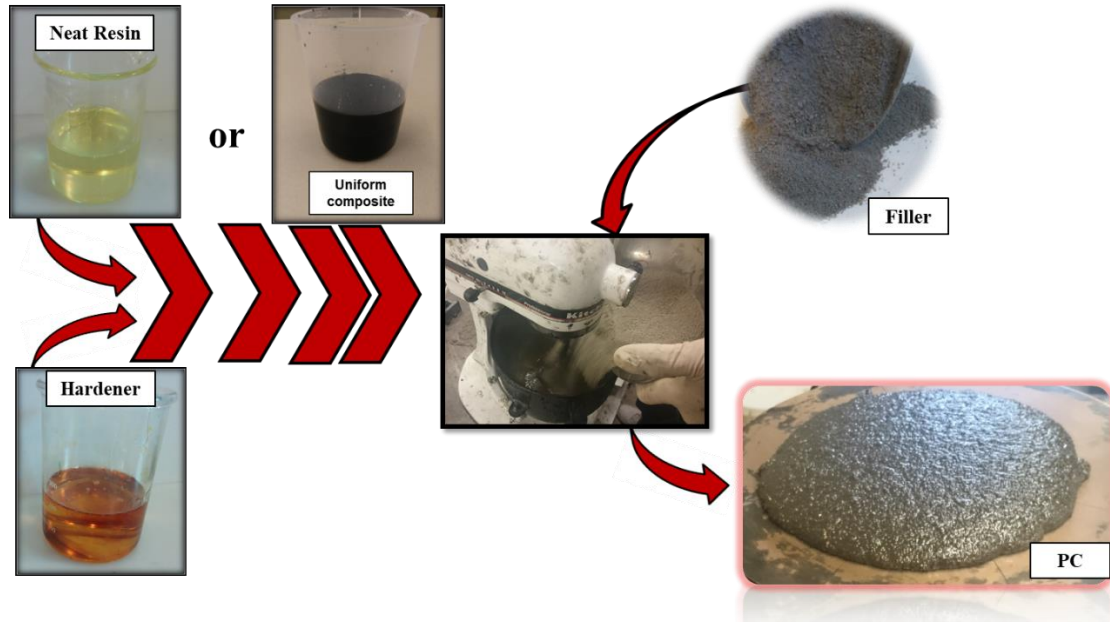
Figure 3.6: Schematic of mixing procedure of polymer-cement nanocomposites.

Table 3.1: List of PCNCs used in this study.

| Mixture Abbreviation | Base Material | Nano-particles | Content% |
|---|---|---|---|
| Reference | Microfine cement | None | ---- |
| PCNC1 | Polysulfide Siloxane epoxy | None | ---- |
| PCNC2 | Polysulfide Siloxane epoxy | MWCNTs | 0.5% |
| PCNC3 | Polysulfide Siloxane epoxy | MWCNTs | 1.0% |
| PCNC4 | Polysulfide Siloxane epoxy | MWCNTs | 1.5% |
| PCNC5 | Polysulfide Siloxane epoxy | Nanoclay | 4.0% |
| PCNC6 | Polysulfide Siloxane epoxy | Nanosilica | 1.0% |
| PCNC7 | Polysulfide Siloxane epoxy | Nanoalumina | 2.0% |
| PCNC8 | Novolac epoxy | None | ---- |
| PCNC9 | Novolac epoxy | MWCNTs | 0.5% |
| PCNC10 | Novolac epoxy | MWCNTs | 1.0% |
| PCNC11 | Novolac epoxy | MWCNTs | 1.5% |
| PCNC12 | Novolac epoxy | Nanoclay | 4.0% |
| PCNC13 | Novolac epoxy | Nanosilica | 1.0% |
| PCNC14 | Novolac epoxy | Nanoalumina | 2.0% |
| PCNC15 | Novolac epoxy | Nanoalumina | 0.5% |
| PCNC16 | Novolac epoxy | Nanoalumina | 1.0% |
| PCNC17 | Novolac epoxy | Nanoalumina | 1.5% |
| PCNC18 | Novolac epoxy | Nanoalumina | 3.0% |
| PCNC19 | Novolac epoxy | Nanoalumina | 4.0% |

Table 3.2: Mix proportions for Polysulfide siloxane epoxy nanocomposites kg/m$^3$.

| Mix designation | Resin | Hardener | Filler | Nanomaterials | Nano content |
|---|---|---|---|---|---|
| PCNC1 | 288 | 128 | 1570 | None | 0.0 |
| PCNC2 | 288 | 128 | 1570 | MWCNTs | 1.44 |
| PCNC3 | 288 | 128 | 1570 | MWCNTs | 2.88 |
| PCNC4 | 288 | 128 | 1570 | MWCNTs | 4.32 |
| PCNC5 | 288 | 128 | 1570 | Nanoclay | 11.52 |
| PCNC6 | 288 | 128 | 1570 | Nanosilica | 2.88 |
| PCNC7 | 288 | 128 | 1570 | Nanoalumina | 5.76 |

Table 3.3: Mix proportions for Novolac epoxy nanocomposites kg/m$^3$.

| Mix designation | Resin | Hardener | Filler | Nanomaterials | Nano content |
|---|---|---|---|---|---|
| PCNC8 | 288 | 128 | 1570 | None | 0.0 |
| PCNC9 | 288 | 128 | 1570 | MWCNTs | 1.44 |
| PCNC10 | 288 | 128 | 1570 | MWCNTs | 2.88 |
| PCNC11 | 288 | 128 | 1570 | MWCNTs | 4.32 |
| PCNC12 | 288 | 128 | 1570 | Nanoclay | 11.52 |
| PCNC13 | 288 | 128 | 1570 | Nanosilica | 2.88 |
| PCNC14 | 288 | 128 | 1570 | Nanoalumina | 5.76 |
| PCNC15 | 288 | 128 | 1570 | Nanoalumina | 1.44 |
| PCNC16 | 288 | 128 | 1570 | Nanoalumina | 2.88 |
| PCNC17 | 288 | 128 | 1570 | Nanoalumina | 4.32 |
| PCNC18 | 288 | 128 | 1570 | Nanoalumina | 8.64 |
| PCNC19 | 288 | 128 | 1570 | Nanoalumina | 11.52 |

## 3.2 Phase I: Steel-cement interface

### *3.2.1 Bond strength with steel surface*

The effect of incorporating nano-particles on the bond strength between polymer cement nanocomposite and steel was examined using a standard slant shear test following ASTM C882 (ASTM 2005). Composite cylinders with 50 mm diameter and 100 mm height were cast. The steel part with dimensions shown in Figure 3.7(a) was sandblasted to a minimum 4 mil clean surface roughness profile and was placed in a cylindrical mold. Polymer cement nanocomposite overlay was then cast on top of the steel in two layers. Each layer was compacted to ensure uniform filling of the mold and the final surface was leveled. In the case of reference mix, the overlay material was cement mortar. After 24 hours, the specimens were demolded and were allowed to cure for 7 days in air for the polymer cement nanocomposites and in water for the cement mortar. Figure 3.7(b) shows the slant shear specimen after it was demolded. After curing, the specimens were tested under a uniaxial compressive as shown in Figure 3.8. The slant shear test was conducted as a displacement control test with a loading rate of 0.036 mm/sec. The bond strength was determined as the average shear strength was computed as shown in equation (3.1).

$$\tau_{max} = \frac{P_{max}}{A} \quad \dots\dots\dots\dots\dots\dots\dots\dots\dots\dots\dots\dots\dots\dots\dots\dots\dots\dots\dots\dots\dots(3.1)$$

Where $P_{max}$ is the maximum load, A is the inclined contact area and $\tau_{max}$ is the maximum average shear strength.
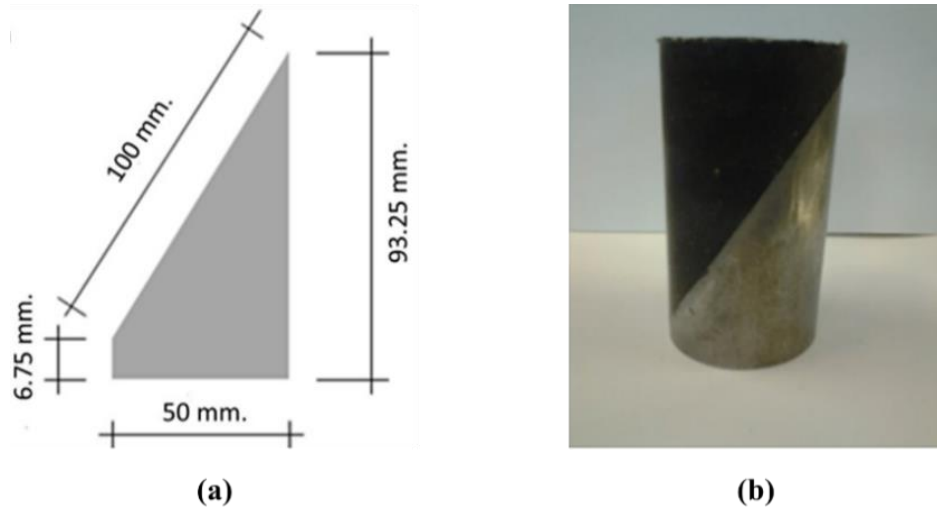
Figure 3.7: (a) Steel part dimensions (b) composite cylinder for slant shear test
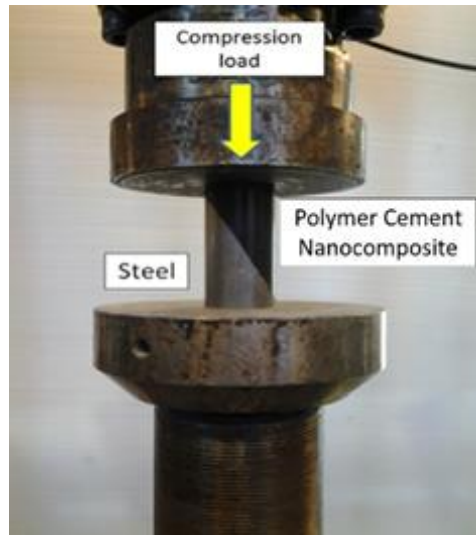


Figure 3.8: Slant shear test setup

Load-displacement data from the slant shear tests for the Polysulfide Siloxane epoxy cement nanocomposites in Figure 3.9 and Novolac epoxy cement nanocomposites in Figure 3.10. Load-displacement response of the reference microfine cement material is also shown in Figure 3.9 and Figure 3.10.
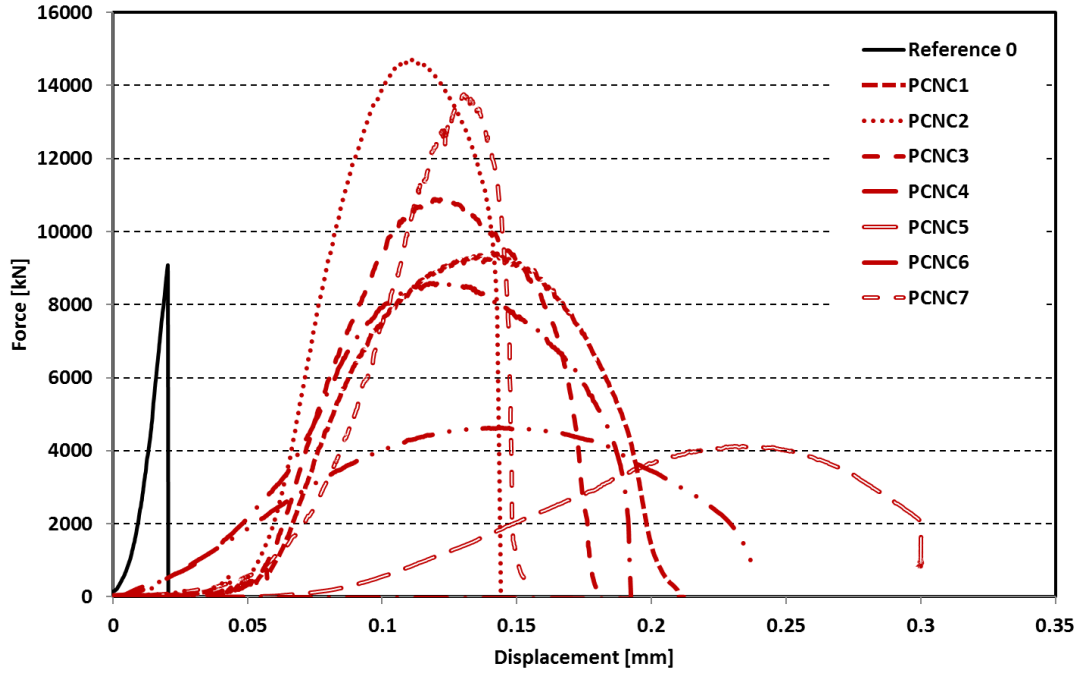
Figure 3.9: Load-displacement curves of reference microfine cement material and Polysulfide Siloxane epoxy cement nanocomposites
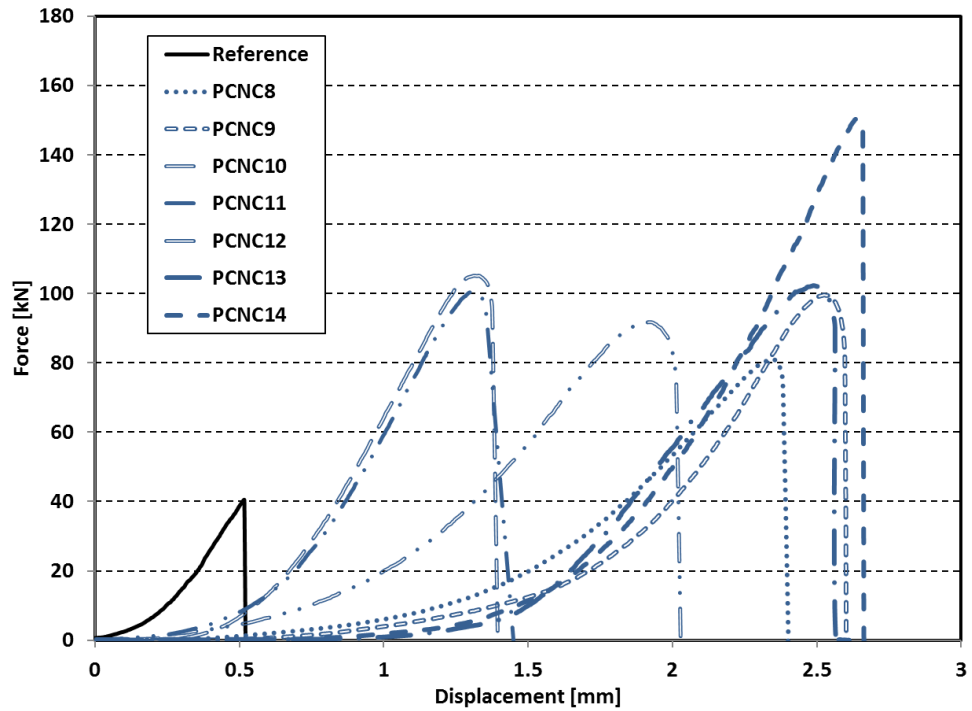


Figure 3.10: Load-displacement curves of reference microfine cement material and Novolac epoxy cement nanocomposites.

The bond strength was calculated from equation 3.1 using the maximum force during the slant shear test. The strength of five specimens for each material was used to calculate the mean bond strength values shown in Figure 3.11. The neat Polysulfide Siloxane epoxy has similar bond strength to that of the reference cement material. However, incorporating 0.5% wt. MWCNTs and 2.0% wt. nanoalumina increased the bond strength of Polysulfide Siloxane epoxy by 49%. On the other hand, dispersing nanoclay and nanosilica in the epoxy resin of the polysulfide Siloxane epoxy system decreased the bond strength between the polymer cement nanocomposite and the steel surface by 59% and 52% respectively. Both nanosilica and nanoclay include silica tetrahedral, which seem to have an adverse effect on the adhesion of Polysulfide Siloxane epoxy with steel substrates.

The bond strength of all Novolac epoxy cement nanocomposites were significantly higher than the reference cement mortar. The bond strength of the neat Novolac epoxy was 102% higher than the reference cement material. Adding MWCNTs did not make a significant improvement of bond strength of the Novolac epoxy cement nanocomposites, perhaps because the COOH functional group may not be suitable for Novolac epoxy. The best improvement in the bond strength of Novolac cement nanocomposites was obtained by dispersing 2.0% nanoalumina in the Novolac epoxy resin (PCNC14), increasing the bond strength by more than 200% compared with the reference cement material. Using nanoclay (PCNC12) and nanosilica (PCNC13) resulted in bond strength improvement of 134% and 138%, respectively. The improvement in bond strength using nanosilica particles suggests that Novolac epoxy can interact with nanosilica without adversely affecting its properties. The ability of alumina based particles to improve bond strength with steel by

29

forming chemical bond of alumina oxides that further bonds the steel surface to the epoxy adhesive has been previously reported (Pocius 2012).
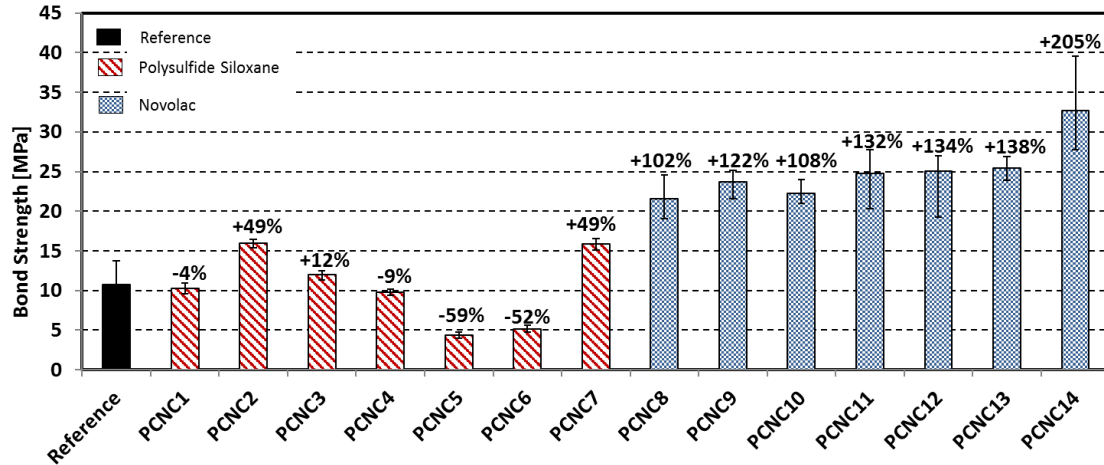


Figure 3.11: Mean bond strength for reference microfine cement material and all fourteen polymer cement nanocomposites.

### 3.2.2 *Flowability of Polymer Cement Nanocomposites*

As all the investigated materials are suggested seal repair materials, these materials need to be flowable in order to be easily injected in the cracks. Thus, the effect of incorporating the nanoparticles in the epoxy on the flowability has to be investigated. The flowability test was conducted according to ASTM C1437 (ASTM 2007) on the polymer cement nanocomposites. The flowability cone used in the tests has a 70 mm smaller diameter and 100 mm larger diameter. The height of the cone is 50 mm. The cone was positioned in the center of the flow table and then it was filled with the mixture in two layers. Each layer was tamped 20 times to ensure uniform filling of the cone. Afterwards, the cone was lifted in 4 seconds. Using the flow table, 25 strikes were applied to the specimen in 15 seconds. Four readings of the specimen in four direction separated by 45° were taken after the 25 strikes using the test caliber. The sum of the four readings represents

the flowability of the slurry. Figure 3.12 shows filling of the flowability cone and reading of flowability with the test caliber.



(a)                                    (b)

Figure 3.12: (a) Filling the flowability cone (b) taking readings using test caliber.

Flowability results for reference microfine cement material and all fourteen PCNCs tested are shown in Figure 3.13. The flowability of all polysulfide siloxane cement nanocomposites were less than the reference cement materials. In contrast, the flowability of all Novolac epoxy cement nanocomposites were greater than the reference cement material. The results indicate that mixtures that included nanoparticles had a reduced flowability compared to the neat epoxy cement nanocomposites. Incorporating 0.5% MWCNTs and 2.0% nanoalumina had the least effect on flowability of polymer cement nanocomposites for both types of epoxies while 4.0% nanoclay and 1.0% nanosilica decreased the flowability the most.
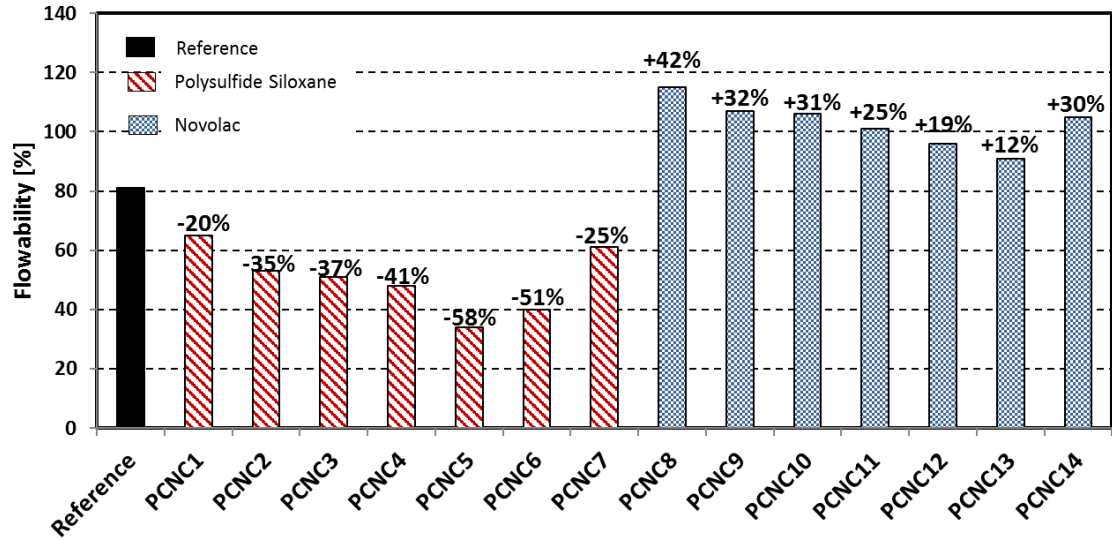
Figure 3.13: Flowability results for the reference microfine cement material and all fourteen polymer nanocomposites.

Slant shear and flowability results presented above show that all Novolac epoxy polymer-cement nanocomposites shows superior performance over polysulfide siloxane epoxy. Furthermore, incorporating 2.0% ANPs in Novolac epoxy PCNC shows the highest improvement in bond strength with steel surface. In addition, incorporating ANPs reduced the flowability of Novolac epoxy PCNC by only 8%. Thus, extended investigation of Novolac epoxy PCNC incorporating ANPs was conducted.

### 3.2.3 *Extended investigation of Novolac epoxy PCNCs incorporating ANPs*

Additional five Novolac epoxy PCNC incorporating 0.5%, 1.0%, 1.5%, 3.0%, and 4.0% ANPs were prepared. The bond strength with steel surface was examined using slant shear test as illustrated in section 3.2.1. Figure 3.14 shows the mean bond strength of all Novolac epoxy PCNC incorporating ANPs compared to neat Novolac epoxy PCNC (PCNC8). Slant shear results shows that there is a direct relation between the amount of ANPs incorporated and the improvement in bond strength of PCNC only up to 2.0% ANPs.

32

Additional content of ANPs (Higher than 2.0%) have an adverse effect and it decrease the improvement in the bond strength. This results can be explained by the fact that with this high content of ANPs (Higher than 2.0%), the effectiveness of dispersion process was affected which results in agglomerated nanoparticles.
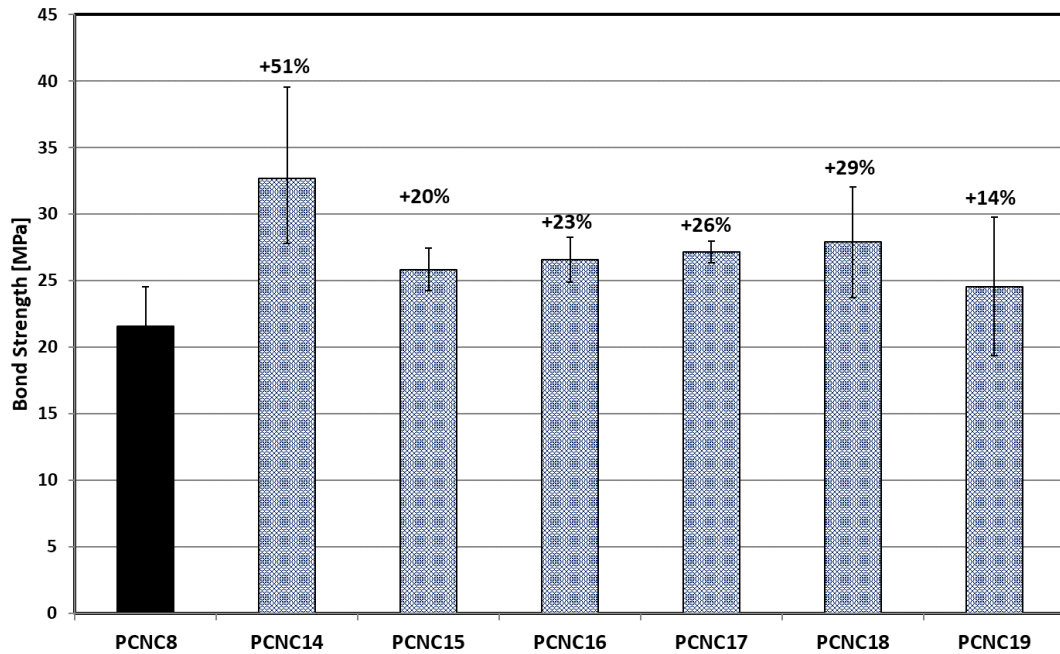


Figure 3.14: Mean bond strength for all Novolac epoxy PCNC.

Figure 3.15 shows the flowability results of all Novolac epoxy PCNC incorporating ANPs compared to neat Novolac epoxy PCNC. Flowability results show that the higher content of nanoparticles incorporated the lower the flowability of PCNCs. However, this relationship is not linear for all ANPs content. As shown in Figure 3.15, incorporating low content of ANPs in Novolac PCNC (from 0.5% to 2.0%) results in less than 9% reduction in the flowability of PCNC. On the other hand, incorporating higher content on ANPs (3.0% and 4.0%) results in 20% to 26% reduction in the flowability of PCNCs. This can also be explained by the agglomerations of nanoparticles that results from dispersing such a high content of ANPs.
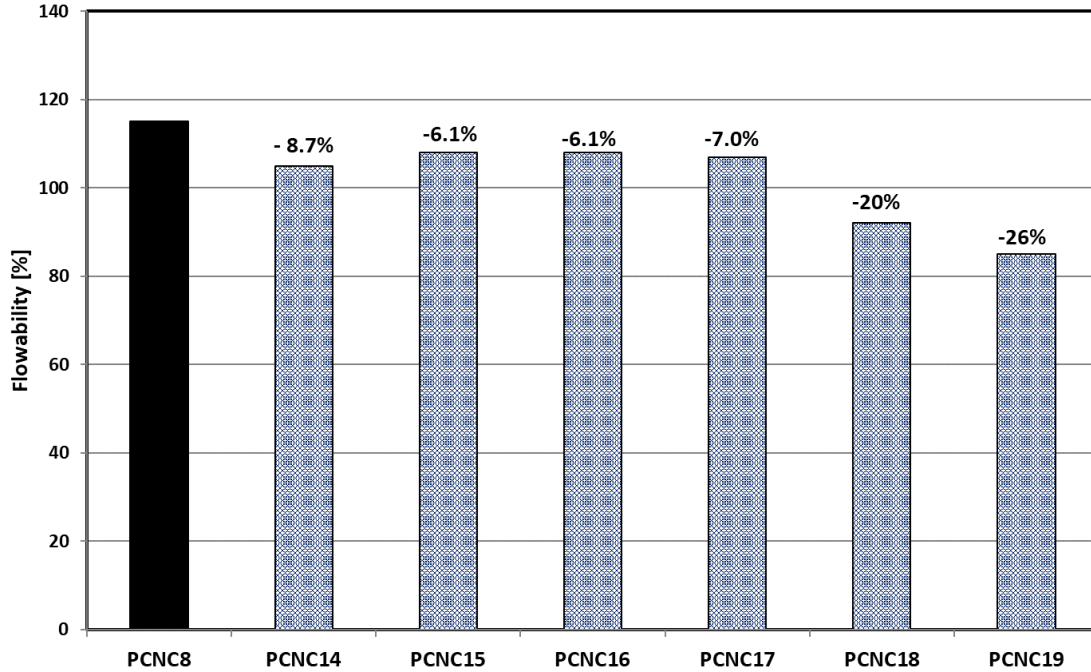
Figure 3.15: Flowability results for all Novolac epoxy PCNC.

Based on the flowability and slant shear tests' results, it was concluded that Polysulfide Siloxane epoxy is not suitable seal repair material of wellbores microannulus cracks due to its significantly low flowability and bond strength which are two main characteristics of any seal repair material. Thus, the Polysulfide Siloxane was eliminated as a potential seal repair material for wellbores microannulus cracks in this research. In addition, the results of using Aluminum Nanoparticles (ANPs) showed a great potential in improving the bond strength of polymers nanocomposites.

Although incorporating 2.0% ANPs in Novolac epoxy showed the highest improvement in bond strength with steel surfaces, it also showed significantly high variability in the bond strength results. This variability was observed also with 3.0% and 4.0% ANPs. This can be explained by a non-uniform dispersion and agglomerated nanoparticles due to the high content. Moreover, it was observed that there was no

significant improvement in the bond strength with incorporating 1.5% ANPs when compared to 1.0% ANPs. On the other hand, incorporating 0.5% and 1.0% ANPs in Novolac epoxy showed 20% and 23% increase in the bond strength respectively in addition to only 6.0% reduction in flowability. Thus, Novolac epoxy incorporating ANPs with highest content limited to 1.0% of polymer weight was selected in the rest of this study.

## 3.3   Phase II: Cement-rock formation interface

### 3.3.1   Push-out test

The bond strength at the cement-shale interface was tested using push-out test. Two sets of specimens were prepared for push-out tests as shown in Figure 3.16. The first set was used to measure the bond strength between the shale and Type G cement paste. A shale core of 25.4 mm diameter and a length greater than 30 mm was fixed in the center of a steel cylinder with an outer diameter of 100 mm and thickness of 3.2 mm; cement paste was then cast around the shale to produce cylindrical specimens with a diameter of 101.4 mm and height of 50.8 mm. The second set of specimens was prepared to investigate the bond strength of the seal repair materials injected in an artificial microannulus between cement paste and shale. Hollow Type G cement cylindrical specimens confined with steel cylinders with inner diameter of 27 mm, outer diameter of 101.4 mm, and height of 50.8 mm were cast first. These specimens were cured at 100% humidity environment at room temperature for 28 days. After the cement cylinder was cured, the shale core with a diameter of 25.4 mm was placed in the center of the hole, which produced a gap or microannulus between the cement paste and shale of nominally 800 μm. Seal repair material was then supplied along the top shale-cement contact and allowed to flow under gravity into the microannulus as shown in Figure 3.17. The seal repair material was added into the crack until the seal repair material no longer flowed into the crack. Five seal repair materials were tested in this test:  standard microfine cement, Novolac epoxy, and Novolac epoxy with 3 different contents of ANPs (0.25 wt.%, 0.5 wt.%, and 1.0 w.%). ANPs were added as a weight percentage of the epoxy total weight. Novolac Epoxy and ANPs were selected to this test

based on the results of followability and slant shear tests of PCNCs as explained in section 3.2.3.
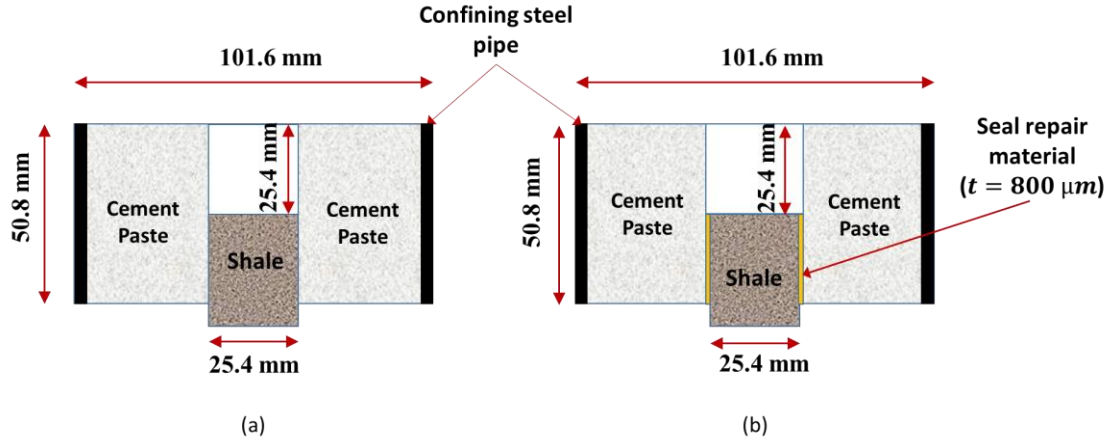


Figure 3.16: Schematic of the push-out test specimens for (a) first set of specimens and (b) second set of specimens.



Figure 3.17: Placing seal repair material at the cement-shale microannulus.

All specimens were tested at age 7 days after sealing (or curing for reference specimens). Cement specimens were cured in 100% humidity while polymer nanocomposites specimens were air cured at room temperature.

The push-out test setup is shown in Figure 3.18. The push-out test was conducted under two-stage displacement control protocol. The test started with a rate of 0. 1 mm/min for the first 5 mm, after which the loading rate was increased to 1.0 mm/min. Test load and

displacement were recorded using sampling rate of 1 Hz. The initial lower displacement rate allowed bond failure to take place at low strain rate. The greater displacement rate post-peak was used to reduce the total test time to about 1 hour. The bond strength was then calculated using equation (3.2).

$$\tau = \frac{P}{\pi DL} \ldots\ldots\ldots\ldots\ldots\ldots\ldots\ldots\ldots\ldots\ldots\ldots\ldots\ldots\ldots\ldots\ldots\ldots\ldots\ldots\ldots\ldots\ldots\ldots(3.2)$$

where $\tau$ is the interfacial bond strength, P is the peak load, D is the diameter of the shale core of 25.4 mm, and L is the embedment length of 25.4 mm.
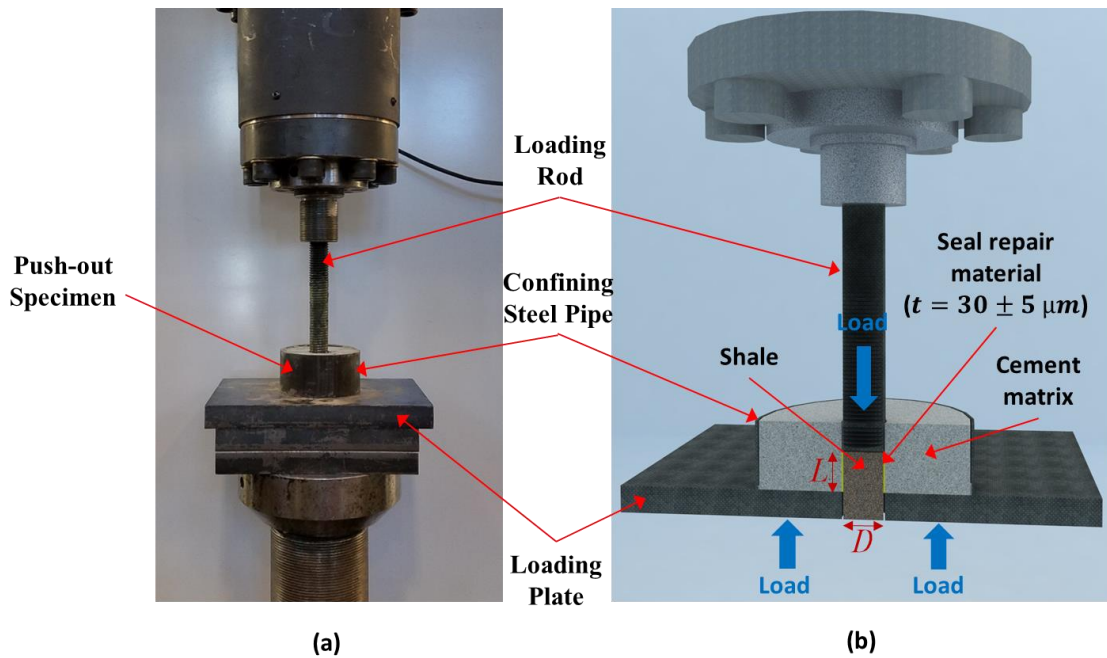


Figure 3.18: (a) Push-out test setup and (b) Push-out test schematic.

Median load-displacement curves of specimens with different seal repair materials are shown in Figure 3.19. It is obvious that microfine cement as seal repair material has a very low shear capacity and very low energy absorption (represented by the area under the curve) compared with all the epoxy nanocomposite seal repair materials. Compared to neat epoxy, the nanocomposite with 0.25% ANPs does not appear to have increased shear capacity or energy absorption. However, it is apparent that adding 0.5 % ANPs to the epoxy

38

improved both the shear capacity and its energy absorption significantly; little additional benefit appears to be gained by increasing the ANP to 1.0%.
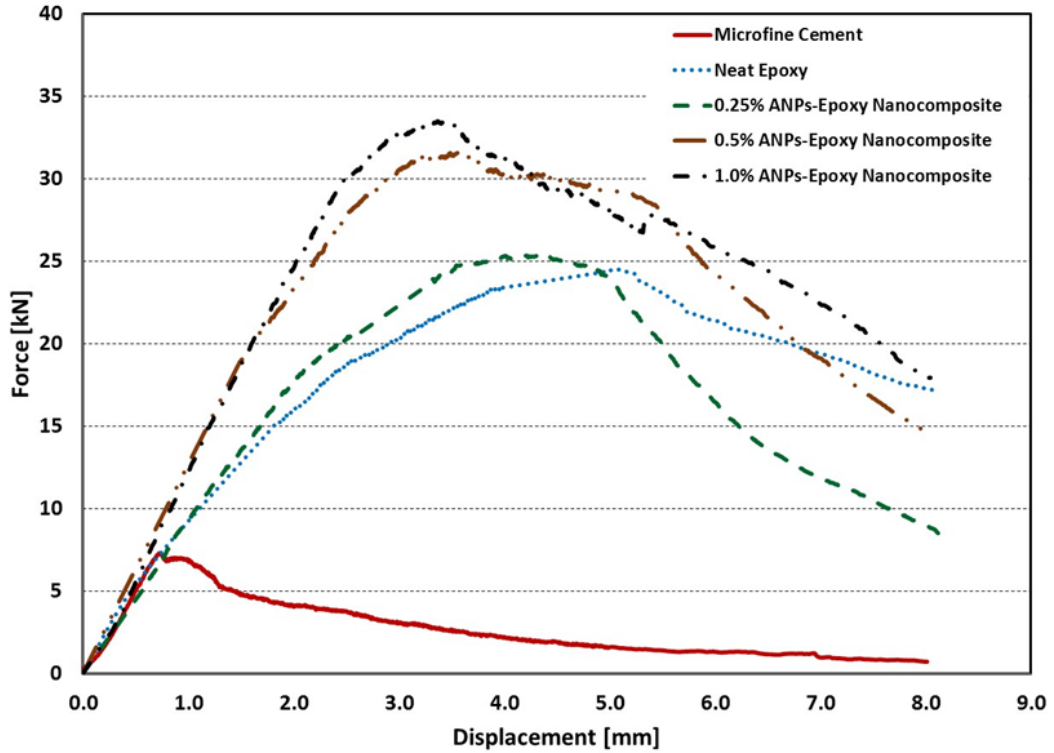


Figure 3.19: Median load-displacement curves of specimens sealed with microfine cement and epoxy-based materials.

Figure 3.20 shows the bond strength of the reference case (cement case around shale) and all seal repair materials. Table 3.4 shows the bond strength results for all seal repair materials compared to reference case. As visual observations show, the failure of all specimens occur at the shale/ANPs-epoxy nanocomposites interface. Statistical analysis using student t-test with 95% level of confidence shows that the reduction of bond strength of microfine cement was statistically insignificant. However, the increase in the bond strength of all ANPS-epoxy nanocomposites is statistically significant when compared with the reference case or the microfine cement.

39
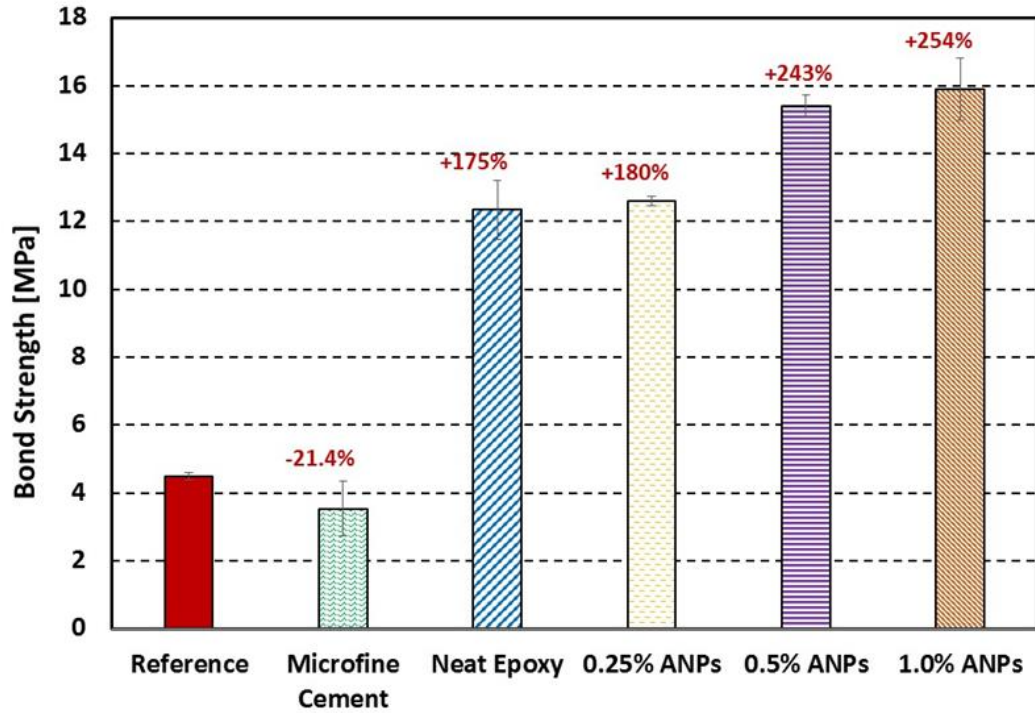
Figure 3.20: The bond strength of the reference case and all seal repair materials.

Table 3.4: The bond strength of the reference case and all seal repair materials.

| Material | Reference | Microfine cement | Neat Epoxy | 0.25% ANPs | 0.5% ANPs | 1.0% ANPs |
|---|---|---|---|---|---|---|
| Bond Strength [MPa] | 4.49±0.1 | 3.53±0.82 | 12.34±0.9 | 12.6±0.1 | 15.4±0.3 | 15.89±0.9 |

Table 3.5 shows shear stiffness defined as the slope of the linear part of the load-displacement curve, displacement at peak load, and toughness calculated as the area under load-displacement curve.

Table 3.5: shear stiffness, displacement at peak load, and toughness for all seal repair materials.

| Material | Microfine cement | Neat Epoxy | 0.25% ANPs | 0.5% ANPs | 1.0% ANPs |
|---|---|---|---|---|---|
| Shear stiffness [kN/mm] | 11.02±0.09 | 10.86±0.49 | 10.67±0.75 | 11.11±0.13 | 11.21±0.5 |
| Displacement at peak load [mm] | 0.75±0.01 | 4.84±0.2 | 4.09±0.13 | 3.54±0.06 | 3.39±0.04 |
| Toughness [N.ma] | 21.69±0.44 | 145.7±0.46 | 141.4±12.2 | 180.7±1.87 | 186.7±2.38 |

The displacement at peak load for microfine cement and ANPs-epoxy nanocomposites is shown in Figure 3.21. Although the results show that incorporating ANPs in the epoxy resin significantly reduces the displacement at peak load, the displacement at peak load of all ANPs-epoxy nanocomposites was significantly higher than microfine cement. Figure 3.22 Shows The toughness of ANPs-epoxy nanocomposites compared to microfine cement. Statistical analysis shows that the difference of stiffness among all seal repair material was insignificant. It was also found that the difference in toughness between all ANPs-epoxy nanocomposites and microfine cement was statistically significant. However, there was no significant difference in toughness between neat epoxy and 0.25% ANPs-epoxy nanocomposite.
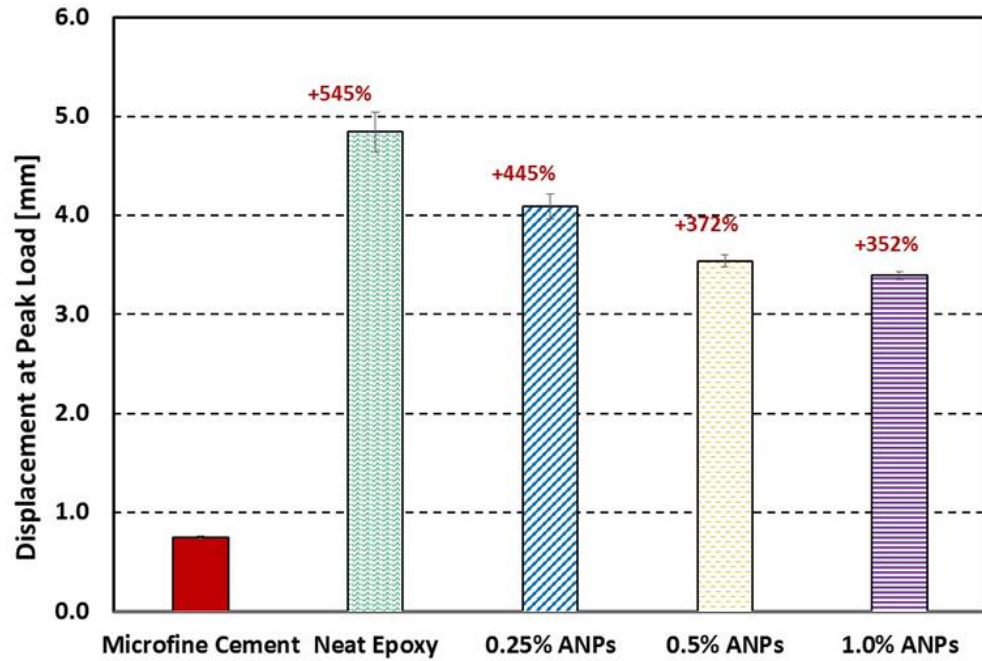
Figure 3.21: Displacement at peak load of the microfine cement and all ANPs-epoxy nanocomposites
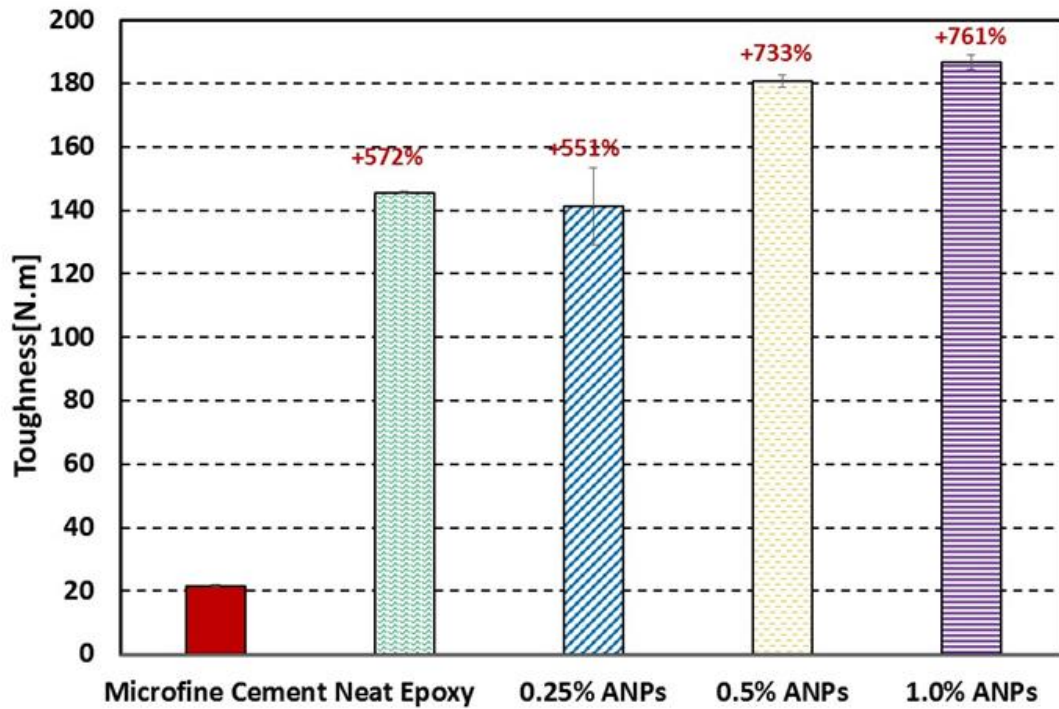


Figure 3.22: Toughness for the microfine cement and all ANPs-epoxy nanocomposites

*3.3.2    Viscosity of Polymer Nanocomposites*

Viscosity test was conducted using rotational Viscometer (Figure 3.23) following AASHTO T316 (AASHTO 2010). The viscosity was measured for all material at room temperature (22 ℃). SC4-21 needle spindles, rotating at 20 rpm, were used for viscosity measurements. The spindles were allowed to rotate for 1 minute, after which three readings were taken at 15-second intervals. The test was performed as per the AASHTO standard.



Figure 3.23: Rotational Viscometer.

Figure 3.24 shows the viscosity measurements for ANPs-epoxy nanocomposites compared with microfine cement. It was found that all ANPs-epoxy nanocomposites have viscosity lower than microfine cement. It was also found that incorporating ANPs in epoxy resin have a minor effect on epoxy viscosity. The maximum increase in viscosity of ANPs-epoxy polymer nanocomposite was found to be 8.2% compared with that of neat epoxy. Statistical analysis using student t-test with 95% level of confidence shows that the

difference in viscosity of ANPs-epoxy nanocomposites was significantly different than that of microfine cement.
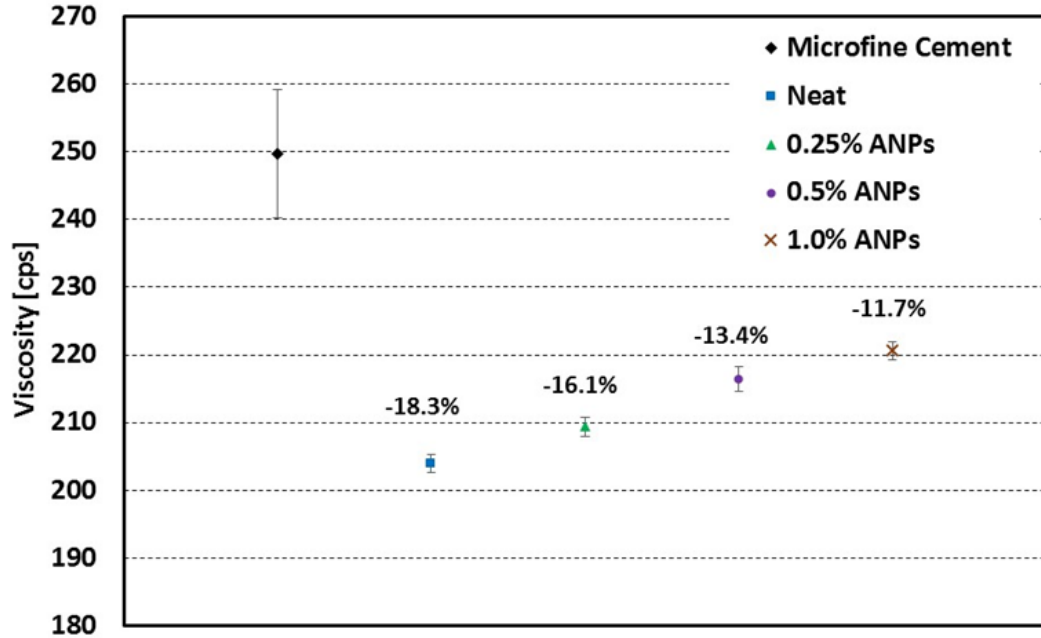


Figure 3.24: Comparison of the viscosity between polymer nanocomposites incorporating 0% (Neat) 0.25%, 0.5%, and 1.0% ANPs and microfine cement.

### 3.3.3    *Microscopic investigation*

Light microscopes with two different levels of magnification (100X and 500X) were used to observe the shale-cement interface with the different seal repair materials. Photomicrographs of the sealed shale interface with Type G cement paste using microfine cement, neat epoxy, and 1.0% ANPs-epoxy polymer nanocomposite are presented in Figure 3.25, Figure 3.26 and Figure 3.27 respectively. As shown in Figure 3.25, using microfine cement as a seal repair material a gap at the shale-cement interface can be observed. It is important to note that such gap was not uniform and the width of the gap ranges from 3 μm up to 40 μm along the interface. These gaps might be formed due to shrinkage of microfine cement during its hydration. These large gaps between microfine

cement and shale surface could explain the reduction in bond strength in case of microfine cement compared to reference case.
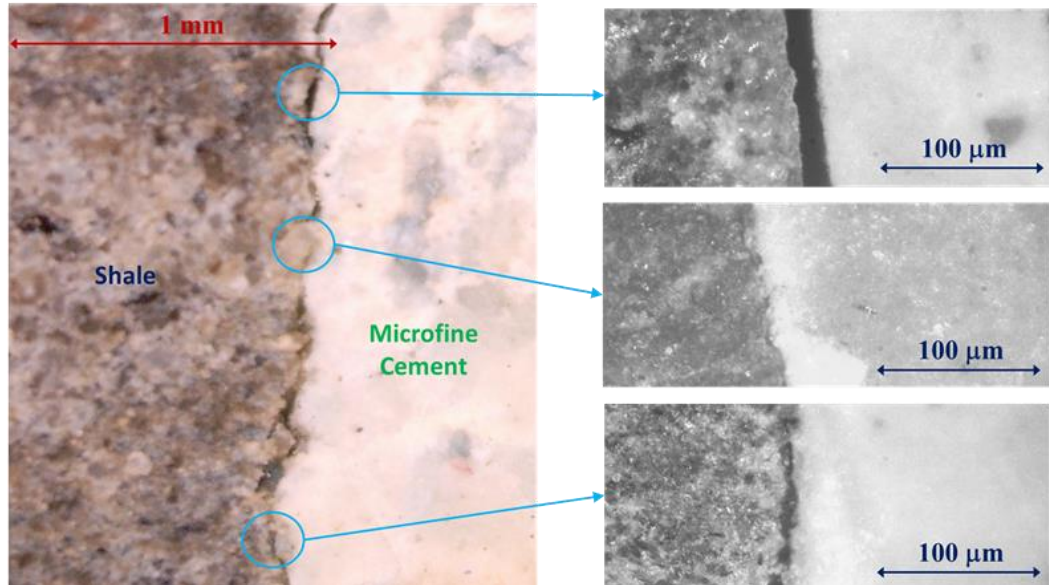


Figure 3.25: Microscopic images of shale-microfine cement interface with two different levels of magnification showing areas with gap between microfine cement and shale.

Photomicrographs of the shale-cement interface sealed with the neat epoxy and 1.0% ANPs-epoxy nanocomposite, shown in Figure 3.26 and Figure 3.27, respectively, show no gaps and demonstrate the ability of epoxy with and without ANPs to flow and seal the shale-cement interface. A close look at Figure 3.26 and Figure 3.27 shows the ability of the ANPs-epoxy nanocomposite to penetrate into the porous shale interface and fill the microcracks at the shale surface. This ability of epoxy and ANPs-epoxy nanocomposite to penetrate the shale microcrack network at the interface enables creating mechanical interlocks in addition to the adhesion between epoxy and shale. These interfacial microcracks at the shale surface also provide potential leakage pathways and thus compromise wellbore seal integrity. The penetration of the epoxy nanocomposite seal

repair material does not only improve the shale-cement bond strength, but it also seals

leakage pathways adjacent to the interface and thus improves wellbore seal integrity.
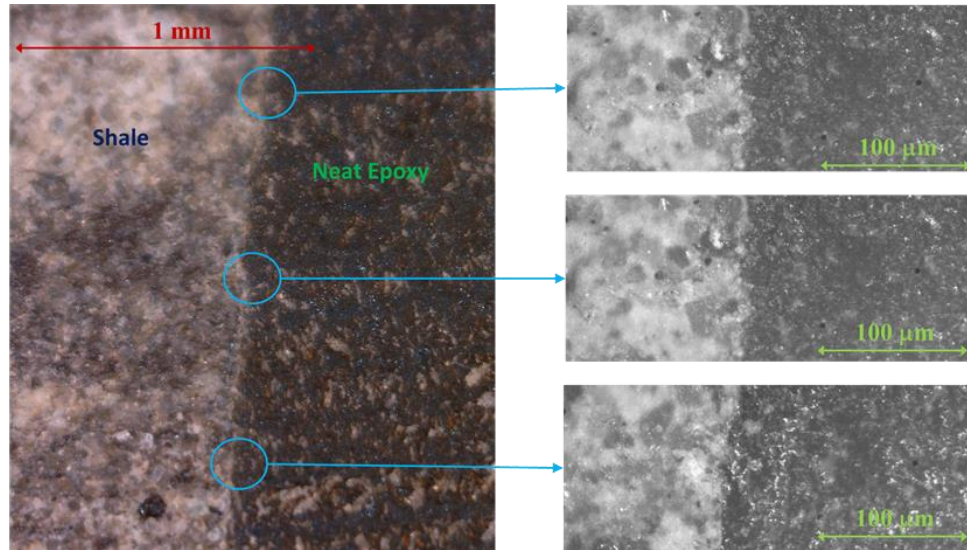


Figure 3.26: Microscopic images of shale-neat epoxy interface with two different levels of magnification showing the ability of the neat epoxy seal repair material to completely fill the gap at the shale-cement interface.
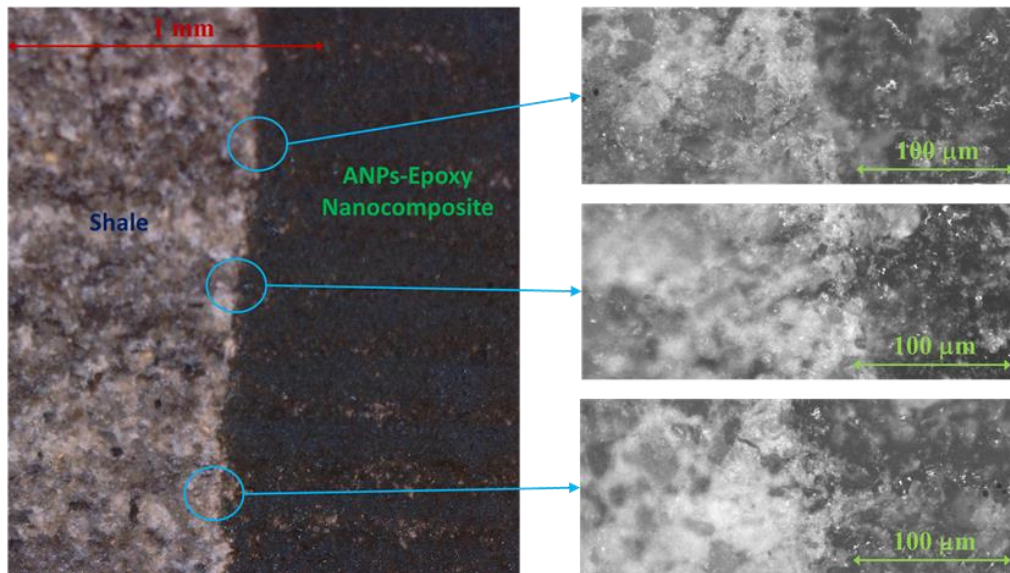


Figure 3.27: Microscopic images of shale-1.0% ANPs-epoxy polymer nanocomposite interface with two different levels of magnification showing the ability of the epoxy seal repair material to completely fill the gap at the shale-cement interface.

### 3.3.4 Fourier Transform Infrared (FTIR) Analysis

FTIR analysis was conducted on neat polymer specimen and specimen incorporating 1.0% ANPs. A PerkinElmer FTIR with the Universal Attenuated Total Reflectance (UATR) accessory was used for the analysis (Figure 3.28). The spectra were recorded with a horizontal ATR accessory and a DiComp crystal (composed of a diamond ATR with a zinc selenide focusing element). For each sample, 4000 scans were collected at a resolution of $4\ cm^{-1}$. The spectra were then converted to absorbance using the Kramers-Kronig equation for FTIR analysis(Griffiths and De Haseth 2007).
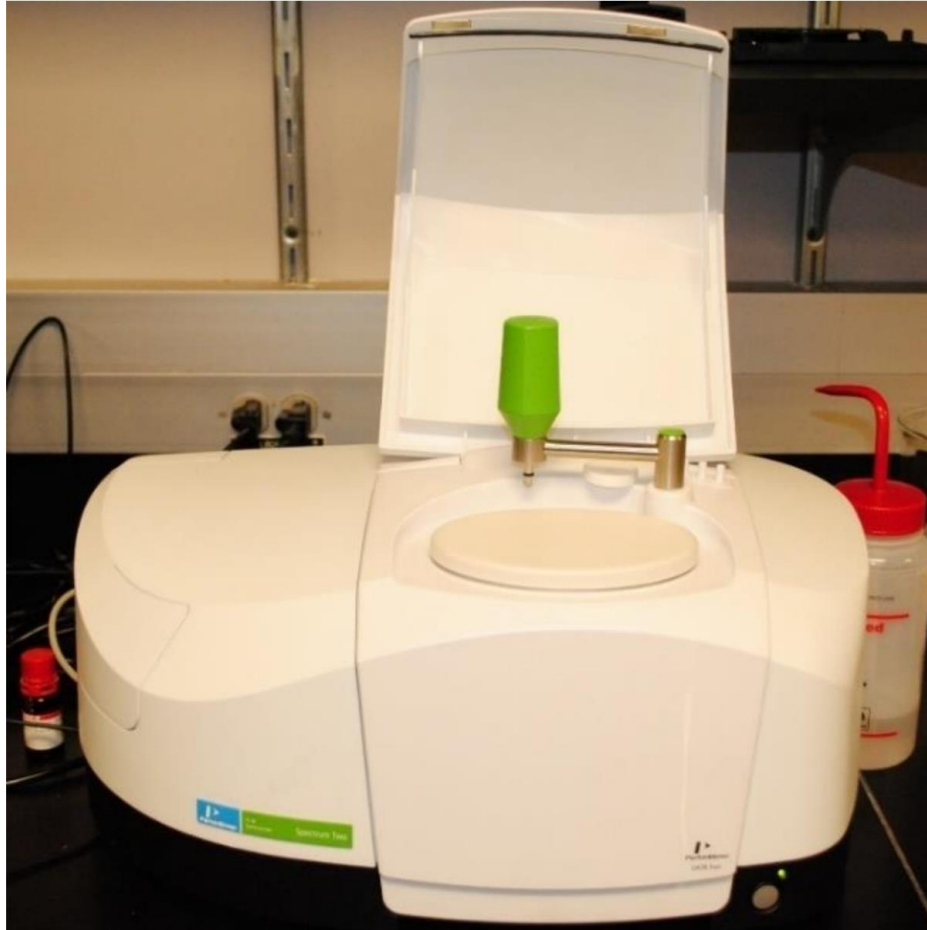


Figure 3.28: PerkinElmer FTIR machine.

FTIR spectra of neat epoxy and epoxy incorporating nano-alumina (0.5 and 1.0% ANPs) were obtained to compare chemical changes of the curing process of epoxy as shown in Figure 3.29. The FTIR spectra show the traditional band of epoxy where absorption bands corresponding to C-H appear at (2850–2930 cm$^{-1}$), epoxide ring ($\sim$825 cm$^{-1}$), N-H band of primary amines (1585– 1610 cm$^{-1}$), O-H groups ($\sim$3350 cm$^{-1}$), C-N band (1030–1115 cm$^{-1}$) and ether bands ($\sim$1230 cm$^{-1}$). The general illustrations of the chemical structures of the Novolac epoxy resin and its curing process can be found elsewhere (Golru et al. 2014). It can be clearly observed that addition of a small amount of ANPs (0.5 or 1.0%) to the epoxy resin caused a significant increase in the epoxy ring, O-H and primary N-H band intensity. This may be attributed to the effect of ANPs on the curing behavior of the epoxy matrix. The curing reaction of the epoxy resin proceeds through the amines presented in the polyamide curing agent(Van den Brand 2004).
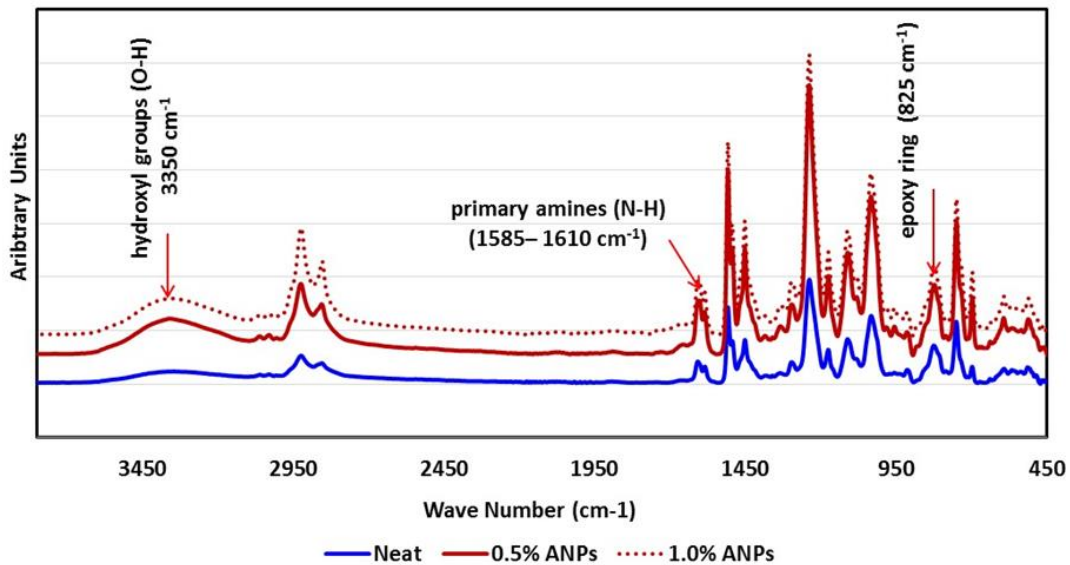
Figure 3.29: FTIR spectra of neat epoxy and epoxy incorporating 0.5 and 1.0 % ANPs showing the significant changes appearing in the spectra using ANPs compared to the neat epoxy.

It is interesting to note that both ANPs contents give the same effect on the curing process of epoxy. Based on the curing mechanism and the results obtained from FTIR analysis, it can be concluded that the curing reaction was affected by the presence of a relatively small amount of ANPs about 0.50%. This can be understood from the higher peak intensities of the epoxy ring ($\sim$830 cm$^{-1}$) and O-H groups ($\sim$3350 cm$^{-1}$) for the epoxy-ANPs nanocomposite compared with neat epoxy. This can be explained by the ability of ANPs to hinder epoxy curing due to steric hindrance effect of ANPs reported by Ramezanzadeh et. al.(Ramezanzadeh, Attar, and Farzam 2011). The steric hindrance effect results in decreasing the reactivity between the epoxy functional groups and polyamide hardener. Such effect is attributed to the amphoteric nature of alumina nanoparticles (Kardar, Ebrahimi, and Bastani 2008, Golru, Attar, and Ramezanzadeh 2014). The ability of ANPs to limit epoxy curing makes the unreacted epoxy groups available to react with other interfaces that epoxy is adhered to. This explains the ability of ANPs-epoxy nanocomposite to have much improved bond strength to both shale and cement paste compared with neat epoxy. The above FTIR observations explain the increase in the sealed shale-cement bond strength by 29% when ANPs were incorporated in the epoxy resin compared with neat epoxy.

### 3.3.5  *Dynamic Mechanical Analyses (DMA)*

The effect of ANPs on crosslinking of epoxy was investigated using dynamic mechanical analyses (DMA). The crosslinking density was determined by applying the theory of rubbery elasticity using equation (3.3) (Hill 1997).

$$\nu_e = \frac{E'}{3RT}\dots\dots\dots\dots\dots\dots\dots\dots\dots\dots\dots\dots\dots\dots\dots\dots\dots\dots\dots\dots\dots\dots\dots\dots(3.3)$$

Where $\upsilon_e$ is the crosslinking density, E' is storage modulus in the rubbery plateau, T is the temperature in Kelvin corresponding to the storage modulus value, and R is Gas Constant. The rubbery plateau was considered to be at temperature 50 ℃ above glass transition temperature $T_g$ (Lee and Yee 2001). The storage modulus at rubbery plateau was measured using DMA Q800 (Figure 3.30). The molecular weight between crosslinks can be calculated using equation (3.4).

$$M_c = \frac{\rho}{\upsilon_e} \dots\dots\dots\dots\dots\dots\dots\dots\dots\dots\dots\dots\dots\dots\dots\dots\dots\dots\dots\dots\dots\dots\dots\dots\dots\dots\dots\dots(3.4)$$

Where $M_c$ is molecular weight between crosslinks and $\rho$ is the density of the polymer nanocomposite. As the crosslinking of a polymer resin increases when the molecular weight between crosslinks decreases (Lee and Yee 2001, Liang and Pearson 2009), A measure for the degree of crosslinking $X_{link}$ is suggested here as an inverse for the molecular weight between crosslinks in a unit volume as in equation (3.5).

$$X_{link} = \frac{1}{M_c} = \frac{\upsilon_e}{\rho} \dots\dots\dots\dots\dots\dots\dots\dots\dots\dots\dots\dots\dots\dots\dots\dots\dots\dots\dots\dots\dots\dots\dots\dots.(3.5)$$

Where $X_{link}$ is a measure of the degree of crosslinking of the polymer nanocomposite.
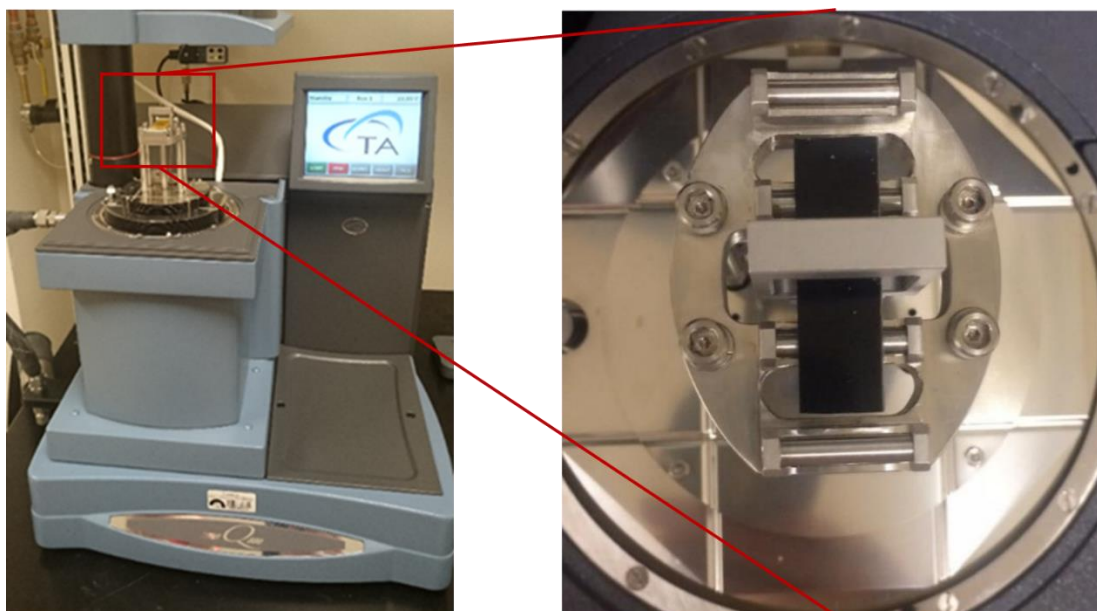
Figure 3.30: DMA Q800 with 3-point bending clamp.

To confirm the significance of ANPs on epoxy cross-linking, DMA testing was conducted on neat epoxy and epoxy incorporating 0.25%, 0.5%, and 1.0% ANPs. The suggested degree of crosslinking measure ($X_{Link}$) was calculated using equations (3.3), (3.4) and (3.5). Figure 3.31 shows the degree of crosslinking for neat epoxy, 0.25% ANPs-epoxy nanocomposites, 0.5%-ANPs epoxy nanocomposite and 1.0% ANPs-epoxy nanocomposite. The results show that incorporating 0.25% ANPs in the epoxy resin reduces the cross linking by only 4.9% which can explain the insignificant change in bond strength between ANPs-epoxy nanocomposites incorporating 0% (Neat) and 0.25% ANPs. On the other side, incorporating 0.5% and 1.0% ANPs reduces epoxy crosslinking by 15.8% and 16.4% respectively. The above analysis confirms the FTIR observations and is consistent with the bond strength results.
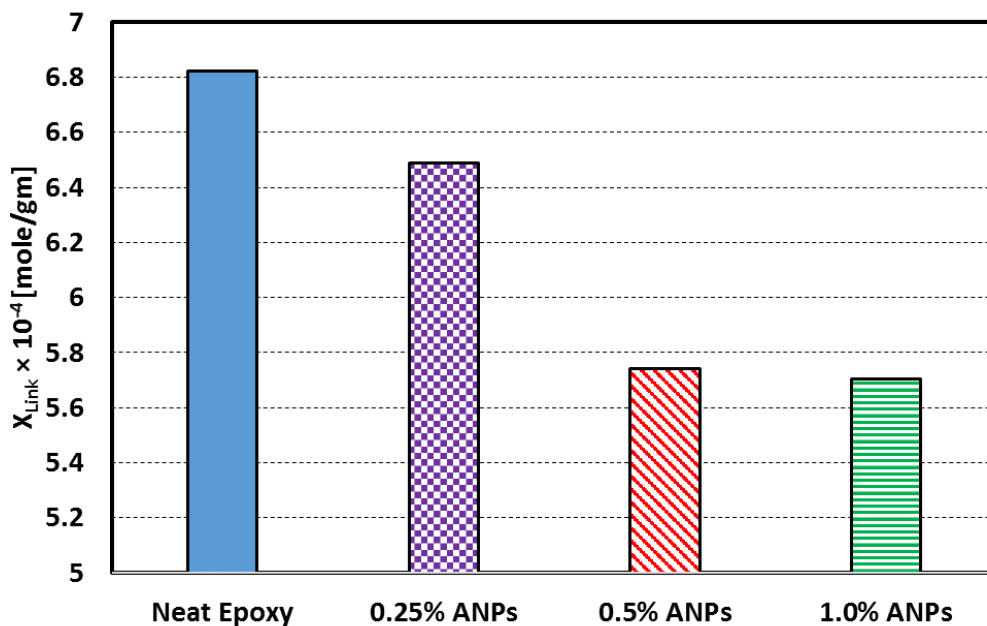
Figure 3.31: $X_{link}$: A measure of the degree of crosslinking for neat epoxy, 0.25% ANPs-epoxy nanocomposite, 0.5% ANPs-epoxy nanocomposite, and 1.0% ANPs-epoxy nanocomposite.

The relation between the bond strength and the content of ANPs in polymer nanocomposites is shown in Figure 3.32. It was observed that the relation between the content of ANPs and bond strength is almost a step function and can be divided in to 3 regions. In region 1, with very low content ($< 0.25\%$) on ANPs, the low content of ANPs was not enough to achieve the full chemical reaction as it is shown in $X_{link}$ measurements (Figure 3.31). This results in insignificant improvement (only 2%) in bond strength. Increasing the content of ANPs to 0.5% (Region 2) resulted in a step increase in the bond strength with 25% improvement in the bond strength. This can be explained by the existence of enough ANPs to interrupt the epoxy crosslinking process and significantly improve the bond strength. With higher content of ANPS (1.0%), only 3% increase in the bond strength was achieved when compared to 0.5%. This limited increase can be explained by that 0.5% ANPs was enough to complete the chemical reaction and interrupt

the crosslinking process which can be concluded from $X_{link}$ measurements (Figure 3.31) and the rest of the ANPs content worked as reinforcement. Due to the small particles size (50nm) and the relatively low content for reinforcement, only limited improvement was observed. Thus, it can be concluded that the optimum ANPs content to achieve the highest effective improvement to cost ratio is 0.5% of the polymer weight.
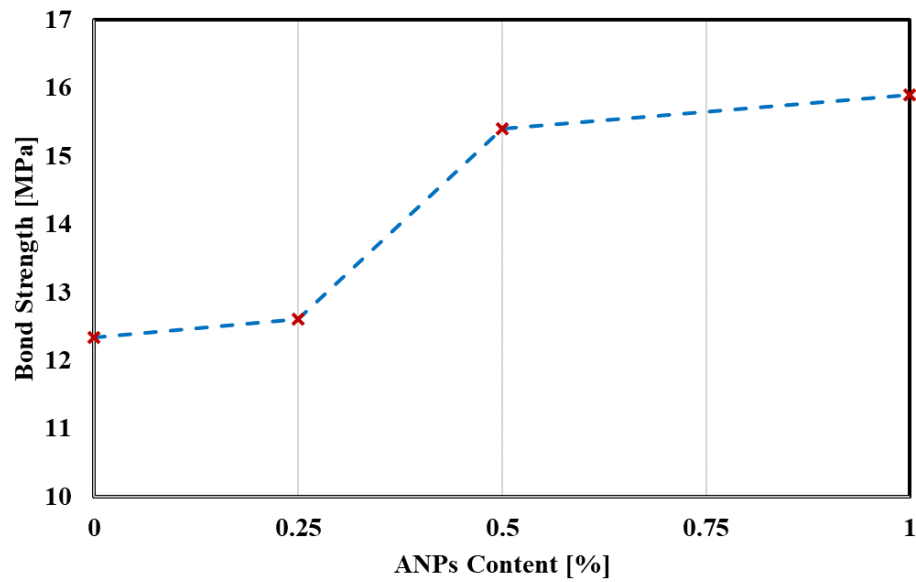
Figure 3.32: The relation between the bond strength and the content of ANPs in polymer nanocomposites.

## 3.4 Phase III: Penetrability study

In this chapter, the ability of the proposed seal repair material to fill thin (30 μm) microcracks was investigated. Neat Novolac epoxy was selected from the previously investigated seal repair materials for this study due to its physical properties. Based on the followability and viscosity results showed in sections 3.2.2 and 3.3.2 respectively, Neat Novolac epoxy showed the highest potential, among the seal repair materials investigated in phase I and II, to be able to fill such thin microcracks. In addition to microfine cement and neat Novolac epoxy, methyl methacrylate (MMA) and nanomodified MMA (NM-MMA) were considered for this study. NM-MMA was prepared by dispersing 0.50 wt.% aluminum nanoparticles (ANPs) in the MMA resin following the dispersing method elaborated in section 3.1.7.

### 3.4.1 Physical properties of seal repair material

To assess the capability of seal repair material to fill 30 μm microcracks, the physical properties, including viscosity, surface tension, and contact angle with cement paste surface, for all seal repair materials used in this investigation were measured.

### 3.4.1.1 Viscosity measurements

Viscosity tests were conducted using a rotational Viscometer as explained in section 3.3.2. The viscosity of investigated seal repair materials is shown in Fig. 3.33. It was found that Novolac epoxy has 18.4% lower viscosity than microfine cement while MMA and NM-MMA both have 99.6% lower viscosity than microfine cement. These extremely low viscosities of MMA and NM-MMA result in a higher rate of flow of the seal repair materials through the microcracks. This high flow rate allows the seal repair

material to penetrate further in the microcrack before hardening and results in an efficient

seal of the microcrack.
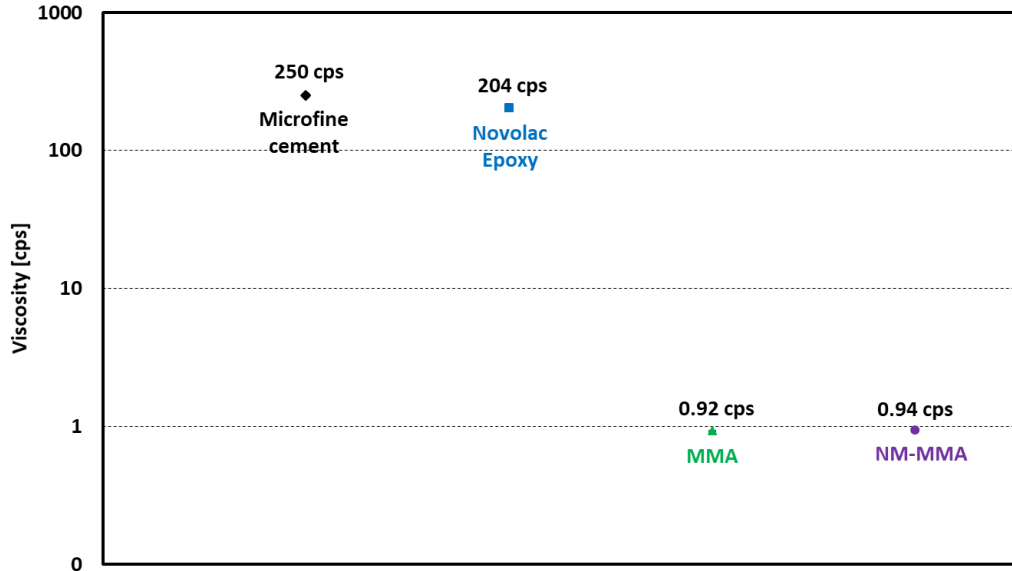


Figure 3.33: Viscosity measurements of all seal repair materials: Log scale is used to enable display with order of magnitude change in viscosity.

### 3.4.1.2   *Surface tension*

The surface tension of the seal repair materials was measured using KRUSS force

tensiometer K100 (Figure 3.34) standard plate surface tension test. The test was conducted

by submerging a standard platinum plate in the investigated liquid to achieve a wetted

depth of 6 mm. The plate was then pulled-out of the liquid with a speed of 10 mm/min.

The force required to pull-out the plate was measured and the surface tension of the liquid

was calculated using Wilhelmy plate method.
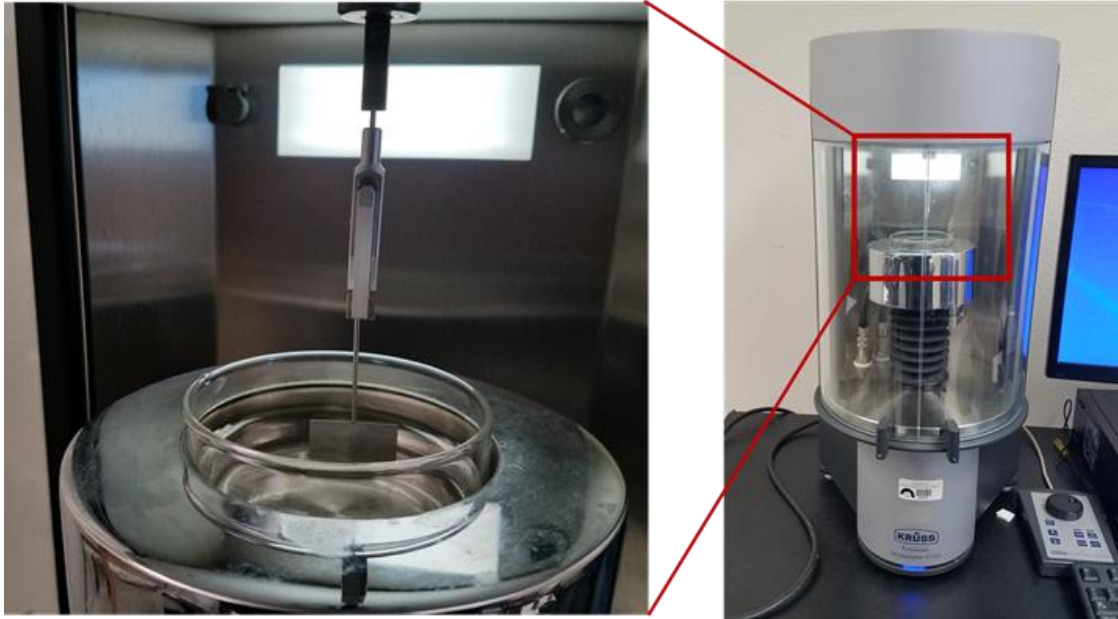
Figure 3.34: KRUSS force tensiometer K100 machine.

The surface tension measurements of investigated seal repair materials are shown in Figure 3.35. Novolac epoxy has 17.7% lower surface tension than microfine cement. This low surface tension allows epoxy to fill smaller microcracks than what microfine cement can fill. On the other hand, it was found that MMA and NM-MMA seal repair materials have 43.2% and 42.7% lower surface tension than microfine cement, respectively, and 31% and 30.5%, respectively, lower than Novolac epoxy. This significantly low surface tension allows MMA to flow through such small microcracks (30 μm) and completely fill the gap and achieve seal integrity. It was also found that incorporating ANPs has no noticeable effect on either viscosity or surface tension of MMA.
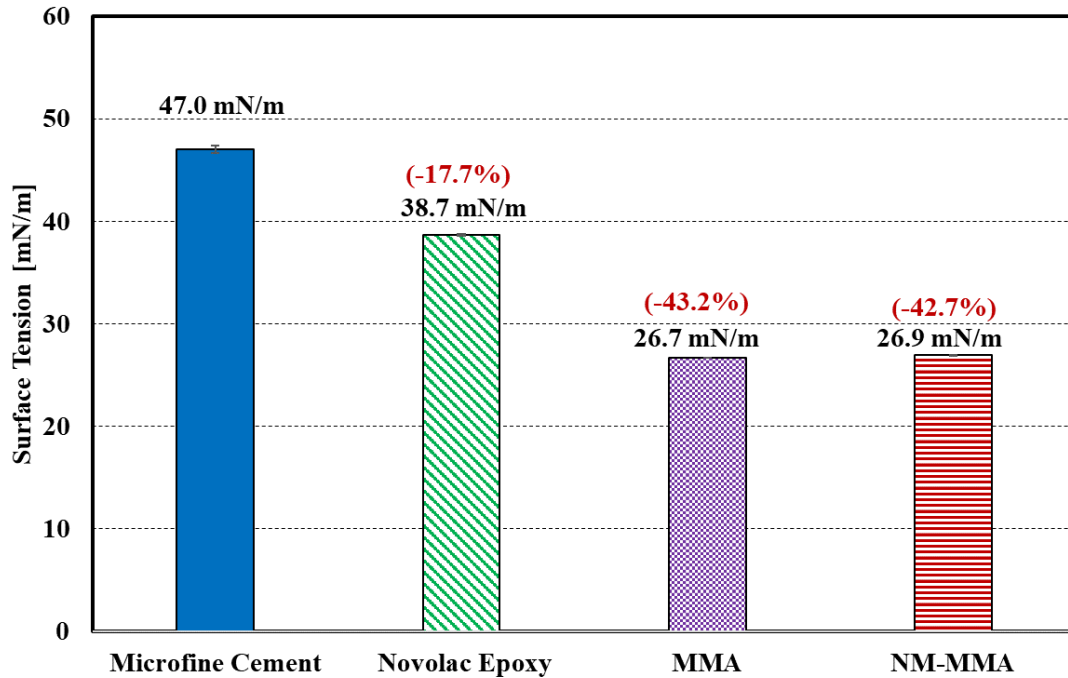
Figure 3.35: Surface tension seal repair materials: % above the bars represents the difference of Penetrability Index of seal repair material compared with microfine cement.

### 3.4.1.3  *Contact angle with cement paste surface*

Contact angle of seal repair material with Type G cement paste surface was measured by allowing a drop of seal repair material to fall on a hardened cement paste surface from 1 cm height. A high resolution camera was used to take a photo of the seal repair material drop before it was absorbed by the cement paste (Courard 1999). DinoCapture 2.0 angle measurement tool was then used to measure the contact angle of each seal repair material.

The contact angle measurements of investigated seal repair materials with Type G cement paste surface are shown in Figure 3.36. The measurements show that the contact angle of Novolac epoxy, MMA, and NM-MMA are 27%, 62%, and 59% lower than the contact angle of microfine cement with Type G cement paste surface respectively. The measurements also show that the contact angle of MMA and NM-MMA are 48% and 44%

lower than Novolac epoxy. On the other hand, incorporating ANPs in MMA resulted in a very limited increase in the contact angle of MMA with cement paste by 7% only.
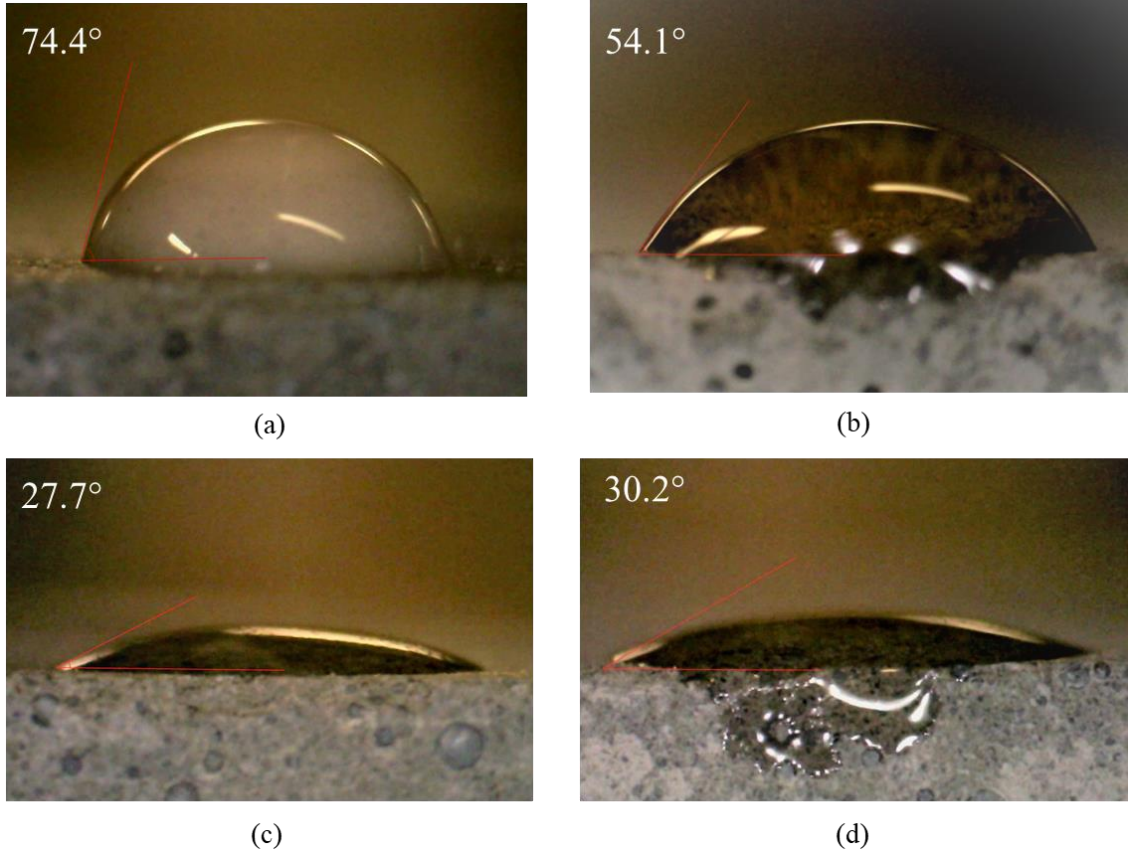


Figure 3.36: Contact angle measurements for (a) Microfine cement, (b) Novolac epoxy, (c) MMA, and (d) NM-MMA.

### 3.4.1.4 *Penetrability of seal repair materials*

The ability of a seal repair material to replace other fluids (e.g. air or water) is proportional to its surface tension and contact angle (Blunt 2017). To compare the penetrability of seal repair materials in this study, we calculated the capillary pressure ($P_c$) based on Young-Laplace equation shown in equation (3.6) (Tiab and Donaldson 2015).

$$P_c = \frac{2\gamma_r \cos\theta_r}{r_c} \dots\dots\dots\dots\dots\dots\dots\dots\dots\dots\dots\dots\dots\dots\dots\dots\dots\dots(3.6)$$

where $P_c$ is the capillary pressure [Pa], $\gamma_r$ is the seal repair material surface tension [N/m], $\theta_r$ is the seal repair material contact angle, and $r_c$ is half of the crack width [m]. The calculated capillary pressure for all seal repair materials is shown in Figure 3.37. The results show that Novolac epoxy, MMA, and NM-MMA have 8.1%, 31.0%, and 30.8% lower capillary pressure in a 30 μm capillary crack than microfine cement respectively. Moreover, MMA and NM-MMA were found to have 24.9% and 24.6% lower capillary pressure than Novolac epoxy respectively. These results show that MMA and NM-MMA seal repair material will be able to penetrate smaller microscale defects than both microfine cement and Novolac epoxy under similar conditions. On the other hand, incorporating ANPs in MMA seal repair material resulted in a very insignificant increase in the capillary pressure of MMA by less than 1.0%.
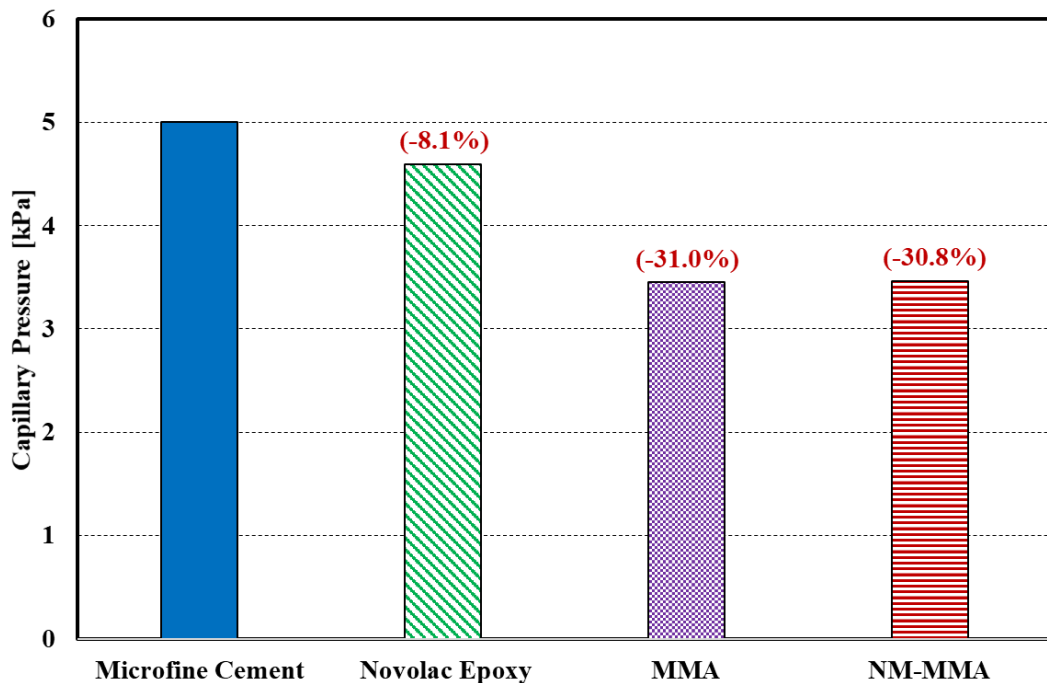


Figure 3.37: Capillary Pressure of all seal repair materials in a 30 μm microcrack; % above the bars represents the difference of Capillary Pressure of seal repair material compared with microfine cement.

### 3.4.2   Bond strength

Push-out test specimens were prepared as shown in Figure 3.38 to measure the bond strength of seal repair materials. Push-out test was conducted as explained in section 3.3.1.
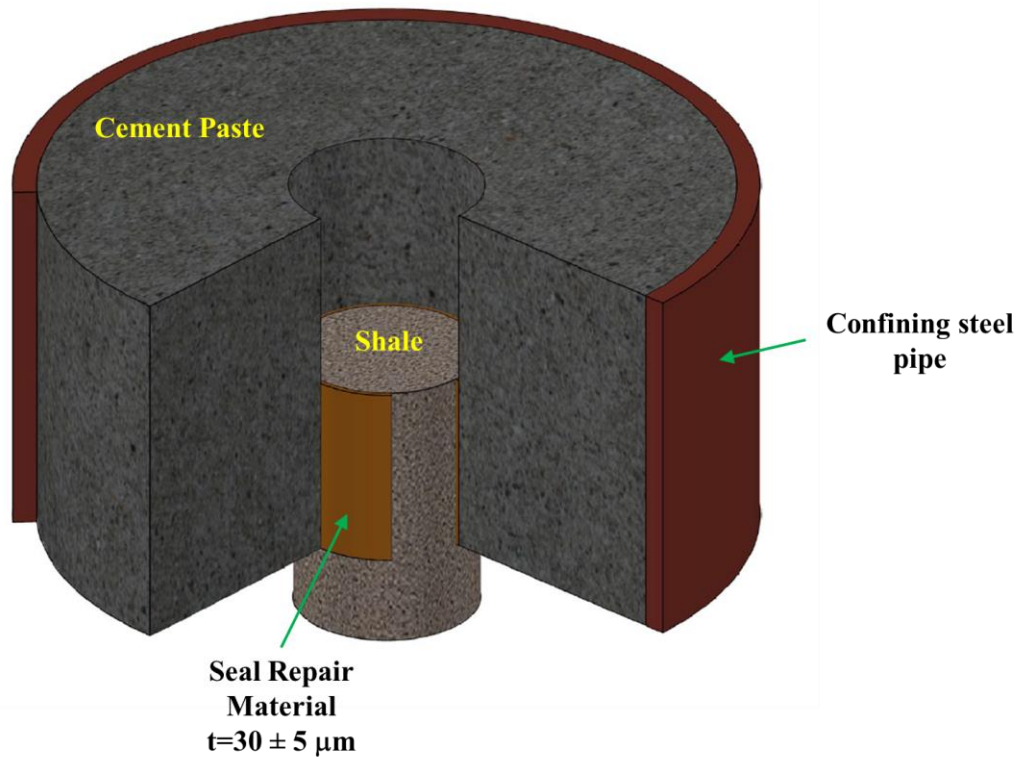


Figure 3.38: Schematic of push-out test specimen for 30 µm microcracks.

All push-out specimens were loaded until failure. Failure was defined as the point at which the load dropped below 50% of the maximum load. Median load-displacement curves of specimens sealed with different seal repair materials are shown in Figure 3.39. The load-displacement curves show that microfine cement has very low bond strength compared with polymer seal repair material. It was also observed that MMA-based seal repair materials have almost 100% higher bond strength than Novolac epoxy seal repair material, and about 1000% higher than microfine cement. Incorporating ANPs has no significant effect on the bond strength of the seal repair material. However, incorporating

ANPs significantly improved the displacement at failure of the seal repair material indicating significant improvement in ductility.
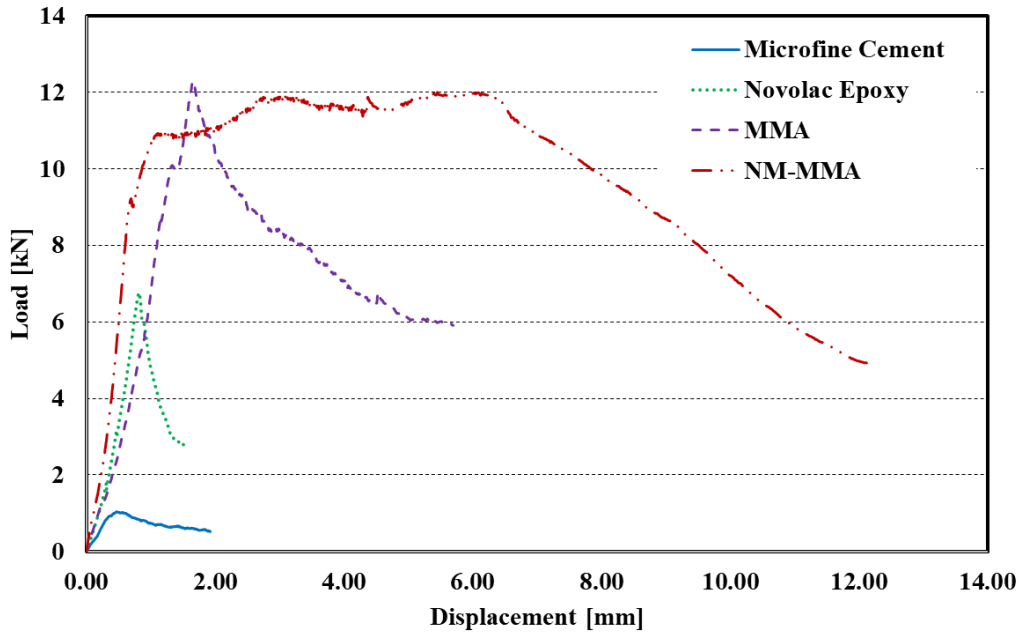


Figure 3.39: Median load-displacement curves of specimens sealed with microfine cement, Novolac epoxy, MMA, and NM-MMA polymer nanocomposite.

The apparent bond strength of seal repair materials was calculated using equation 3.2. Figure 3.40 shows the bond strength of investigated seal repair materials. The results show an increase in the apparent bond strength of Novolac epoxy, MMA, and NM-MMA by 554%, 1088%, and 1061% compared to microfine cement. Statistical analysis using student t-test with 95% level of confidence shows that the increase of bond strength of Novolac epoxy, MMA, and NM-MMA compared to microfine cement was statistically significant. However, the reduction in the bond strength of NM-MMA is statistically insignificant when compared with neat MMA seal repair material.
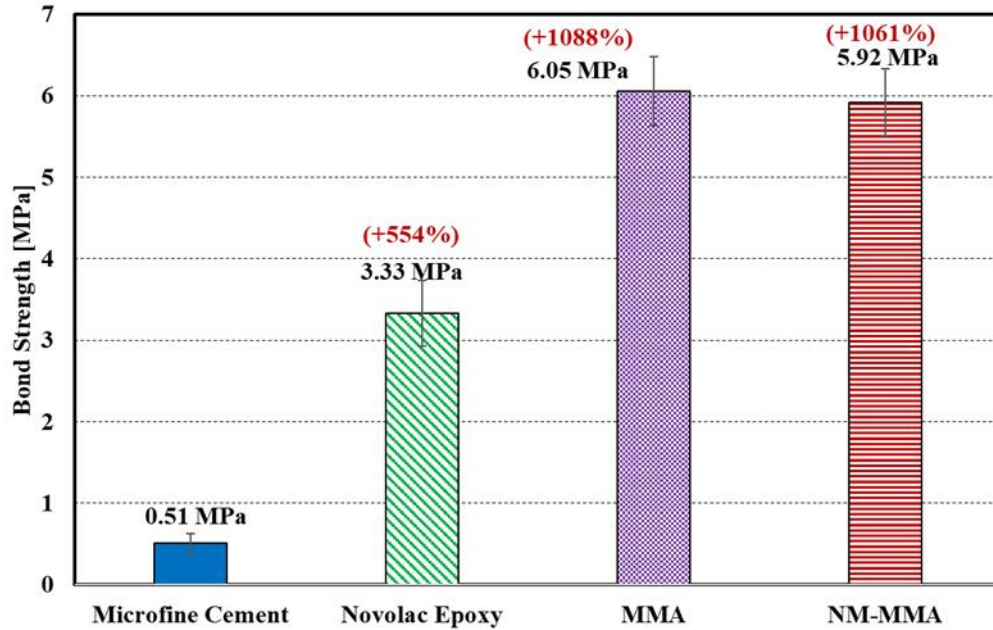
Figure 3.40: The apparent bond strength of all seal repair materials; % above the bars represents the difference of bond strength of seal repair material compared with microfine cement currently used in the field.

Figure 3.41 shows the displacement at failure for seal repair materials. Using Novolac epoxy as seal repair material reduced the displacement at failure by 34.9% compared with microfine cement. However, this reduction was found to be statistically insignificant. On the other hand, the displacement at failure of specimens sealed with MMA and NM-MMA was found to increase the displacement at failure by 156% and 468%, respectively, compared to microfine cement.

The toughness of push-out specimens was calculated as the area under the load-displacement curve until failure (Figure 3.42). It was found that the toughness was increase by 223%, 2638%, and 8135% for Novolac epoxy, MMA, and NM-MMA, respectively, compared to microfine cement. These results show that incorporating 0.5% ANPs in MMA was able to increase the displacement at failure and toughness of push-out specimens by 122% and 201% respectively. It is important to note that such increase in ductility and

toughness of seal repair material will have a significant effect on seal efficiency. A seal repair material with relatively high strength and very high failure displacement and ability to absorb energy will show much improved efficiency compared to current sealing technology.
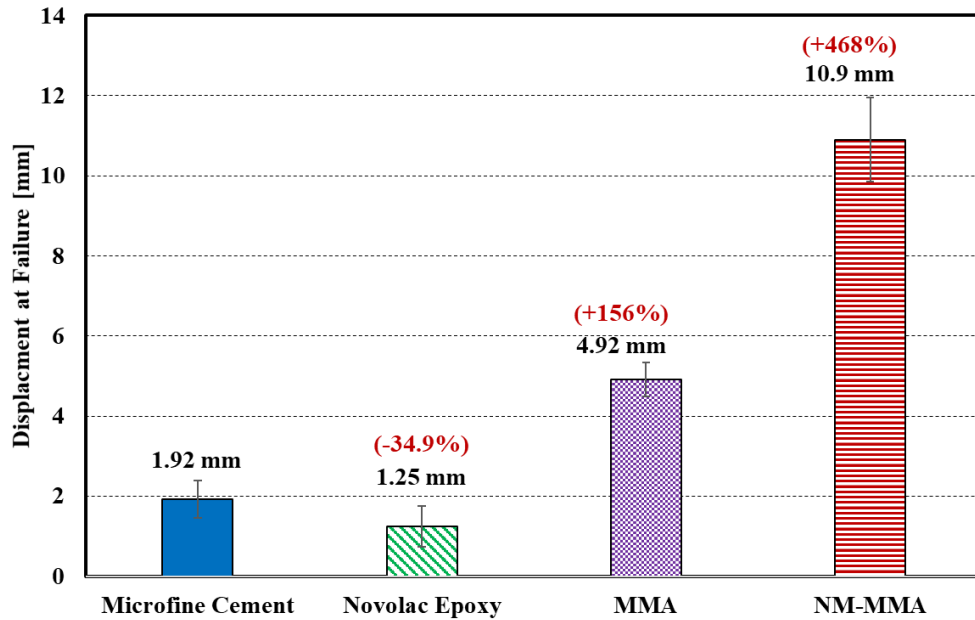


Figure 3.41: Displacement at failure of all seal repair materials; % above the bars represents the difference of bond strength of seal repair material compared with microfine cement.
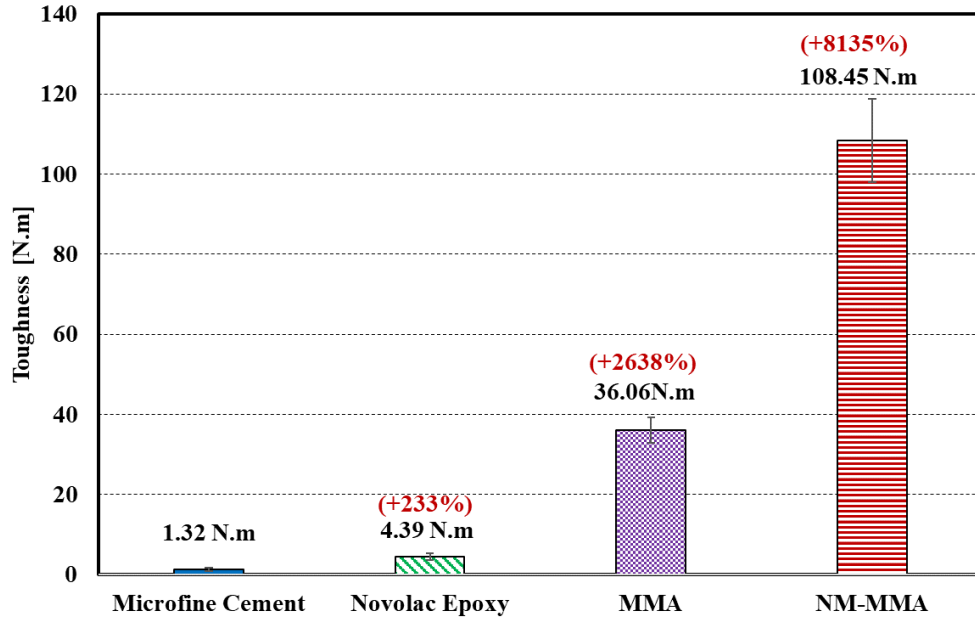
Figure 3.42: Toughness of all seal repair materials; % above the bars represents the difference of bond strength of seal repair material compared with microfine cement.

### 3.4.3    Microscopic investigation

Microscopic investigation of the cement-shale interface was conducted to explain the bond strength. Figure 3.43 and Figure 3.44 show photomicrographs of cement-shale interfaces sealed with microfine cement and Novolac epoxy respectively. Figure 3.43 shows that microfine cement has a very limited penetration in the cement-shale interface. Moreover, Novolac epoxy was found to discreetly fill the cement-shale interface as shown in Figure 3.44. This shows that both microfine cement and Novolac epoxy were not able to fill the 30 μm microcracks. This explains the relatively low bond strength of both materials. This also explains the reduction in the values of the bond strength measured compared with those reported in section 3.3.1 for sealing of 800 μm microcracks. On the other hand, NM-MMA was able to completely fill 30 μm microcracks as shown in Figure 3.45. In addition, NM-MMA was able to penetrate into the shale and cement surfaces which can be explained by the capillary effect.
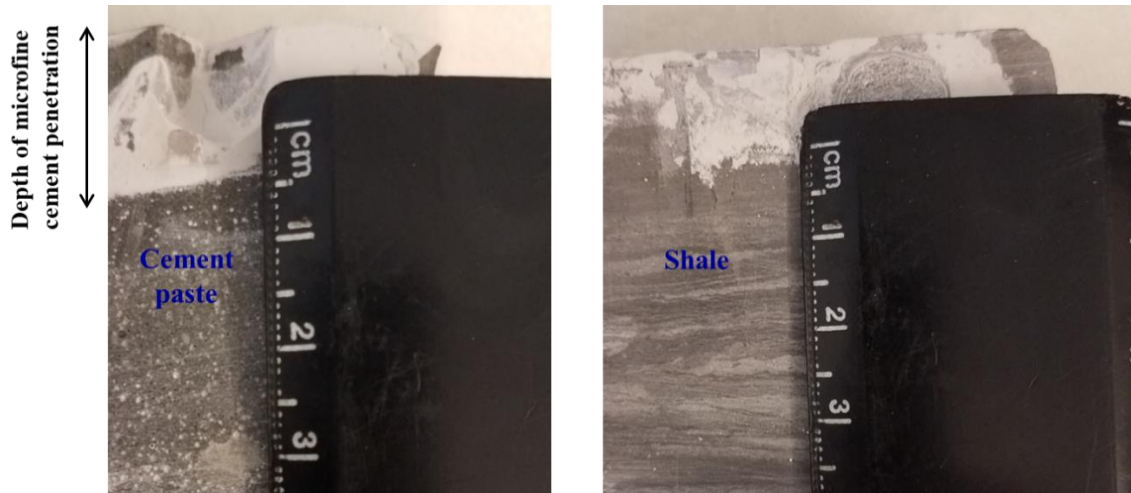
Figure 3.43: Microscopic images of cement-shale interface sealed with microfine cement with two different sides showing depth of microfine cement penetration of cement paste and shale sides.
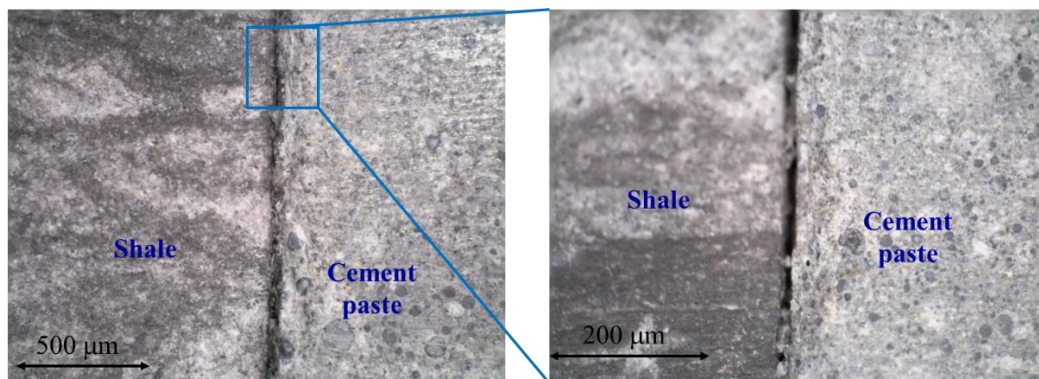


Figure 3.44: Microscopic images of cement-shale interface sealed with Novolac epoxy with two different levels of magnification showing gabs in sealed interface. Right photo at high magnification shows the inability of epoxy to penetrate 30 μm microcracks.
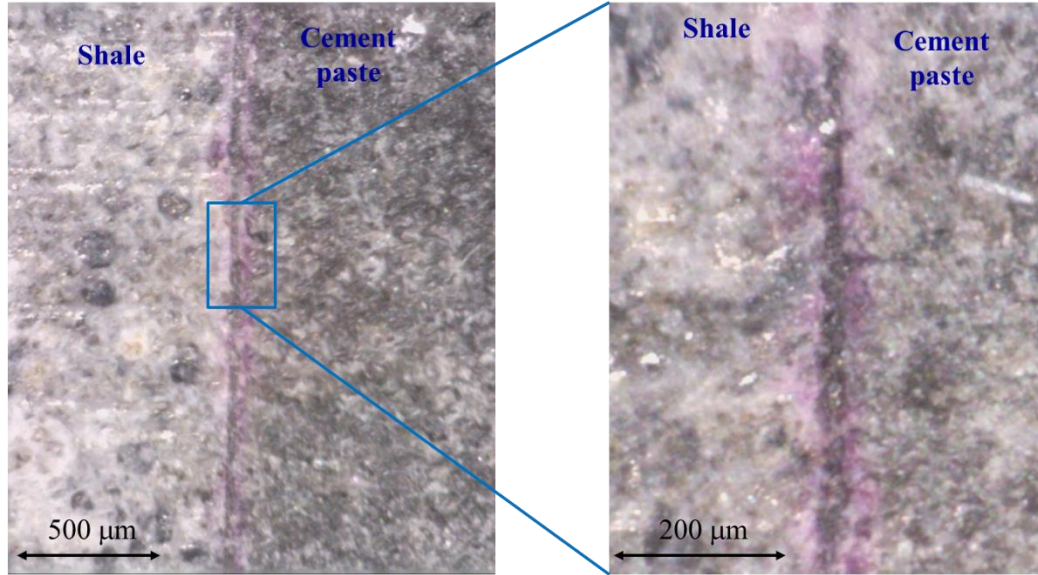
Figure 3.45: Microscopic images of cement-shale interface sealed with NM-MMA with two different levels of magnification showing the ability of the NM-MMA seal repair material to completely fill the gap at the shale-cement interface. Right photo proves the ability of NM-MMA to fill the microcracks and infiltrate both shale and cement paste sides.

### 3.4.4   Dynamical Mechanical Analysis (DMA)

The effect of incorporating ANPs in MMA on the viscoelastic behavior of MMA polymer nanocomposites was investigated using DMA Q800. MMA and NM-MMA specimens were subjected to constant tension stress of 3.5 MPa for 20 minutes. Afterward, the strain was allowed to recover for 40 minutes. The change of strain with time was recorded and the creep compliance was calculated using equation 3.7.

$$J(t) = \frac{\varepsilon(t)}{\sigma_0} \text{.............................................................................................................(3.7)}$$

where $J(t)$ is the creep compliance [MPa$^{-1}$], $\varepsilon(t)$ is the time dependent strain, $\sigma_0$ is the applied constant stress [MPa]. The viscoelastic behavior of MMA and NM-MMA obtained from creep test is shown in Figure 3.46. The creep compliance calculated using equation 3.7 is presented in Figure 3.47. For consistency, the initial creep compliance for

both MMA and NM-MMA was considered at time of 2 seconds for all specimens and it was found to be $2394 \pm 135.7$ $\mu m^2/N$ and $1988.2 \pm 159.9$ $\mu m^2/N$ for MMA and NM-MMA respectively. This represents a decrease of 17% in creep compliance due to incorporating 0.5 wt.% ANPs in MMA resin. Furthermore, the strain recovery was found to be $77.3 \pm 2.4\%$ and $83.0 \pm 2.1\%$ for MMA and NM-MMA respectively. Moreover, the elastic modulus of MMA and NM-MMA was found to be $418.6 \pm 23.4$ MPa and $505.2 \pm 41.9$ MPa respectively.
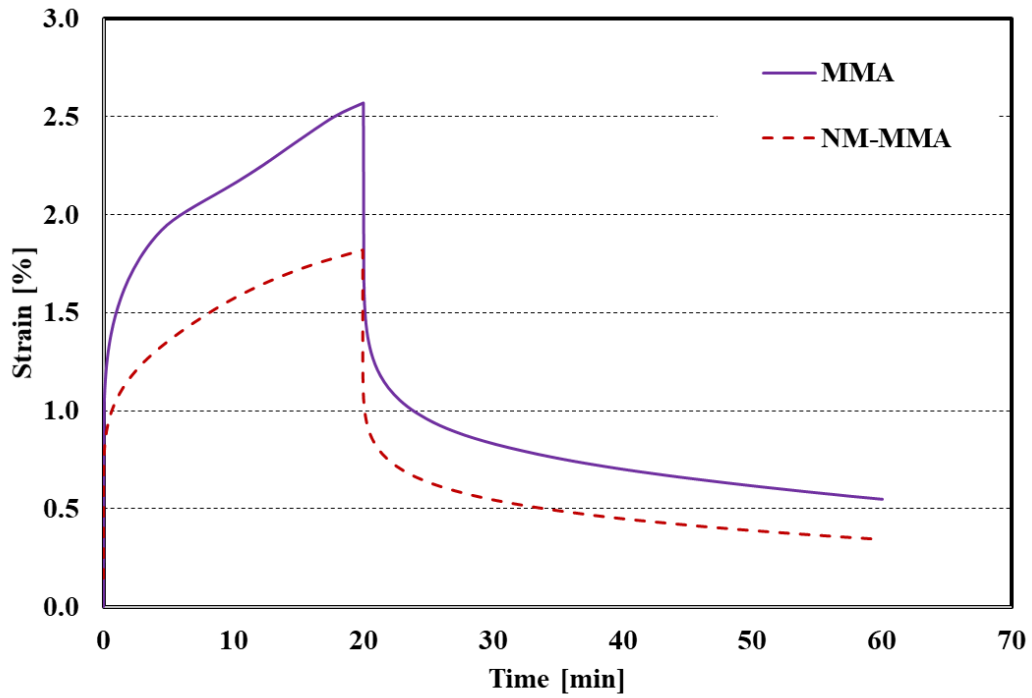
Figure 3.46: The viscoelastic behavior of MMA and NM-MMA obtained from creep test.
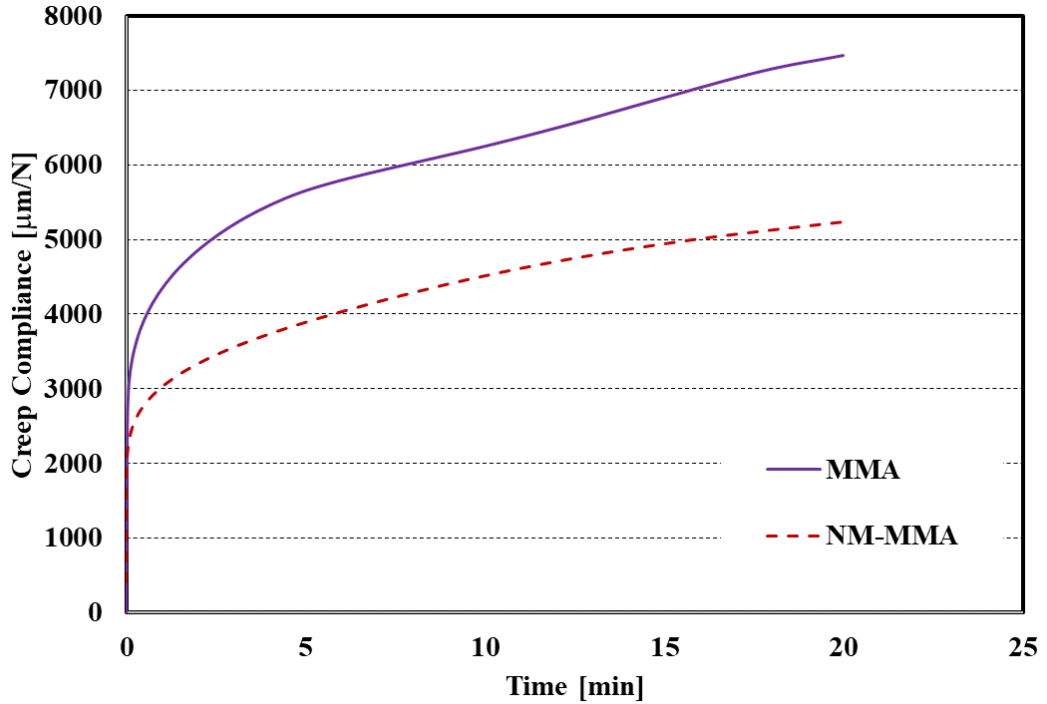
Figure 3.47: Creep Compliance of MMA and NM-MMA calculated from equation 3.7.

To investigate the reinforcement effect of nanoparticles on the mechanical behavior of polymer nanocomposites, several models were developed to estimate the mechanical properties of the composite. The ability of two models to estimate the mechanical properties of the MMA/ANPs polymer nanocomposite was investigated. The elastic modulus of the NM-MMA was estimated using the modified rule of mixture presented by equation 3.8 after Kuo et al. (2005).

$$E_c = \eta E_p V_p + E_m V_m \dots\dots\dots\dots\dots\dots\dots\dots\dots\dots\dots\dots\dots\dots\dots\dots\dots\dots\dots(3.8)$$

where $E_c$ is the composite modulus of elasticity [MPa], $E_p$ is the particles modulus of elasticity [MPa], $E_m$ is the matrix modulus of elasticity [MPa], $V_p$ is the particles volume fraction, $V_m$ is the matrix volume fraction, and $\eta$ is strengthening coefficient. The modulus of elasticity of ANPs was assumed to be 393 GPa after Naous et al. (2006). The matrix

68

modulus of elasticity was measured using DMA and the strengthening coefficient for ANPs was assumed to be $\approx 0.1$ for particles with aspect ratio $\approx 1$ (Kuo et al. 2005). Moreover, the Halpin–Tsai equation presented in equation 3.9 and equation 3.10 was also examined to estimate the modulus of elasticity of NM-MMA polymer nanocomposite (Naous et al. 2006)

$$E_c = E_m \left( \frac{1+\xi \eta V_p}{1-\eta V_p} \right) \dots\dots\dots\dots\dots\dots\dots\dots\dots\dots\dots\dots\dots\dots\dots\dots\dots\dots\dots\dots\dots\dots\dots\dots\dots\dots(3.9)$$

$$\eta = \frac{\frac{E_p}{E_m}-1}{\frac{E_p}{E_m}+\xi} \dots\dots\dots\dots\dots\dots\dots\dots\dots\dots\dots\dots\dots\dots\dots\dots\dots\dots\dots\dots\dots\dots\dots\dots\dots\dots(3.10)$$

The constant $\xi$ was assumed to be 2 for spherical particles like ANPs (Naous et al. 2006). The estimated modulus of elasticity of NM-MMA using the modified rule of mixture and the Halpin–Tsai method compared with the measured value are shown in Figure 3.48. The calculations show that the modified rule of mixture overestimated the polymer nanocomposite modulus of elasticity by more than 29% while he Halpin–Tsai underestimated the modulus by more than 15%. Failure of both models to estimate the modulus of MMA-ANPs polymer nanocomposite can be explained by the fact that these models are micromechanics models that do not take into account the potential chemical reaction between the nanoparticles and the polymer matrix. Such chemical reaction can alter the microstructure and the mechanical properties of the matrix and thus would result in change in the polymer nanocomposite properties.
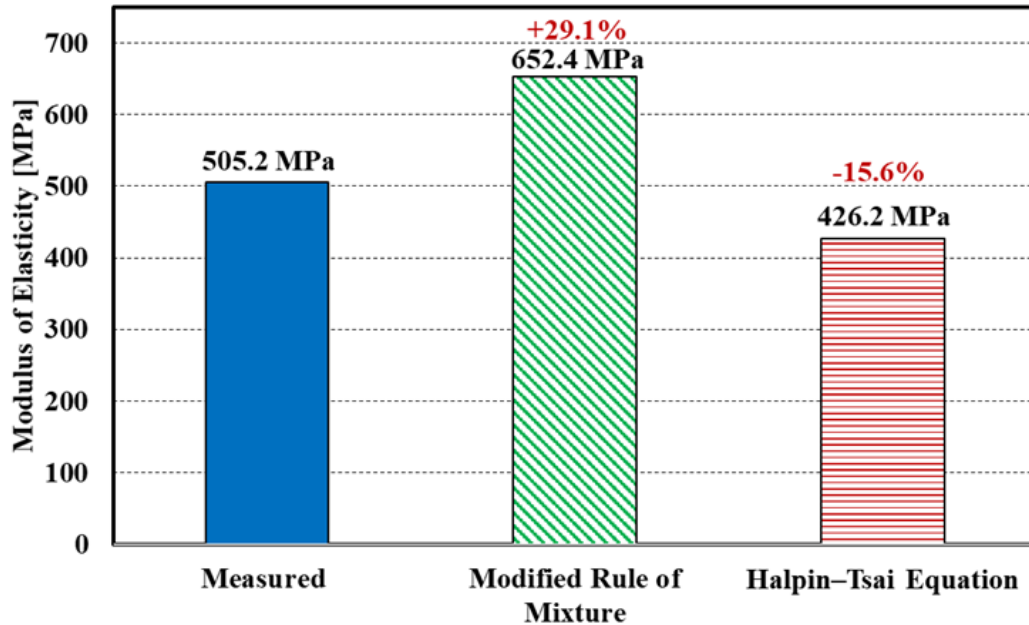
Figure 3.48: The estimated modulus of elasticity of NM-MMA using modified rule of mixture and Halpin–Tsai method compared to the measured value; % above the bars represents the difference of estimated modulus of elasticity compared with measured value..

### 3.4.5   X-ray Diffraction (XRD)

Microstructural investigation using X-ray Diffraction (XRD) was conducted to achieve further understanding of the effect of incorporating ANPs in MMA resin. XRD was conducted using Rigaku, SmartLab XRD machine (Figure 3.49). The machine is equipped with copper k alpha tube and 1 dimensional silicon strip detectors D/teX. The scan was conducted from 0 to 90 degrees with 0.02 degrees' step and scan rate of 6 degrees/min.
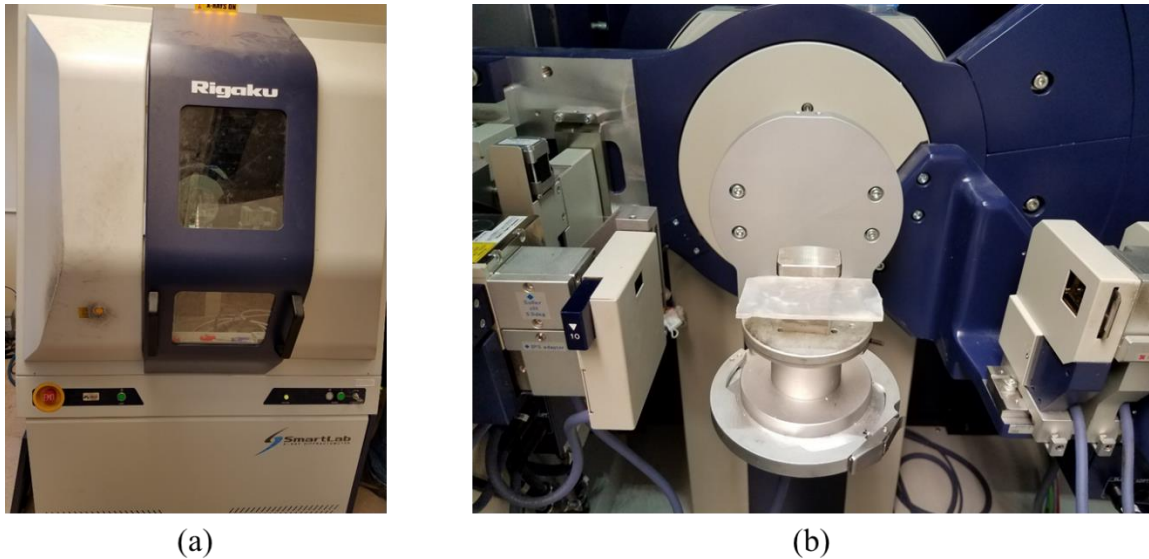
Figure 3.49: (a) Rigaku SmartLab XRD machine and (b) MMA sample on XRD sample holder.

Polymers with semi-crystalline microstructure are well known to have higher plastic deformation than aligned cross-linked polymers (Parks and Ahzi 1989, Bartczak, Cohen, and Argon 1992, G'sell and Dahoun 1994). In addition, it was also reported that the increase in degree of crystallinity in polymeric matrix would result in increase in the elastic modulus (Ferry 1980). XRD scans for both MMA and NM-MMA specimens were conducted to investigate the effect of incorporating ANPs on the degree of crystallization of MMA (Figure 3.50). It can be observed from the XRD scans that two peaks (at $2\theta$ of 24° and 68°) were detected in the NM-MMA spectroscopy that are not observable in the neat MMA profile. These peaks can be associated to 3-Methyl-1,5-diphenyl-4,5,9, 13b-tetrahydro, which is considered a crystallized organic structure. The new peaks can be associated with the increase in the degree of polymer crystallization (Bai et al. 1998). This explains the significant increase in the failure displacement/ductility and the decrease in creep compliance in the case of NM-MMA seal repair material compared with standard MMA.
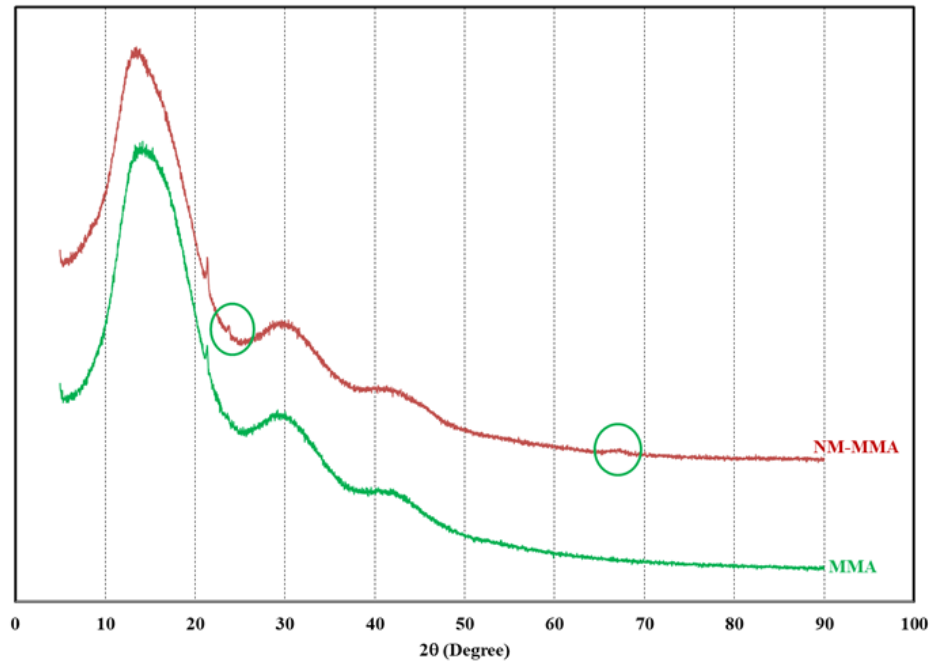
Figure 3.50: XRD scans for both MMA and NM-MMA specimens.

## 3.5  Phase IV: Seal performance investigation

The performance of seal repair material was defined in this research by the efficiency of seal repair material in sealing microannuli and its ability to withstand harsh environmental conditions. The efficiency of seal repair material was investigated using integrated seal testing specifically developed to test seal performance. On the other hand, durability test was used to investigate seal repair material's ability to withstand harsh environmental condition. Based on the results from Phase I, II, and II, MMA and Novolac epoxy PNCs incorporating 0% and 0.5% ANPs were selected for the final phase of this research.

### 3.5.1  Integrated seal testing

The efficiency of seal repair material to seal microannuli was defined by the percentage reduction in gas permeability at the cement-steel interface. The gas permeability was calculated using equation 3.11 based on Darcy's law following Gatlin (1960) and based on the assumption of linear (viscous) flow.

$$k = \frac{2Q\mu LP_{sc}}{A(P_1^2 - P_2^2)} \dots\dots\dots\dots\dots\dots\dots\dots\dots\dots\dots\dots\dots\dots\dots\dots\dots\dots\dots\dots\dots(3.11)$$

Where, $k$ is the gas permeability [m$^2$], $Q$ is the volumetric gas flow rate [m$^3$/s], $\mu$ is the viscosity of the gas [kg/m.s], $L$ is the length of the gas flow path [m]. $P_{sc}$ is the midpoint pressure value between upstream and downstream pressures [Pa], $A$ is the cross-sectional area of the flow [m$^2$], $P_1$ is the upstream pressure [Pa], and $P_2$ is the downstream pressure [Pa]. In case of non-linear flow, Forchheimer equation expressed by equation 3.12 which accounts for the flow non-linearity can be used (Forchheimer 1901).

$$-\nabla P = \frac{\mu}{kA}Q + \frac{\beta\rho}{A^2}Q^2 \quad \text{..............................................................(3.12)}$$

Where, ∇P is the pressure gradient [Pa/m], β is the inertial coefficient [m$^{-1}$] and ρ is the gas density [kg/m$^3$]. Equation 3.8 can be re-written as presented in equation 3.13 (Zeng and Grigg 2006).

$$\frac{MA(P_1^2 - P_2^2)}{2zRT\mu L\rho Q} = \frac{1}{k} + \beta\frac{Q\rho}{\mu A} \quad \text{.......................................................(3.13)}$$

Where *M* is the gas molecular weight [kg/mol], *z* is the gas compressibility factor (the value can be approximated to 1 (Davis 1992)), *R* the universal gas constant [8.314 kg.m$^2$/s$^2$.K.mol], and *T* is the gas temperature [K]. This equation is written in the form of strain line where 1/k is the intercept with y axis and β is the slope. Previous studies showed that Forchheimer equation can be used to calculate the permeability through fractures (Nowamooz, Radilla, and Fourar 2009, Zhang and Nemcik 2013, Javadi et al. 2014, Stormont et al. 2018)

As it is shown in equations 3.11, 3.12, and 3.13, calculating the permeability requires measuring the volumetric gas flow rate at the cement-steel interface. In the case of relatively large flow rate, flowmeters with reading ranges from 5 to 150 standard cm$^3$/min. For smaller ranges, soap bubble flow meter or pressure drop-off method was used to calculate the volumetric gas flow rate as presented in equation 3.14 (Jannot and Lasseux 2012).

$$Q = \frac{dP}{dt}\frac{V}{P_{avr}} \quad \text{.........................................................................(3.14)}$$

Where $Q$ is the gas volumetric flow rate [m³/s], $\frac{dP}{dt}$ is rate of change in pressure with time [Pa/s], $V$ is the volume of the upstream gas reservoir [m³], and $P_{avr}$ is average upstream gas pressure in the considered segment [Pa]. Once the gas permeability is measured, the hydraulic aperture can be estimated using the cubic law (equation 3.15) assuming that the gas flows only through the microannulus at cement-steel interface (Stormont et al. 2018).

$$h^3 = \frac{12kA}{w} \dotfill (3.15)$$

Where $h$ is the hydraulic aperture [m] and $w$ is the length of the microannulus [m]. To investigate the efficiency of seal repair materials to seal microannulus cracks, sealed & unsealed test specimens were prepared and tested in two stages. Stage 1, where cement-steel interface was characterized and stage 2, where the sealed interface was tested under casing pressure cycles.

### 3.5.1.1 Sample preparation

The specimen was made of 2.35 mm thick steel casing with an outer diameter of 60 mm confined with 20 mm thick cement sheath to simulate the cement-steel interface of the wellbores. Integrated seal test specimen in shown in Figure 3.51. The cement was mixed following the mixing method in ASTM C305 (ASTM 2014a) with mixing proportions as presented in Table 3.6. While a typical water/binder ratio in wellbore cementing is 0.45 (API 2009), a water/binder ratio of 0.3 was selected for this research to achieve higher cement strength than typical. The high strength was needed so that any flaws/cracks generated would be at the cement-steel interface and not in the cement sheath itself. This would allow the microannulus to govern gas permeability of the system rather cement

sheath cracks/porosity. The specimens were then cured for 7 days at 50 °C and 100% humidity.

Table 3.6: Mixing proportions of cement sheath [kg/m$^3$].

| Cement (Type G) | 1290 |
|---|---|
| Silica Fume | 129 |
| Water | 430 |
| Superplasticizer | 8.6 |
| Water/binder ratio | 0.3 |
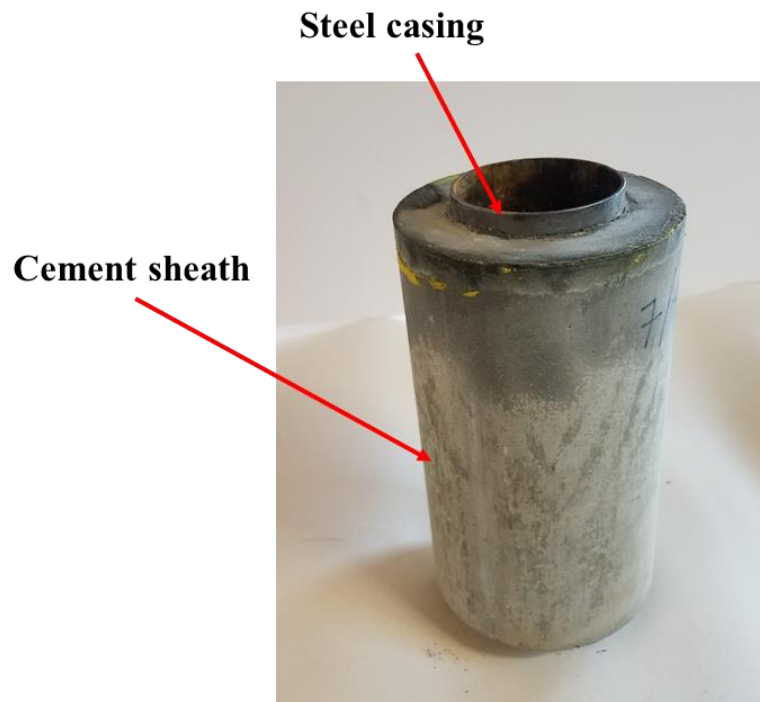


Figure 3.51: Integrated seal test specimen.

To create microannulus cracks, the steel casing was debonded from the cement sheath using dry ice as shown in Figure 3.52. Afterwards, the seal repair material was injected into the microannulus at the cement-steel interface. This process was conducted by introducing the seal repair material at one end of the integrated test specimen. Vacuum pressure was then applied at the other end of specimen until the seal repair material was observed at the other end of the specimen. The setup used for the injection of seal repair

material and schematic of sealed specimen are shown in Figure 3.53 and Figure 3.54 respectively.



Figure 3.52: Debonding steel casing from the cement sheath using dry ice.
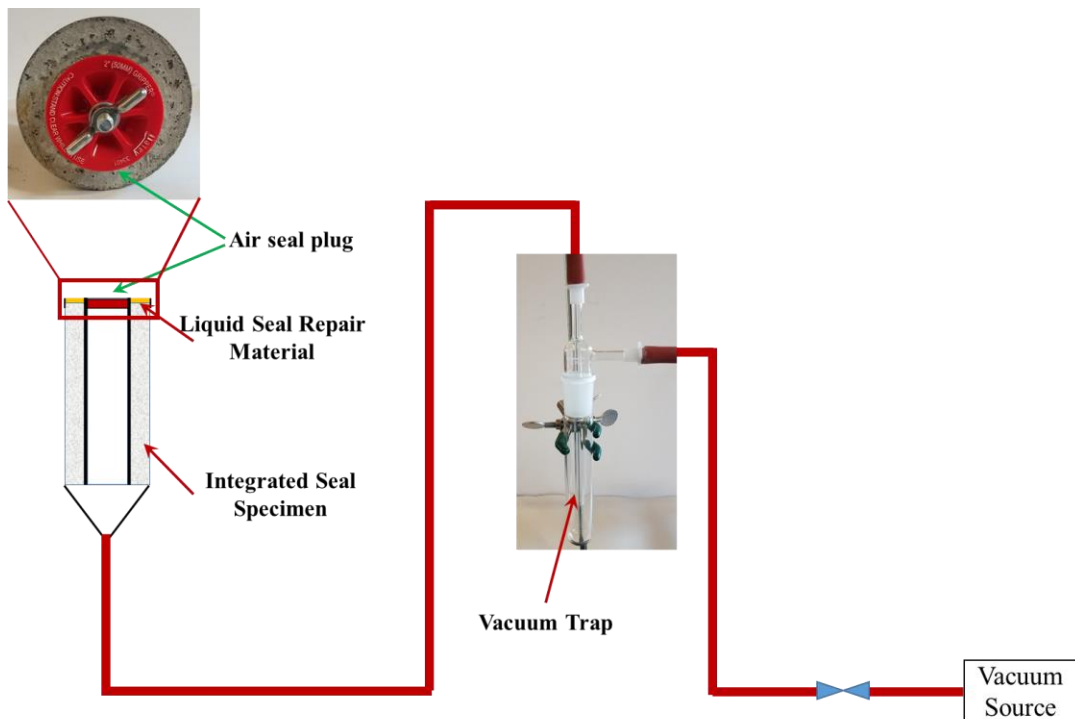


Figure 3.53: Schematic of seal repair material injection setup.
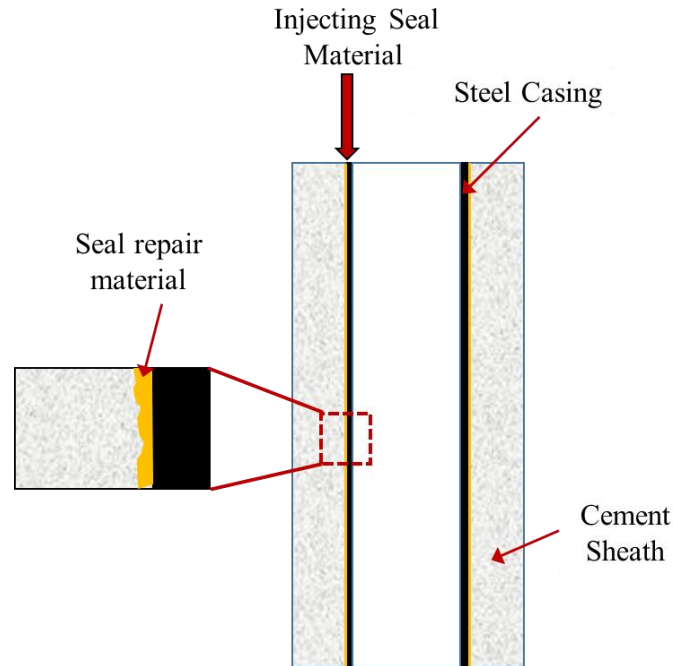
Figure 3.54: Schematic of integrated seal test specimen.

### 3.5.1.2  Cement-steel interface characterization

The efficiency of seal repair material to seal microannuli at the cement sheath-steel interface was investigated by measuring the permeability of the cement-steel interface for an integrated seal specimen at the intact, debonded, and sealed stages for each seal repair material. The gas flow rate through the interface was measured using pressure drop-off method. First, a 786 cm$^3$ pressure reservoir was subjected to vacuum until the pressure stabilized in the system. Afterwards, the vacuum source was closed and the specimen was subjected to the vacuum pressure. Meanwhile, the steel casing was sealed using a tube plug to allow the air to only flow through the cement-steel interface (gas flow though the cement sheath was neglected due to its low permeability (Hamami, Turcry, and Aït-Mokhtar 2012, Powers and Brownyard 1946)). The change of pressure with time was recorded using DAQ system with sampling rate of 10 Hz. Figure 3.55 shows a schematic of the cement-steel interface characterization setup. Once the flow rate was obtained, the permeability of the

78

cement-steel interface was calculated using Forchheimer equation. Finally, the efficiency

of seal repair material was calculated using Equation 3.16.
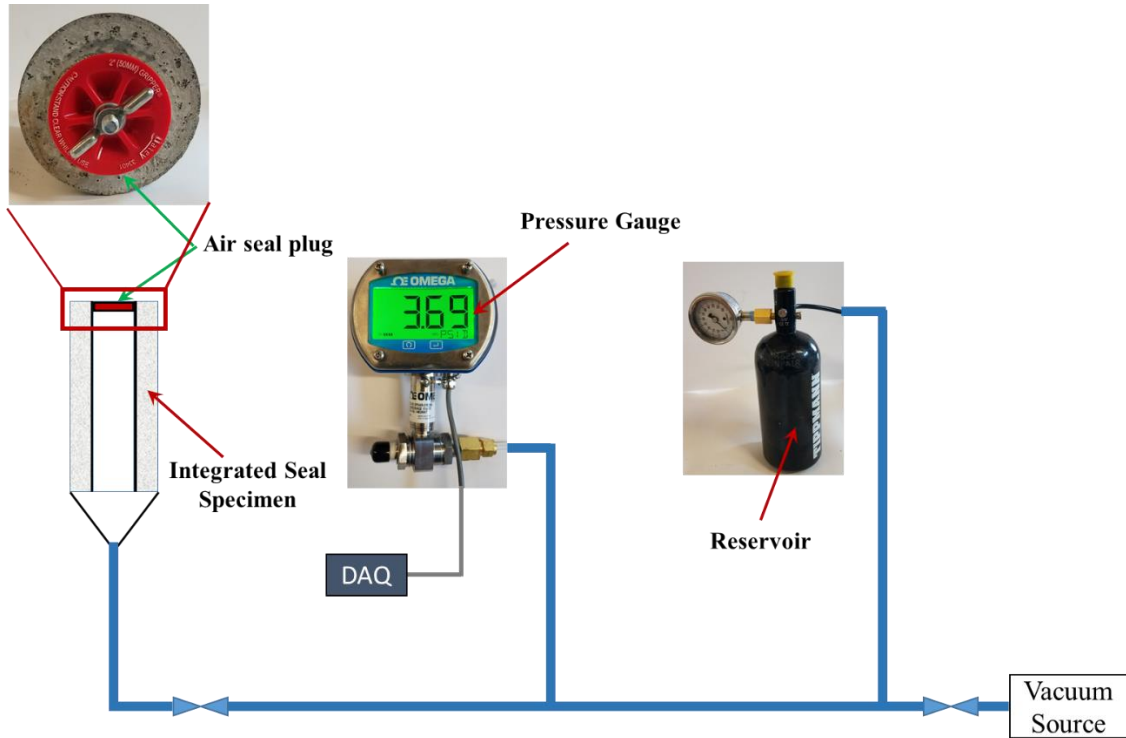


Figure 3.55: Schematic of the cement-steel interface characterization setup.

$$E = \frac{\log K_d - \log K_r}{\log K_d - \log K_i}\%\text{.......................................................................................................}(3.16)$$

Where, $E$ is efficiency of seal repair material [%], $K_r$ is the permeability of

specimen (sealed) [m²], $K_d$ is the permeability of specimen (debonded) [m²], and $K_i$ is the

permeability of intact reference specimen [m²].

The permeability and the hydraulic aperture of debonded and sealed integrated seal

specimens for each seal repair material in addition to the permeability and the hydraulic

aperture of the reference intact specimen are presented in Table 3.7 and Table 3.8

respectively. The relatively high values of permeability of reference intact specimen and

seal samples can be due to leaks in the characterization setup. However, the setup was used

for the characterization measurements of all samples. Thus, the efficiency calculations and comparisons would be valid.

The seal efficiency of investigated seal repair materials is shown in Figure 3.56. The results show that the efficiency of microfine cement efficiency was limited to 24%. Despite the fact that Novolac epoxy PNCs partially penetrated the microannulus at the cement-steel interface, PNCs seal efficiency of 91% and 79% were observed for neat Novolac epoxy and Nano modified Novolac epoxy with 0.5% ANPs (NM-Novolac) respectively. This relatively high efficiency can be explained by the fact that even with partial penetration, Novolac epoxy PNCs were able to seal the microannuli and reduce the gas permeability. The reduction in seal efficiency of Novolac epoxy to that with ANPs attributed to the fact that incorporating ANPs increases epoxy viscosity which reduces the ability of PNCs to penetrate microannuli. On the other hand, MMA and NM-MMA were able to demonstrate seal efficiency of 97% and 103% respectively. These results show that MMA and NM-MMA were able to completely penetrate and fill the microannuli at the cement sheath-steel interface and block gas permeation. This resulted in measured permeability values even lower than the permeability of the reference intact specimen. Moreover, it was observed that incorporating ANPs resulted in reduction in the seal efficiency of Novolac epoxy while it did not have the same effect on MMA. This can be explained by the fact that incorporating ANPs in MMA had a negligible effect on the viscosity and surface tension of MMA.

Table 3.7: Permeability of intact, debonded, and sealed integrated seal specimens [$m^2$].

| Seal Repair Material | Reference Intact Specimen | Debonded Specimen | Sealed Specimen |
|---|---|---|---|
| Microfine Cement | | $2.33\times10^{-14}$ | $72\times10^{-16}$ |
| Novolac | | $2.29\times10^{-14}$ | $2.86\times10^{-16}$ |
| NM-Novolac | $1.84\times10^{-16}$ | $1.13\times10^{-14}$ | $4.29\times10^{-16}$ |
| MMA | | $0.48\times10^{-14}$ | $2.14\times10^{-16}$ |
| NM-MMA | | $1.48\times10^{-14}$ | $1.62\times10^{-16}$ |

Table 3.8: Hydraulic aperture of intact, debonded, and sealed integrated seal specimens [μm].

| Seal Repair Material | Reference Intact Specimen | Debonded Specimen | Sealed Specimen |
|---|---|---|---|
| Microfine Cement | | 18.7 | 12.6 |
| Novolac | | 18.6 | 4.3 |
| NM-Novolac | 3.7 | 14.7 | 4.9 |
| MMA | | 11.1 | 3.9 |
| NM-MMA | | 16.1 | 3.6 |
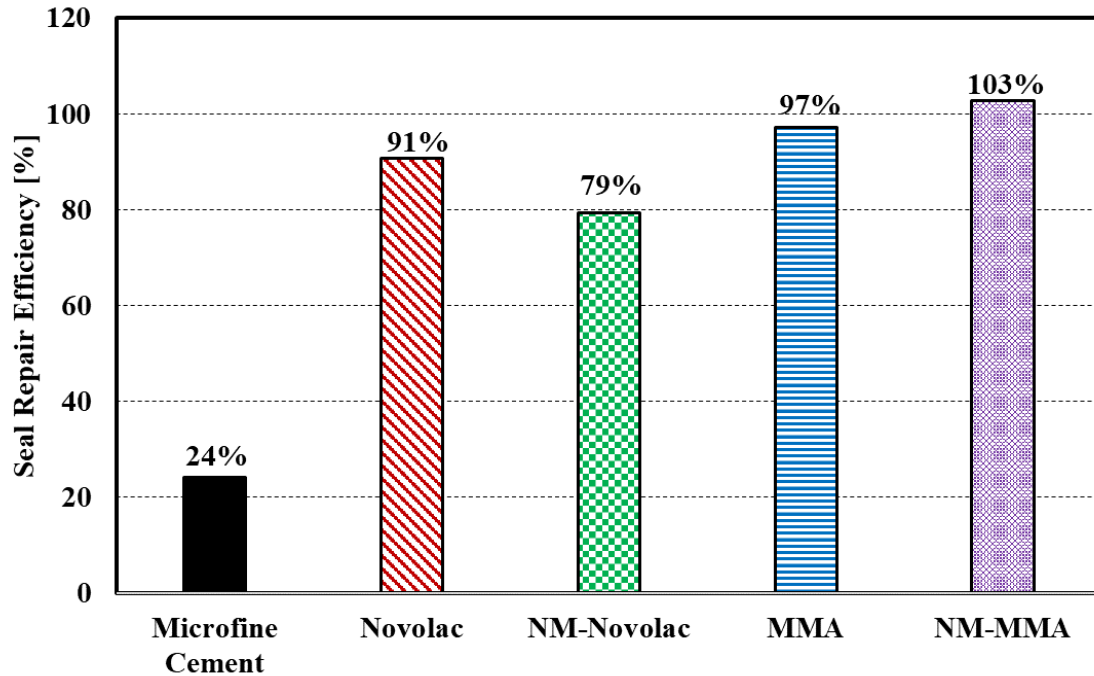
Figure 3.56: Seal efficiency of different seal repair materials used for restoring wellbore seal integrity.

### 3.5.1.3 Casing pressure cycles

To investigate the performance of seal repair material under cyclic pressure, pressure vessel setup which is capable of applying up to 35 MPa and 25 MPa confining and casing pressure respectively was used. Constant confining pressure and cycles of casing pressure were applied. Meanwhile, inert gas (Nitrogen) was allowed to flow at the cement-steel interface. The flow rate was measured and gas permeability was calculated. In this investigation, confining pressure of 0.34 MPa (50 psi) was applied to ensure that there is no flow bypass between the specimens and the pressure vessel's bladder. Cycles of casing pressure ranging from 0.7 to 10.3 MPa (100 to 1500 psi) were then applied. The change of microannulus permeability versus the number of pressure cycles was recorded until loss of integrity was observed. Figure 3.57 shows the pressure vessel setup.
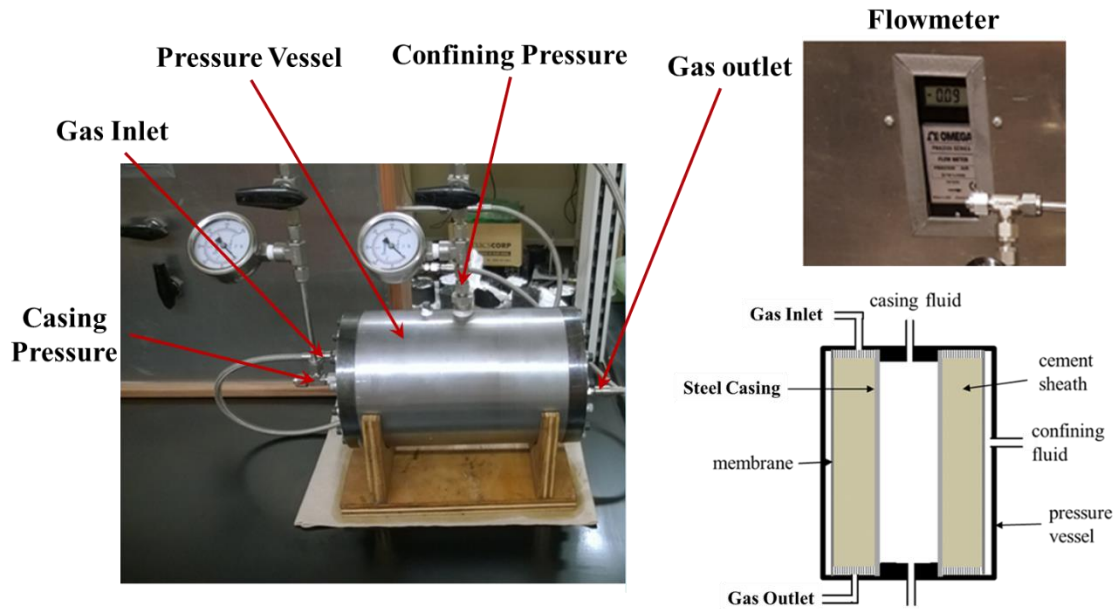
Figure 3.57: Integrated seal test setup.

The number of casing pressure cycles applied until loss of seal integrity of sealed specimens is presented in Figure 3.58. Seal integrity was considered to fail when the seal efficiency of integrated seal specimens dropped to 50% of its initial value. Experimental observations show that the number of cycles to seal integrity loss of specimens sealed with NM-MMA was two order of magnitude higher than the specimens sealed with microfine cement respectively. The very poor efficiency of microfine cement in sealing microannulus and its inability to withstand any cycles of stress surprising given the fact it is the standard seal repair material used by the industry. It was also found that the failure of the seal integrity of specimen sealed MMA and NM-MMA were due to crack of cement sheath and not due to failure of the seal repair material as shown in Figure 3.59 and Figure 3.60. Although in both MMA and NM-MMA sealed specimens' loss of seal integrity was due to cracks in the cement sheath, it was found that there is 45% increase of number of cycles associated with incorporating ANPs in MMA. This significant improvement can be explained by the ability of MMA based materials to impregnate the cement sheath-steel

interface as well as the cement sheath in the vicinity of the interface. The higher ductility of NM-MMA compared to MMA improved the energy dissipation of cement sheath. This conclusion is supported by an observation that post cyclic tests, one single crack in the specimen sealed with MMA was observed compared with the two cracks in the specimen sealed with NM-MMA as shown in Figure 3.59 and Figure 3.60.
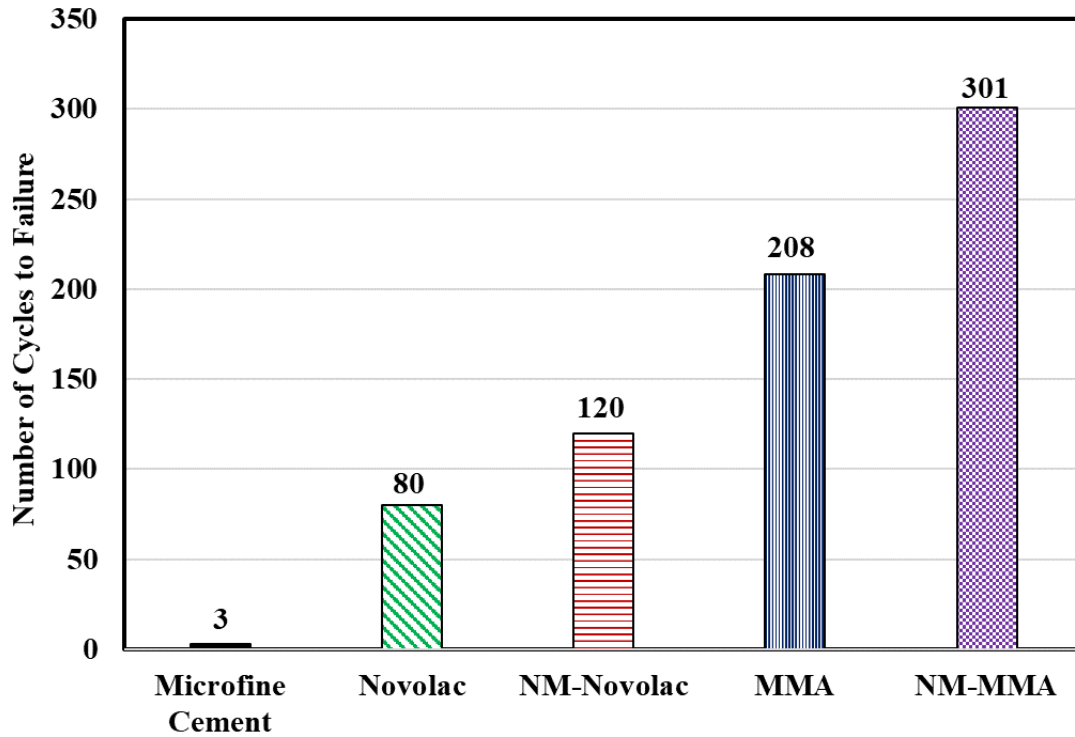


Figure 3.58: Number of casing pressure cycles applied until failure of seal integrity of sealed specimens.

Figure 3.59: Post cyclic test integrated seal specimen sealed with MMA showing a single longitudinal crack in the cement sheath.



Figure 3.60: Post cyclic test integrated seal specimen sealed with NM-MMA showing two longitudinal cracks in the cement sheath.

The change of seal efficiency of seal repair materials with the number of casing pressure cycles is presented in Figure 3.61. It was found that microfine cement was able to only hold one casing pressure cycle after which its efficiency dropped from 24% to 12% in only 2 cycles. Novolac epoxy and NM-Novolac epoxy were able to withstand 10 cycles

before any significant loss of efficiency was observed. After the first 10 cycles, Novolac epoxy's efficiency rapidly drop from 90% to 80%. Afterwards, the efficiency was found to be stable for 30 cycles. Novolac seal efficiency then dropped rapidly. On the other hand, NM-Novolac epoxy did not follow the same 3-staged cycles-efficiency curves as observed in neat Novolac epoxy. NM-Novolac epoxy showed gradual reduction in efficiency with increased number of casing pressure cycles. The behavior of integrated seal test specimen sealed with NM-Novolac epoxy did not have the steady state stage where the seal efficiency was constant with increased number of casing pressure cycles that was observed with neat Novolac epoxy. The gradual loss of seal efficiency of NM-Novolac epoxy compared with neat Novolac can be explained by the relatively higher bond strength of NM-Novolac epoxy to steel compared with neat Novolac epoxy (Genedy et al. 2014). The absence of the steady state stage of the cycles-efficiency curve was due to the increase in the viscosity associated with incorporating ANPs in Novolac epoxy. This increase in viscosity limited the penetration depth of NM-Novolac epoxy. This hypothesis can also be supported by the increase of efficiency observed at 90 cycles. This increase did not hold and the drop of efficiency immediately continued afterwards.
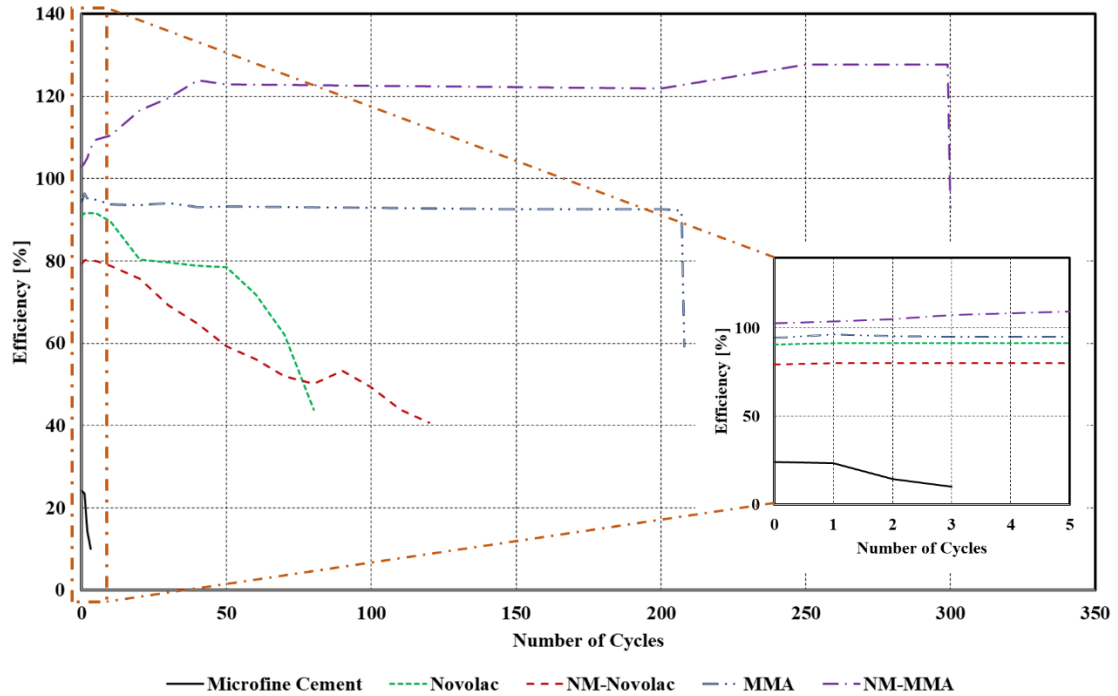
Figure 3.61: Change of seal efficiency of seal repair materials with number of casing pressure cycles.

For MMA, no significant loss of seal efficiency was observed until cracking of the cement sheath occurred at 208 cycles. Moreover, NM-MMA showed significant increase in seal efficiency with cycles of casing pressure reaching 301 cycles. This increase of efficiency was due to the improved ductility resulted from incorporating ANPs in MMA PNCs. With increasing the casing pressure, the steel casing applied pressure on the seal repair material at the cement-steel interface forcing it to fill open microannuli and reduce the permeability of the interface. When the pressure is released, ductile seal repair material such as MMA would return to its original state with almost no change of permeability while brittle materials such as microfine cement would fail under such extreme deformations. On the other hand, Improvement in seal efficiency of specimen sealed with NM-MMA due to applying casing pressure can be explained in Figure 3.62. Prior to applying casing pressure, some gaps at the cement sheath surface could remain unfilled after injecting NM-MMA

seal repair materials as shown in Figure 3.62(a). Applying casing pressure would allow steel casing to expand forcing NM-MMA seal repair material against the surface of the cement sheath and close unfilled gaps as shown in Figure 3.62(b). Once the casing pressure is released, NM-MMA seal repair material would expand and retain its the new shape (Figure 3.62(c)) due to its significant high ductility resulting in improved in seal efficiency despite the increase in casing pressure cycles. It can be concluded from performance investigation that NM-MMA is the most suitable seal repair material to restore wellbore seal integrity.
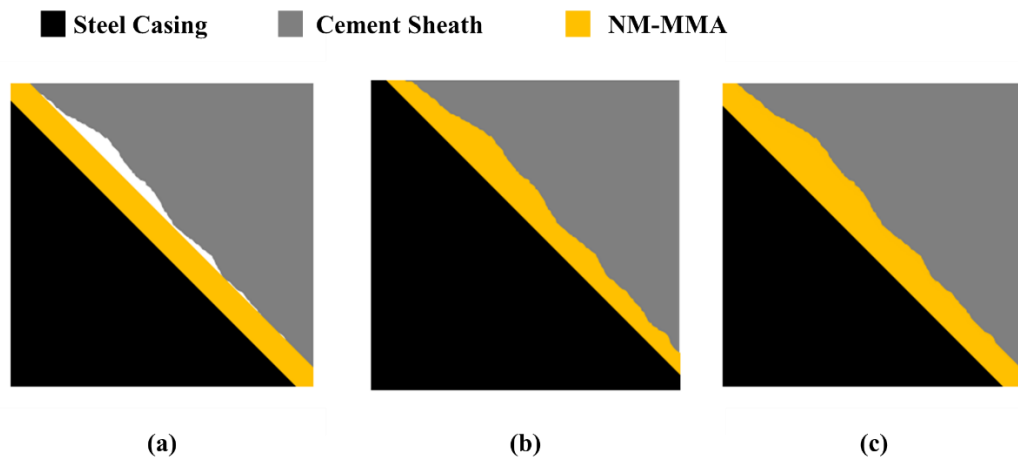


Figure 3.62: Effect of casing pressure cycles on cement-steel interface sealed with NM-MMA: (a) Prior to applying casing pressure, (b) Maximum casing pressure applied, and (c) Casing pressure released.

### 3.5.2 Durability study

The wellbore environment is very aggressive due to the existence of carbonated water, saline, and other chemicals in addition to the high pressure and elevated temperature (Kutchko et al. 2007, Duguid and Scherer 2010, Huet, Prevost, and Scherer 2010, Zhang and Bachu 2011, Matteo et al. 2018). The resistance of polymer nanocomposites to wellbore environmental condition was investigated. The durability of seal repair material

was investigated using weight loss test. For durability study tests, samples of the seal repair materials were exposed to the following environmental conditions:

1- Air

2- Deionized Water

3- Carbonated Brine

4- Crude Oil

5- High temperature and pressure

The exposure to water, carbonated brine, and crude oil was conducted by immersion test following ASTM D543-14 (ASTM 2014c). Polymer nanocomposites and microfine cement specimens as shown in Figure 3.63 was immersed in the chemicals listed above. Carbonated brine used in the investigation was designed after the flow back brine from Marcellus gas wells in Pennsylvania, USA (Haluszczak, Rose, and Kump 2013). Exposure to high temperature and pressure was conducted using reactor setup shown in Figure 3.64. The temperature in the reactor was maintained at 80° C and Nitrogen gas was injected into the reactor and pressure was maintained at 10.3 MPa (1500 psi) for 7 days.



(a)                                      (b)
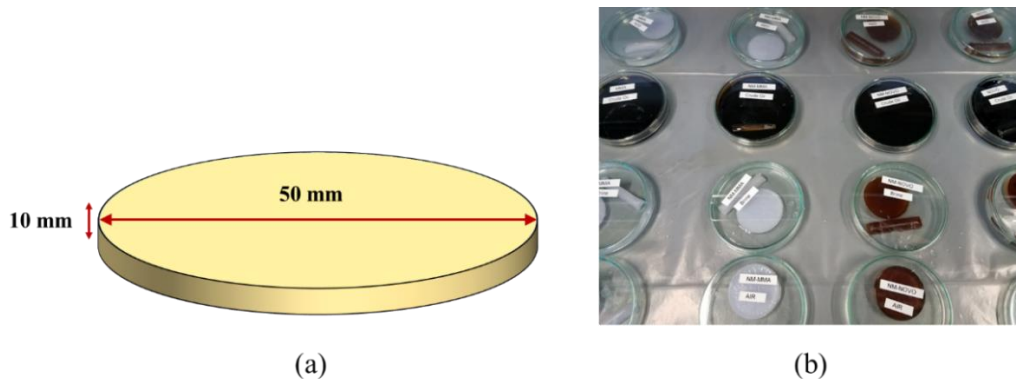
Figure 3.63: Weight loss test (a) Specimen dimensions and (b) specimens in different chemicals.
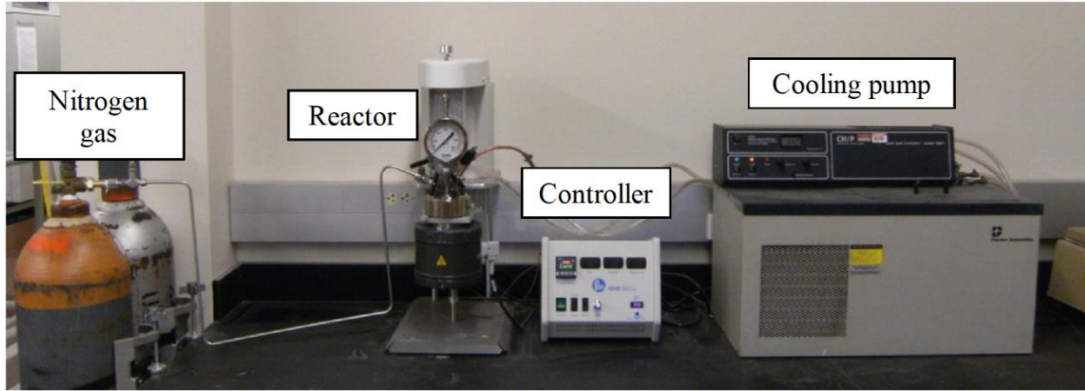
Figure 3.64: High temperature and pressure reactor setup.

Selected polymer nanocomposites were tested for weight loss after subjected to harsh environmental condition based on ASTM D543-14 and ASTM C771-14 (ASTM 2014b, c). The percentage of weight loss of each polymer nanocomposite exposed to each environmental condition was calculated using equation 3.17.

$$WL = \frac{W_f - W_i}{W_i} \dots\dots\dots\dots\dots\dots\dots\dots\dots\dots\dots\dots\dots\dots\dots\dots\dots\dots\dots\dots\dots\dots(3.17)$$

Where $WL$ is the weight loss, $W_i$ is the initial weight before exposure, and $W_f$ is the weight after exposure. To measure the weight after exposure, the polymer nanocomposite (or microfine cement) specimens was taken out of the chemical, washed with DI water, dried with clean cloth, then immediately weighted to the nearest 0.01 gm. The results of the weight loss study are presented in Table 3.9.

Table 3.9: Weight loss results for selected seal repair materials and microfine cement [%].

|  | Air | DI Water | Carbonated Brine | Crude Oil | High Temperature and Pressure |
|---|---|---|---|---|---|
| Microfine Cement | 4.95% | 2.32% | 8.24% | 13.3% | 18.94% |
| Novolac epoxy | 0.00% | -2.20% | -0.25% | 0.00% | -1.61% |
| NM-Novolac epoxy | 0.00% | -0.35% | -0.24% | -0.03% | -1.96% |
| MMA | 1.15% | 1.01% | 1.50% | 1.37% | 1.51% |
| NM-MMA | 0.33% | 0.43% | 0.81% | 0.43% | 0.99% |

The durability study showed that chemical exposure has no weight loss effect on Novolac epoxy PNCs. Moreover, microfine cement showed weight losses ranges between 5% up to 19%. This very high weight loss percentages were due to the fact that exposure to harsh environmental conditions resulted in significant cracking of microfine cement specimens that allowed small fractions to fall apart as shown in figure 3.65. On other hand, the weight loss of neat MMA PNCs was found to be in the range between 1% and 1.5%. However, incorporating ANPs in MMA was able to significantly improve the durability of MMA PNCs. Although the results showed that harsh wellbore's environmental conditions have higher effect on MMA based PNCs than on Novolac epoxy based PNCs, that effect of wellbore environment on MMA based PNCs was still significantly lower than the effect on microfine cement.
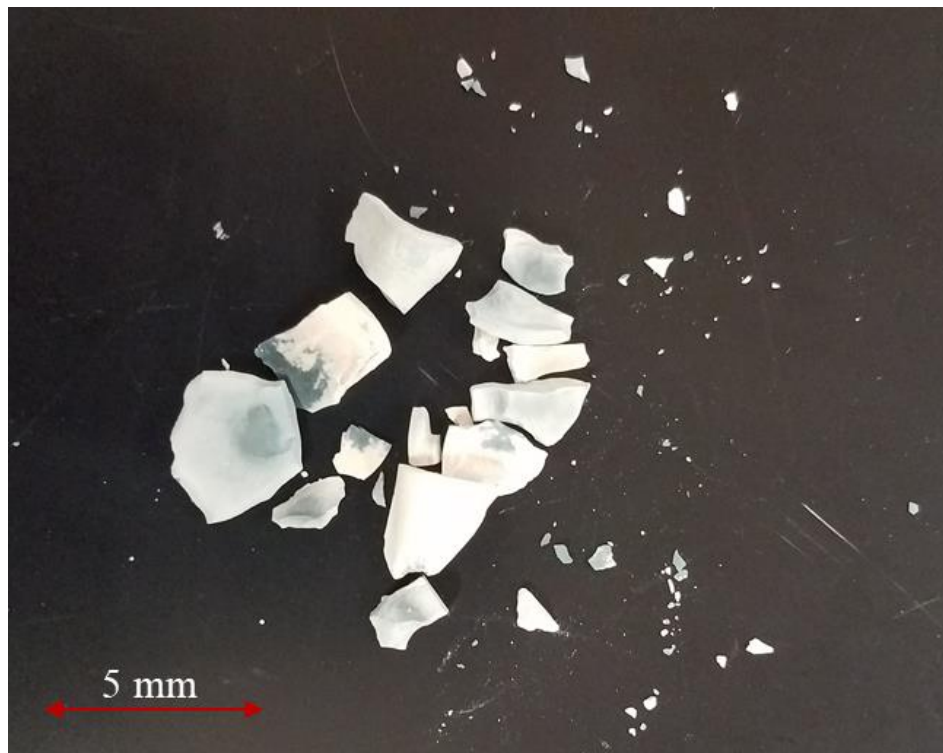


Figure 3.65: Microfine cement fractions falling apart due to harsh environmental conditions.

# Chapter 4. Conclusions

In this dissertation, a new seal repair material to restore wellbore seal integrity was developed. An efficient seal repair material should have good bond strength with both steel and rock formations. In addition, seal repair material should be able to fill thin microcracks at both the interfaces (microannuli) and withstand harsh wellbore environmental conditions. This investigation was conducted in four consecutive phases: Phase (I) Cement-steel interface, Phase (II) Cement-rock formation interface, Phase (III) Penetrability of seal repair material, and Phase (IV) Investigating performance of sealed interfaces in realistic wellbore conditions. In this chapter, the conclusions of this investigation are presented then followed by the recommendations and suggestions for future work.

## 4.1   Conclusions

The flowability and bond strength of 19 polymer cement nanocomposites (PCNCs) with steel surfaces were investigated. First, 7 Polysulfide Siloxane epoxy based PCNCs and 7 Novolac epoxy based the PCNCs were examined. While incorporating nanoparticles resulted in reduction of flowability of PCNCs, it was observed that the nanoparticles effect on Polysulfide Siloxane epoxy PCNCs was much higher than their effect on Novolac epoxy PCNCs flowability. It was also observed that all Novolac epoxy PCNCs have higher flowability than microfine cement while all Polysulfide Siloxane epoxy PCNCs have lower flowability than microfine cement. It became apparent that Polysulfide Siloxane epoxy might not be a suitable seal repair material for wellbores.

Moreover, COOH functionalized MWCNTs were able to improve the bond strength of Polysulfide Siloxane epoxy with 49% over standard microfine cement. Other

nanoparticles such as silica and alumina based nanoparticles showed an adverse effect on bond of Polysulfide Siloxane epoxy. On the other hand, COOH functionalized MWCNTs showed an insignificant improvement of Novolac epoxy bond strength to steel surfaces. However, incorporating silica and alumina based nanomaterials made significant improvement in bond strength in Novolac epoxy. Incorporating 2.0 wt.% aluminum nanoparticles (ANPs) in Novolac epoxy PCNC showed the highest bond strength with steel surfaces (200% compared with microfine cement) and it had a very low effect on PCNC flowability (only 8% lower than neat Novolac epoxy PCNC). Thus, an extended investigation of Novolac epoxy PCNCs incorporating 0.5% to 4.0% ANPs was conducted.

The extended investigation on incorporating ANPs in Novolac epoxy showed that 2.0 wt.% resulted in the highest improvement in bond strength with steel surfaces. The extended investigation also showed relatively high variability in the bond strength. This variability was observed also with 3.0% and 4.0% ANPs. Moreover, it was observed that there was no significant improvement in the bond strength with incorporating 1.5% ANPs when compared to 1.0% ANPs. On the other hand, incorporating 0.5% and 1.0% ANPs in Novolac epoxy showed 20% and 23% increase in the bond strength, respectively, in addition to only 6.0% reduction in flowability. It can be concluded that Novolac epoxy incorporating up to 1.0 wt.% ANPs results in the best seal performance considering both flowability and bond strength. It was decided to only consider Novolac epoxy in Phase II of the investigation.

In Phase II, viscosity measurements were obtained to investigate the feasibility of using Novolac epoxy PNCs as seal repair material. Moreover, push-out tests were conducted to examine the bond strength of the cement paste-shale interface sealed with

microfine cement and Novolac epoxy PNCs incorporation 0% (Neat), 0.25%, 0.5%, and1.0% ANPs. The bond strengths were compared with a reference case where Type G cement paste was cast directly around the shale core. Microstructural investigations were also conducted to understand the behavior at the interface using microscopic images, FTIR and DMA.

Viscosity tests showed that all Novolac epoxy PNCs incorporating ANPs have viscosities that are comparable to that of microfine cement, which might enable using PNCs incorporating ANPs as seal repair material for microannulus cracks. Push-out test showed that microfine cement has a bond strength that is 21% lower than the reference case. In contrast, Novolac epoxy PNCs incorporating ANPs showed bond strength up to 250% higher than the reference case. Microscopic investigation of the shale-cement interface showed that microfine cement was unable to completely fill the 800 μm gap, and microcracks along the interface with widths up to 40 μm remained open and unsealed. However, no gap was observed with ANPs-epoxy nanocomposites. In addition, the displacement at peak load and the toughness of PNCs were up to 545% and 761% higher than the displacement at peak load and toughness of microfine cement respectively.

Furthermore, FTIR and DMA measurements showed that incorporating ANPs in Novolac epoxy PNCs were able to interrupt the epoxy crosslinking process of PNCs and reduce the crosslinking density. This process allows free epoxy groups and improves the bond strength with shale surfaces. Moreover, DMA crosslinking measurements showed that 0.5% ANPs was enough to complete the chemical reaction and interrupt the crosslinking process, the rest of the alumina nanoparticles worked as particular reinforcement in the epoxy matrix. Due to the small particle size (50 nm) and the relatively

94

low content for reinforcement, only limited improvement of ANPs as reinforcement was observed. Thus, it can be concluded that the optimum ANPs content to achieve the highest effective improvement to cost ratio is 0.5% of the polymer weight.

In Phase III, the ability of MMA and NM-MMA incorporating ANPs in addition to Neat Novolac epoxy PNCs to penetrate thin microannuli (below 30 μm) was investigated. MMA and NM-MMA were included in this investigation due to their superior flowability and potential to fill very thin microcracks compared with Novolac epoxy and microfine cement. A penetrability study based on surface tension and contact angle measurement of seal repair materials with cement paste surface was performed. The investigation indicated that MMA and NM-MMA have the ability to penetrate smaller microannuli than Novolac epoxy and microfine cement under similar conditions. Microscopic investigation of the shale-cement interface was used to scrutinize the hypothesis. Microscopic investigation showed that microfine cement did not flow through 30 μm microcracks and it has a very limited penetration depth. Moreover, Novolac epoxy was also unable to completely fill the microcrack between the shale and the cement sheath. In contrast, MMA-based seal repair materials were able to completely fill the wellbore microcracks.

Moreover, MMA based PNCs showed improved bond strength (1061% higher than microfine cement), excellent ductility (468% higher displacement at failure than microfine cement), and superior toughness (8135% higher than microfine cement). The improved mechanical properties of NM-MMA showed that it would have superior performance as a seal repair material compared with microfine cement currently used as the standard material for microannuli seal. It was found that incorporating 0.5% ANPs by weight in MMA was able to increase the displacement at failure (ductility) and toughness

95

by 122% and 201% respectively. Viscoelastic investigation using DMA showed that incorporating ANPs in MMA matrix reduced creep compliance of NM-MMA by 17% and improved creep recovery by 7.3%. XRD analysis showed that incorporating ANPs in MMA increased the degree of polymer crystallization of MMA enabling significant increase in polymer ductility and toughness and a reduction of polymer creep compliance.

In Phase IV, we examined the integrated performance of selected seal repair materials. The performance of seal repair materials was evaluated based on their efficiency to seal cement-steel interface, the ability to withstand cyclic casing pressure, and the ability to withstand harsh environmental conditions. A seal efficiency parameter was defined and the results showed that microfine cement efficiency was limited to 24%. On the other hand, NM-MMA achieved seal efficiency as high as 103%. Moreover, NM-MMA withstood casing pressure cycles two orders of magnitude higher than microfine cement.

The durability investigation showed that microfine cement exposed to wellbore harsh environmental conditions showed weight loss ranges between 5% up to 19%. On the other hand, exposure had no weight loss effect on Novolac epoxy PNCs. Moreover, the weight loss of neat MMA PNCs was found to be in the range between 1% and 1.5%. However, incorporating ANPs in MMA significantly improved the durability of MMA PNCs. Although the results showed that harsh environmental conditions could have a higher effect on MMA based PNCs than on Novolac epoxy based PNCs, that effect on MMA based PNCs was still significantly lower than the effect on microfine cement.

In conclusion, investigations in this dissertation showed that Novolac epoxy and MMA based polymer nanocomposites have a higher bond strength and excellent performance in sealing microannuli at cement-steel and cement-shale interfaces than

microfine cement. Moreover, microstructural investigations proved that incorporating ANPs significantly improved the bond strength and ductility of Novolac epoxy and MMA polymer nanocomposites. In addition, it was found that 0.50 wt.% is the optimal content of ANPs for seal using MMA and Novolac epoxy.

## 4.2   Limitations and future work

### 4.2.1   Bond strength

Bond strength of the seal repair materials in this investigation was evaluated based on its bond with stainless steel and shale. Bond strength with other types of rock such as limestone, granite, and consolidated salt needs to be investigated. In addition, a study on the effect of a rock formation's degree of saturation on the bond strength is recommended. Moreover, the bond strength of seal repair materials with corroded steel casing is also recommended.

### 4.2.2   Chemical exposure and environmental conditions

All experimental work in this investigation was conducted at ambient conditions. Curing seal repair materials and testing under high temperature and pressure conditions would allow better understanding of the behavior of seal repair materials in realistic wellbore conditions. Furthermore, bond strength and sealing efficiency exposed to harsh environmental conditions would be beneficial for further understanding of the efficiency of proposed seal repair materials.

### 4.2.3   Integrated seal testing

For the integrated seal test, the seal repair materials were injected from one end of the test specimens. Sealing the specimens through perforations in the steel casing as shown

in Figure 4.1 would cover other seal situations. In addition, investigating the seal efficiency of seal repair materials to seal microannuli with different crack size is needed. Furthermore, evaluating the cement-steel interface using CT scan techniques is recommended. CT investigation would give in-depth understanding of the continuity of microannuli and its effect on the permeability of the interface in addition to the ability of seal repair materials to seal such very thin microannuli. In this study, the seal repair materials were injected into microannuli filled only with air. The ability of seal repair materials to replace other fluids such as water, brine, crude oil, or drilling mud (Bentonite slurry) requires further investigation.
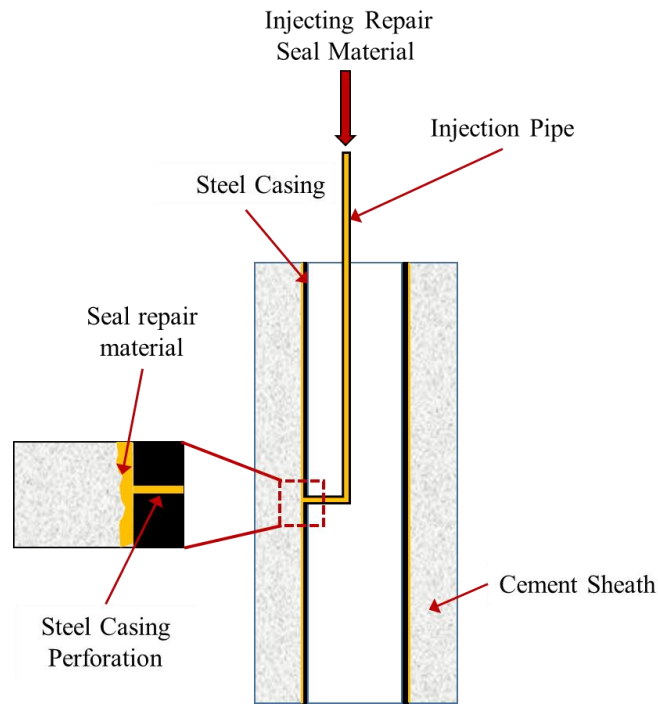


Figure 4.1: Schematic of sealing integrated seal specimen through perforation in the steel casing.

### 4.2.4 Finite Element (FE) modeling

Finite Element (FE) analysis using ABAQUS/CAE simulation environment in order to simulate push-out test with both shale and steel core is recommended for further

understanding of the bond mechanics. Such FE model can then be used to investigate the bond mechanics of the seal repair material with a shale/steel surface. Contact element can be used to define the interface between the shale/steel and cement sheath. In this element, the cohesive behavior of polymer nanocomposites following the bilinear shear stress-slip model shown in Figure 4.2 and equation (4.1) can be defined. The interface interaction parameters including mode II fracture energy ($G_{II}$), shear contact stiffness ($K_t$), and maximum displacement at failure ($\delta_{max}$) can be back solved to match the load-displacement curve generated from the FE model with the load-displacement curve obtained from the experiment. Such model would be very beneficial to simulate the effect of seal repair materials on limiting leakage in wellbores and caverns.

$$G_{II} = \frac{1}{2}\tau_{max}\delta_{max}$$ ……………………..………..………………………………….(4.1)
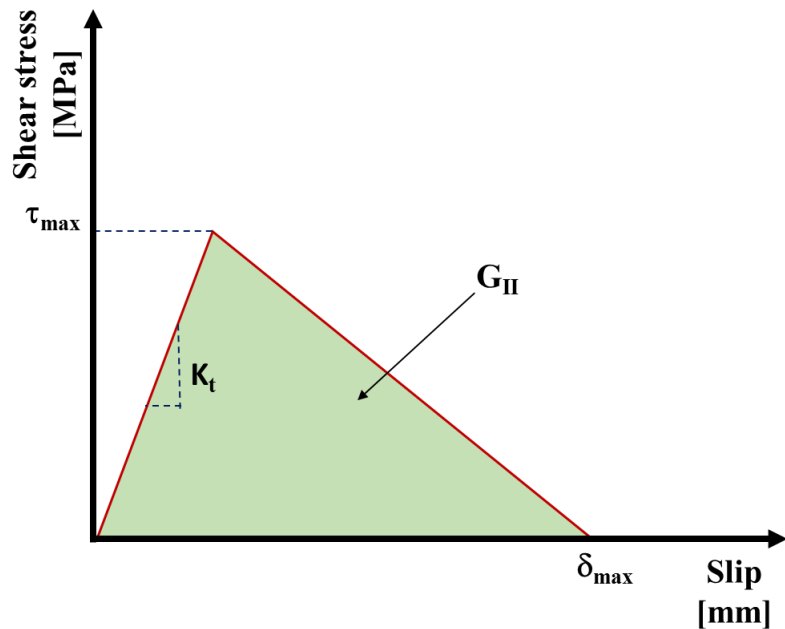


Figure 4.2: Bilinear shear stress-slip interface interaction model.

# References

AASHTO. 2010. AASHTO T316: Standard method of test for viscosity determination of asphalt binder using rotational viscometer.

Abel, M., J. F. Watts, and R. P. Digby. 2004. "The influence of process parameters on the interfacial chemistry of γ-GPS on aluminium: A review." *The Journal of Adhesion* 80 (4):291-312.

Aboubakr, S. H., U. F. Kandil, and M. Reda Taha. 2014. "Creep of epoxy–clay nanocomposite adhesive at the FRP interface: A multi-scale investigation." *International Journal of Adhesion and Adhesives* 54:1-12.

Alberty, M., and Z. Yao. 2018. "A Practical Method to Monitor Wellbore Strengthening Particle Concentration." IADC/SPE Drilling Conference and Exhibition.

Antonio, L., O. D. Barrios, and G. A. M. Rodriguez. 2007. "Swelling packer technology eliminates problems in difficult zonal isolation in tight-gas reservoir completion." Latin American & Caribbean Petroleum Engineering Conference.

API. 2009. 10A, Specification for cements and materials for well cementing. Washington DC: American Petroleum Institute Publishing Services. .

ASTM. 2005. ASTM C882/C882M: Standard test method for bond strength of epoxy-resin systems used with concrete by slant shear.

ASTM. 2007. ASTM C1437: Standard test method for flow of hydraulic cement mortar. Philadelphia, PA: ASTM International.

ASTM. 2014a. C305: Standard Practice for Mechanical Mixing of Hydraulic Cement Pastes and Mortars of Plastic Consistency. Philadelphia, PA: ASTM International.

ASTM. 2014b. C771: Standard Test Method for Weight Loss After Heat Aging of Preformed Tape Sealants. Philadelphia, PA: ASTM International

ASTM. 2014c. D543: Standard practices for evaluating the resistance of plastics to chemical reagents. Philadelphia, PA: ASTM International.

Bagal, J.h, G. Onadeko, P. Hazel, and V. Dagestad. 2016. "Annular Barrier as an Alternative to Squeezes in Challenging Wells: Technology Review and Case Histories."

Bai, S., J. Z. Hu, R. J. Pugmire, D. M. Grant, C. M. V. Taylor, J. B. Rubin, and E. J. Peterson. 1998. "Solid state NMR and wide angle X-ray diffraction studies of supercritical fluid CO2-treated poly (ethylene terephthalate)." *Macromolecules* 31 (26):9238-9246.

Bakar, M., M. Kostrzewa, B. Hausnerova, and K. Sar. 2010. "Preparation and property evaluation of nanocomposites based on polyurethane-modified epoxy/montmorillonite systems." *Advances in Polymer Technology* 29 (4):237-248.

Baldan, A. 2004. "Adhesively-bonded joints and repairs in metallic alloys, polymers and composite materials: adhesives, adhesion theories and surface pretreatment." *Journal of materials science* 39 (1):1-49.

Barlet-Gouédard, V., G. Rimmelé, B. Goffé, and O. Porcherie. 2007. "Well technologies for CO2 geological storage: CO2-resistant cement." *Oil & Gas Science and Technology-Revue de l'IFP* 62 (3):325-334.

Barlet-Gouedard, V., G. Rimmele, B. Goffe, and O. Porcherie. 2006. "Mitigation strategies for the risk of CO2 migration through wellbores." IADC/SPE drilling conference.

Bartczak, Z., R.E. Cohen, and A.S. Argon. 1992. "Evolution of the crystalline texture of high-density polyethylene during uniaxial compression." *Macromolecules* 25 (18):4692-4704.

Bellabarba, M., H. Bulte-Loyer, B.t Froelich, S. Le Roy-Delage, R. van Kuijk, S. Zeroug, D. Guillot, N. Moroni, S. Pastor, and A. Zanchi. 2008. "Ensuring zonal isolation beyond the life of the well." *Oilfield Review* 20 (1):18-31.

Benge, G. 2009. "Improving wellbore seal integrity in CO2 injection wells." SPE/IADC Drilling Conference and Exhibition.

Berry, D. H., and A. Namkanisorn. 2005. "Fracture toughness of a silane coupled polymer-metal interface: Silane concentration effects." *The Journal of Adhesion* 81 (3-4):347-370.

Blunt, M. J. 2017. *Multiphase flow in permeable media: A pore-scale perspective*: Cambridge University Press.

Browning, L. A., and J. D. Smith. 1993. "Analysis of the rate of and reasons for injection well mechanical integrity test failure." SPE/EPA Exploration and Production Environmental Conference.

Carey, B. and C. Gardner. 2012. *Wellbore Integrity Network*(No. LA-UR-12-22410). Los Alamos National Laboratory (LANL).

Carey, J. W., M. Wigand, S. J. Chipera, G. WoldeGabriel, R. Pawar, P. C. Lichtner, S. C. Wehner, M. A. Raines, and G. D. Guthrie. 2007. "Analysis and performance of oil well cement with 30 years of $CO_2$ exposure from the SACROC Unit, West Texas, USA." *International Journal of Greenhouse Gas Control* 1 (1):75-85.

Celia, M. A., S. Bachu, J. M. Nordbotten, S. E. Gasda, and H. K. Dahle. 2005. "-Quantitative estimation of $CO_2$ leakage from geological storage: Analytical models, numerical models, and data needs." In *Greenhouse Gas Control Technologies 7*, 663-671. Elsevier.

Chatterji, J., R. S. Cromwell, B. R. Reddy, and B. J. King. 2001. Resilient well cement compositions and methods. Google Patents.

Checkai, D., S. Bryant, and Q. Tao. 2013. "Towards a frequency distribution of effective permeabilities of leaky wellbores." *Energy Procedia* 37:5653-5660.

Chen, Y., K. Gao, E. S. Davis, D. N. Sinha, C. P., and L. Huang. 2018. "Full-waveform inversion and least-squares reverse-time migration imaging of collimated ultrasonic-beam data for high-resolution wellbore integrity monitoring." *Applied Physics Letters* 113 (7):071903.

Childers, M. I., M. Nguyen, K. A. Rod, P. K. Koech, W. Um, J. Chun, V.Glezakou, D. Linn, T. J. Roosendaal, and T. W. Wietsma. 2017. "Polymer-Cement Composites with Self-Healing Ability for Geothermal and Fossil Energy Applications." *Chemistry of Materials* 29 (11):4708-4718.

Chung, D. D. L. 2000. "Interface engineering for cement-matrix composites." *Composite Interfaces* 8 (1):67-81.

Condor, J., and K. Asghari. 2009. "Experimental study of stability and integrity of cement in wellbores used for CO2 storage."

Cooke Jr, C. E. 1994. Apparatus for determining mechanical integrity of wells. Google Patents.

Courard, L. 1999. "How to analyse thermodynamic properties of solids and liquids in relation with adhesion?" Proceedings of the 2nd International RILEM Symposium ISAP 99.

Crow, W., J. W. Carey, S. Gasda, D. B. Williams, and M. Celia. 2010. "Wellbore integrity analysis of a natural CO2 producer." *International Journal of Greenhouse Gas Control* 4 (2):186-197.

Davies, R. J., S. Almond, R. S. Ward, R. B. Jackson, C. Adams, F. Worrall, L. G. Herringshaw, J. G. Gluyas, and M. A. Whitehead. 2014. "Oil and gas wells and their integrity: Implications for shale and unconventional resource exploitation." *Marine and Petroleum Geology* 56:239-254.

Davis, E. S. 2018. Development of a Novel 3D Acoustic Borehole Integrity Monitoring System. Los Alamos National Lab.(LANL), Los Alamos, NM (United States).

Davis, R. S. 1992. "Equation for the determination of the density of moist air (1981/91)." *Metrologia* 29 (1):67.

De Simone, M., F. L. G. Pereira, and D. M. Roehl. 2017. "Analytical methodology for wellbore integrity assessment considering casing-cement-formation interaction." *International Journal of Rock Mechanics and Mining Sciences* 94:112-122.

Devol-Brown, I., E. Tinseau, D. Bartier, A. Mifsud, and D. Stammose. 2007. "Interaction of Tournemire argillite (Aveyron, France) with hyperalkaline fluids: Batch experiments performed with powdered and/or compact materials." *Physics and Chemistry of the Earth, Parts A/B/C* 32 (1-7):320-333.

Douba, A., M. Genedy, E. N. Matteo, U. F. Kandil, J. Stormont, and M. M. Reda Taha. 2017. "The significance of nanoparticles on bond strength of polymer concrete to steel." *International Journal of Adhesion and Adhesives* 74:77-85.

Duguid, A., and J. Tombari. 2007. "Technologies for measuring well integrity in a CO2 field." Sixth Annual Conference on Carbon Capture and Sequestration—DOE/NETL, May.

Duguid, A., and G. W. Scherer. 2010. "Degradation of oilwell cement due to exposure to carbonated brine." *International Journal of Greenhouse Gas Control* 4 (3):546-560.

Emiroglu, M., A. Douba, R. A. Tarefder, U. F. Kandil, and M. Reda Taha. 2017. "New Polymer Concrete with Superior Ductility and Fracture Toughness Using Alumina Nanoparticles." *Journal of Materials in Civil Engineering* 29 (8):04017069.

Fan, M., J. Li, and G. Liu. 2018. "New Method to Analyse the Cement Sheath Integrity During the Volume Fracturing of Shale Gas." *Energies* 11 (4):750.

Fernandez, C. A., P. K. Koech, W. Um, V. Glezakou, J. Chun, M. I. Childers, M. T. Nguyen, and K. A. Rod. 2018. Self-repairing cement polymer composites and processes of making and using same. Google Patents.

Ferry, J. D.1980. *Viscoelastic properties of polymers*. John Wiley & Sons.

Forchheimer, P. 1901. "Wasserbewegung durch boden." *Z. Ver. Deutsch, Ing.* 45:1782-1788.

Freyer, R., M. Fejerskov, and A. Huse. 2002. "An Oil Selective Inflow Control System." European Petroleum Conference.

G'sell, C., and A. Dahoun. 1994. "Evolution of microstructure in semi-crystalline polymers under large plastic deformation." *Materials Science and Engineering: A* 175 (1-2):183-199.

Gatlin, C. 1960. *Petroleum engineering: drilling and well completions*: Prentice-Hall Englewood Cliffs, NJ, USA.

Genedy, M., Usama .F K., E. N. Matteo, J.n Stormont, and M. M. Reda Taha. 2017. "A new polymer nanocomposite repair material for restoring wellbore seal integrity." *International Journal of Greenhouse Gas Control* 58:290-298.

Genedy, M., M. Stenko, J. Stormont, E. Matteo, T. Dewers, and M. Reda Taha. 2017. Methyl Methacrylate Nanocomposite (MMNC) for Sealing Ultra-Thin Wellbore Microcracks and Methods for Making. USA, Provisional Patent.

Genedy, M., J. Stormont, E. Matteo, and M. Reda Taha. 2014. "Examining epoxy-based nanocomposites in wellbore seal repair for effective CO2 sequestration." *Energy Procedia* 63:5798-5807.

Gojny, F. H., M. H. G. Wichmann, U. Köpke, B. Fiedler, and K. Schulte. 2004. "Carbon nanotube-reinforced epoxy-composites: enhanced stiffness and fracture toughness at low nanotube content." *Composites science and technology* 64 (15):2363-2371.

Golru, S. S., M. M. Attar, and B. Ramezanzadeh. 2014. "Studying the influence of nano-Al 2 O 3 particles on the corrosion performance and hydrolytic degradation resistance of an epoxy/polyamide coating on AA-1050." *Progress in Organic Coatings* 77 (9):1391-1399.

Goodwin, K. J., and R. J. Crook. 1992. "Cement sheath stress failure." *SPE Drilling Engineering* 7 (04):291-296.

Griffin, A. S., M. K. Rahman, J. J. Kim, and M. Reda Taha. 2013. "The Significance of Nanosilica on Degradation of Oil Well Cement in Carbonated Brine Environments." In *Mechanics and Physics of Creep, Shrinkage, and Durability of Concrete: A Tribute to Zdeňk P. Bažant*, 372-379.

Griffiths, P. R., and J. A. De Haseth. 2007. *Fourier transform infrared spectrometry*. Vol. 171: John Wiley & Sons.

Grujicic, M., V. Sellappan, M. A. Omar, N. Seyr, A. Obieglo, M. Erdmann, and J. Holzleitner. 2008. "An overview of the polymer-to-metal direct-adhesion hybrid technologies for load-bearing automotive components." *Journal of Materials Processing Technology* 197 (1):363-373.

Guo, J., W. Pan, J. Fan, and Y. Yu. 2018. "Improving the Performance of Oilwell Cement by Graft-modified PB Latex." *Transactions of Tianjin University*:1-8.

Guthrie, G. D., R. J. Pawar, J. W. Carey, S. Karra, D. R. Harp, and H. S. Viswanathan. 2018. "The mechanisms, dynamics, and implications of self-sealing and CO 2 resistance in wellbore cements." *International Journal of Greenhouse Gas Control* 75:162-179.

Haagsma, A., S. Weber, M. Moody, J. Sminchak, J. Gerst, and N. Gupta. 2017. "Comparative wellbore integrity evaluation across a complex of oil and gas fields within the Michigan Basin and implications for CO2 storage." *Greenhouse Gases: Science and Technology* 7 (5):828-842.

Haluszczak, L. O., A. W. Rose, and L. R. Kump. 2013. "Geochemical evaluation of flowback brine from Marcellus gas wells in Pennsylvania, USA." *Applied Geochemistry* 28:55-61.

Hamami, A. A., P. Turcry, and A. Aït-Mokhtar. 2012. "Influence of mix proportions on microstructure and gas permeability of cement pastes and mortars." *Cement and Concrete Research* 42 (2):490-498.

Harris, K. L., E. F. Vinson, D. L. Bour, D. P. Ewert, and R. R. Gerke. 1992. Repair of microannuli and cement sheath. USA.

Hill, L. W. 1997. "Calculation of crosslink density in short chain networks." *Progress in organic coatings* 31 (3):235-243.

Hodgkinson, E. S., and C. R. Hughes. 1999. "The mineralogy and geochemistry of cement/rock reactions: high-resolution studies of experimental and analogue materials." *Geological Society, London, Special Publications* 157 (1):195-211.

Huet, B. M., J. H. Prevost, and G. W. Scherer. 2010. "Quantitative reactive transport modeling of Portland cement in CO2-saturated water." *International Journal of Greenhouse Gas Control* 4 (3):561-574.

Jannot, Y., and D. Lasseux. 2012. "A new quasi-steady method to measure gas permeability of weakly permeable porous media." *Review of Scientific Instruments* 83 (1):015113.

Javadi, M., M. Sharifzadeh, K. Shahriar, and Y. Mitani. 2014. "Critical Reynolds number for nonlinear flow through rough-walled fractures: The role of shear processes." *Water Resources Research* 50 (2):1789-1804.

Jones, P. J., J. D. Karcher, A. Ruch, A. Beamer, P. Smit, S. Hines, M. R. Olson, and D. Day. 2014. "Rigless Operation to Restore Wellbore Integrity using Synthetic-based Resin Sealants." SPE/EAGE European Unconventional Resources Conference and Exhibition.

Kansas, State of. 2003. Permanent Administrative Regulations, Article 45.—Underground Hydrocarbon Storage Wells And Associated Brine Ponds. edited by Department of Health and Environment. Kansas, USA: State of Kansas, Department of Health and Environment.

Kansas, State of. 2011. Nitrogen/Brine Interface Mechanical Integrity Test (MIT). edited by Department of Health and Environment. Kansas, USA: State of Kansas, Department of Health and Environment.

Kardar, P., M. Ebrahimi, and S. Bastani. 2008. "Study the effect of nano-alumina particles on physical–mechanical properties of UV cured epoxy acrylate via nano-indentation." *Progress in Organic Coatings* 62 (3):321-325.

Kennedy, G. P., A. R. Lawless, A. K. Shaikh, and I. B. Alabi. 2005. "The use of swell Packer's as a replacement and alternative to cementing." SPE Annual Technical Conference and Exhibition.

Kuo, M.C., C.M. Tsai, J.C. Huang, and M. Chen. 2005. "PEEK composites reinforced by nano-sized SiO2 and Al2O3 particulates." *Materials Chemistry and Physics*, *90*(1):185-195.

Kutchko, B. G., B. R. Strazisar, D. A. Dzombak, G. V. Lowry, and N. Thaulow. 2007. "Degradation of well cement by CO2 under geologic sequestration conditions." *Environmental science & technology* 41 (13):4787-4792.

Lacuve, M., A. Chougnet, M. Allouche, and C. Mazard. 2015. "A Method to Improve Adhesion Strength at the Cement/Steel-Casing Interface and its Effect on Cement Evaluation Log Response." Offshore Mediterranean Conference and Exhibition.

Ladva, H. K. J., B. Craster, T. G. J. Jones, G. Goldsmith, and D. Scott. 2005. "The cement-to-formation interface in zonal isolation." *SPE Drilling & Completion* 20 (03):186-197.

Lee, J., and A. F. Yee. 2001. "Inorganic particle toughening I: micro-mechanical deformations in the fracture of glass bead filled epoxies." *Polymer* 42 (2):577-588.

Li, Y., B. Cheng, W. Zhu, H. Xiao, and R. Nygaard. 2017. "Development and evaluation of the coaxial cable casing imager: a cost-effective solution to real-time downhole monitoring for CO2 sequestration wellbore integrity." *Greenhouse Gases: Science and Technology* 7 (5):927-941.

Li, Y., and R. Nygaard. 2018. "A numerical study on the feasibility of evaluating CO2 injection wellbore integrity through casing deformation monitoring." *Greenhouse Gases: Science and Technology* 8 (1):51-62.

Liang, Y. L., and R. A. Pearson. 2009. "Toughening mechanisms in epoxy–silica nanocomposites (ESNs)." *Polymer* 50 (20):4895-4905.

Mansur, A. A. P., D. B. Santos, and H. S. Mansur. 2007. "A microstructural approach to adherence mechanism of poly (vinyl alcohol) modified cement systems to ceramic tiles." *Cement and concrete research* 37 (2):270-282.

Matteo, E. N., B. Huet, C. F. Jové-Colón, and G. W. Scherer. 2018. "Experimental and modeling study of calcium carbonate precipitation and its effects on the degradation of oil well cement during carbonated brine exposure." *Cement and Concrete Research*.

McLaren, R. G., and K. C. Cameron. 1996. *Soil Science, sustainable production and environmental protection*.

Mehta, P. K., and P. J. M. Monteiro. 1976. "Concrete-Microstructure, Properties and Materials. 2006." *Utilization of palm oil fuel ash in concrete: a review*.

Metcalf, A. S., D. L. Purvis, and S. Stilwell. 2009. "Wellbore re-entries and repairs: practical guidelines for cementing new casing inside existing casing." *Drilling contractor* 65 (6).

Michanowicz, D. R., J. J. Buonocore, S. T. Rowland, K. E. Konschnik, S. A. Goho, and A. S. Bernstein. 2017. "A national assessment of underground natural gas storage: identifying wells with designs likely vulnerable to a single-point-of-failure." *Environmental Research Letters* 12 (6):064004.

Mondal, P., S. P. Shah, and L. Marks. 2007. "A reliable technique to determine the local mechanical properties at the nanoscale for cementitious materials." *Cement and Concrete Research* 37 (10):1440-1444.

Nakayama, M., and J. J. Beaudoin. 1987. "A novel technique for determining bond strength development between cement paste and steel." *Cement and Concrete Research* 17 (3):478-488.

Namkanisorn, A., A. Ghatak, M. K. Chaudhury, and D. H. Berry. 2001. "A kinetic approach to study the hydrolytic stability of polymer–metal adhesion." *Journal of adhesion science and technology* 15 (14):1725-1745.

Naous, W., X.Y. Yu, Q.X. Zhang, K. Naito, and Y. Kagawa. 2006. "Morphology, tensile properties, and fracture toughness of epoxy/Al2O3 nanocomposites." *Journal of Polymer Science Part B: Polymer Physics*, *44*(10):1466-1473.

Newell, D. L., and J. W. Carey. 2012. "Experimental evaluation of wellbore integrity along the cement-rock boundary." *Environmental science & technology* 47 (1):276-282.

Ngo, T. D., M. T. Ton-That, S. V. Hoa, and K. C. Cole. 2007. "Preparation and Properties of Epoxy Nanocomposites-Part 1: The Effect of Pre-Mixing on Dispersion of Organoclay." Simha Symposium on Polymer Physics: to celebrate the 95th birthday of Prof. Robert Simha, October 17-18, 2007 and Polymer Nanocomposites 2007: Fourth International Symposium on Polymer Nanocomposites Science and Technology, October 18-19, 2007.

Nowamooz, A., G. Radilla, and M. Fourar. 2009. "Non-Darcian two-phase flow in a transparent replica of a rough-walled rock fracture." *Water resources research* 45 (7).

Osorio, A. G., I. C. L. Silveira, V. L. Bueno, and C. P. Bergmann. 2008. "H 2 SO 4/HNO 3/HCl—functionalization and its effect on dispersion of carbon nanotubes in aqueous media." *Applied Surface Science* 255 (5):2485-2489.

Park, J. H., and S. C. Jana. 2003. "Mechanism of exfoliation of nanoclay particles in epoxy-clay nanocomposites." *Macromolecules* 36 (8):2758-2768.

Parks, D. M., and S. Ahzi. 1989. Polycrystalline plastic deformation and texture evolution for crystals lacking five independent slip systems. MASSACHUSETTS INST OF TECH CAMBRIDGE.

Phillips, A. J., E. Troyer, R. Hiebert, C. Kirkland, R. Gerlach, A. B. Cunningham, L. Spangler, J. Kirksey, W. Rowe, and R. Esposito. 2018. "Enhancing wellbore cement integrity with microbially induced calcite precipitation (MICP): A field scale demonstration." *Journal of Petroleum Science and Engineering*.

Pocius, A. V. 2012. *Adhesion and adhesives technology: an introduction*: Carl Hanser Verlag GmbH Co KG.

Powers, T. C., and T. L. Brownyard. 1946. "Studies of the physical properties of hardened Portland cement paste." Journal Proceedings.

Ramezanzadeh, B., M. M. Attar, and M. Farzam. 2011. "Effect of ZnO nanoparticles on the thermal and mechanical properties of epoxy-based nanocomposite." *Journal of thermal analysis and calorimetry* 103 (2):731-739.

Ravi, K., M. Bosma, and O. Gastebled. 2002. "Improve the economics of oil and gas wells by reducing the risk of cement failure." IADC/SPE Drilling Conference.

Read, D., F. P. Glasser, C. Ayora, M. T. Guardiola, and A. Sneyers. 2001. "Mineralogical and microstructural changes accompanying the interaction of Boom Clay with ordinary Portland cement." *Advances in cement research* 13 (4):175-183.

Reddy, C. M., J. S. Arey, J. S. Seewald, S. P. Sylva, K. L. Lemkau, R. K. Nelson, C. A. Carmichael, C. P. McIntyre, J. Fenwick, and G. Todd Ventura. 2012. "Composition and fate of gas and oil released to the water column during the Deepwater Horizon oil spill." *Proceedings of the National Academy of Sciences* 109 (50):20229-20234.

Ren, Y., Y. Q. Fu, K. Liao, F. Li, and H. M. Cheng. 2004. "Fatigue failure mechanisms of single-walled carbon nanotube ropes embedded in epoxy." *Applied Physics Letters* 84 (15):2811-2813.

Rogers, H. E., D. Allison, and E. D. Webb. 2008. "New equipment designs enable swellable technology in cementless completions." IADC/SPE Drilling Conference.

Roy, P., J. P. Morris, S. D. C. Walsh, J. Iyer, and S. Carroll. 2018. "Effect of thermal stress on wellbore integrity during CO2 injection." *International Journal of Greenhouse Gas Control* 77:14-26.

Rusch, D. W., F. Sabins, and J. Aslakson. 2004. "Microannulus leaks repaired with pressure-activated sealant." In *SPE Eastern Regional Meeting*. Society of Petroleum Engineers.

Seidel, F. A., and T. G. Greene. 1985. "Use of expanding cement improves bonding and aids in eliminating annular gas migration in Hobbs Grayburg-San Andres wells." SPE Annual Technical Conference and Exhibition.

Shi, J., and J. Ming. 2017. "Influence of defects at the steel-mortar interface on the corrosion behavior of steel." *Construction and Building Materials* 136:118-125.

Silva, J. C., and N. B. Milestone. 2018. "Cement/rock interaction in geothermal wells. The effect of silica addition to the cement and the impact of CO 2 enriched brine." *Geothermics* 73:16-31.

Smith, L., M. Smith, and P. Ashcroft. 2011. "Analysis of environmental and economic damages from British Petroleum's Deepwater Horizon oil spill."

Stormont, J. C., S. Garcia Fernandez, M. Reda Taha, and E. N. Matteo. 2018. "Gas flow through cement-casing microannuli under varying stress conditions." *Geomechanics for Energy and the Environment* 13:1-13.

Tavassoli, S., J. F. Ho, M. Shafiei, C. Huh, P. Bommer, S. Bryant, and M. T. Balhoff. 2018. "An experimental and numerical study of wellbore leakage mitigation using pH-triggered polymer gelant." *Fuel* 217:444-457.

Thiercelin, M. J., B. Dargaud, J. F. Baret, and W. J. Rodriquez. 1998. "Cement design based on cement mechanical response." *SPE drilling & completion* 13 (04):266-273.

Thornhill, J., and B. G. Benefield. 1990. *Injection well mechanical integrity*: Office of Research and Development, US Environmental Protection Agency.

Tiab, D., and E. C. Donaldson. 2015. *Petrophysics: theory and practice of measuring reservoir rock and fluid transport properties*. Gulf professional publishing.

Tinseau, E., D. Bartier, L. Hassouta, I. Devol-Brown, and D. Stammose. 2006. "Mineralogical characterization of the Tournemire argillite after in situ interaction with concretes." *Waste Management* 26 (7):789-800.

Torsæter, M., J. Todorovic, and A. Lavrov. 2015. "Structure and debonding at cement–steel and cement–rock interfaces: Effect of geometry and materials." *Construction and Building Materials* 96:164-171.

US DOE. 2016. Strategic Petroleum Reserve Annual Report for Calendar Year 2014. edited by United States Department of Energy. Washington, D.C. : United States Department of Energy.

Uddin, F. 2008. "Clays, nanoclays, and montmorillonite minerals." *Metallurgical and Materials Transactions A* 39 (12):2804-2814.

Van den Brand, J. 2004. *On the adhesion between aluminium and polymers*: TU Delft, Delft University of Technology.

Wetzel, B., P. Rosso, F. Haupert, and K. Friedrich. 2006. "Epoxy nanocomposites–fracture and toughening mechanisms." *Engineering fracture mechanics* 73 (16):2375-2398.

Wilson, DC, AW Eustes, and WW Fleckenstein. 2018. "Lab Testing Cement-Steel Bonding at Shallow Temperature and Pressure Conditions." SPE Western Regional Meeting.

Xu, Y., and D. D. L Chung. 1999. "Carbon fiber reinforced cement improved by using silane-treated carbon fibers." *Cement and concrete research* 29 (5):773-776.

Xue, Z., and T. Hashimoto. 2017. "Geomechanical monitoring of caprock and wellbore integrity using fiber optic cable: Strain measurement from the fluid injection and extraction field tests." *Energy Procedia* 114:3305-3311.

Zeng, J., B. Saltysiak, W. S. Johnson, D. A. Schiraldi, and S. Kumar. 2004. "Processing and properties of poly (methyl methacrylate)/carbon nano fiber composites." *Composites Part B: Engineering* 35 (2):173-178.

Zeng, Z., and R. Grigg. 2006. "A criterion for non-Darcy flow in porous media." *Transport in porous media* 63(1): 57-69.

Zhai, L., G. Ling, J. Li, and Y. Wang. 2006. "The effect of nanoparticles on the adhesion of epoxy adhesive." *Materials Letters* 60 (25-26):3031-3033.

Zhang, M., and S. Bachu. 2011. "Review of integrity of existing wells in relation to CO2 geological storage: What do we know?" *International Journal of Greenhouse Gas Control* 5 (4):826-840.

Zhang, Z., and J. Nemcik. 2013. "Fluid flow regimes and nonlinear flow characteristics in deformable rock fractures." *Journal of hydrology* 477:139-151.

Zhu, J., J. Kim, H. Peng, J. L. Margrave, V. N. Khabashesku, and E. V. Barrera. 2003. "Improving the dispersion and integration of single-walled carbon nanotubes in epoxy composites through functionalization." *Nano letters* 3 (8):1107-1113.

# Appendix A: Interface Characterization Readings

Table 0.1: Interface characterization readings of reference intact specimen.

| Time [sec] | Vacuum Pressure [psig] |
|---|---|
| 0 | -11.0 |
| 188.6 | -10.9 |
| 381.6 | -10.8 |
| 575.7 | -10.7 |
| 770.3 | -10.6 |
| 961.6 | -10.5 |
| 1175.7 | -10.4 |
| 1383.8 | -10.3 |

Table 0.2: Interface characterization readings of microfine cement sealed specimen.

| Debonded | | Sealed | |
|---|---|---|---|
| Time [sec] | Vacuum Pressure [psig] | Time [sec] | Vacuum Pressure [psig] |
| 0 | -7.0 | 0 | -7.0 |
| 8.9 | -6.0 | 16.8 | -6.0 |
| 18.0 | -5.0 | 36.3 | -5.0 |
| 27.8 | -4.0 | 57.0 | -4.0 |
| 37.4 | -3.0 | 81.6 | -3.0 |
| 47.8 | -2.0 | 112.2 | -2.0 |
| 60.7 | -1.0 | 155.7 | -1.0 |

Table 0.3: Interface characterization readings of Novolac epoxy sealed specimen.

| Debonded | | Sealed | |
|---|---|---|---|
| Time [sec] | Vacuum Pressure [psig] | Time [sec] | Vacuum Pressure [psig] |
| 0 | -11.0 | 0 | -11.2 |
| 7.6 | -10.0 | 145.3 | -11.1 |
| 16.0 | -9.0 | 294.0 | -11 |
| 23.5 | -8.0 | 432.8 | -10.9 |
| 32.3 | -7.0 | 583.8 | -10.8 |
| 40.3 | -6.0 | 730.8 | -10.7 |
| 48.4 | -5.0 | 872.1 | -10.6 |
| 57.2 | -4.0 | 1025.6 | -10.5 |

Table 0.4: Interface characterization readings of NM-Novolac epoxy sealed specimen.

| Debonded | | Sealed | |
|---|---|---|---|
| Time [sec] | Vacuum Pressure [psig] | Time [sec] | Vacuum Pressure [psig] |
| 0 | -9.0 | 0 | -11.5 |
| 10.3 | -8.0 | 124.2 | -11.4 |
| 22.0 | -7.0 | 252.0 | -11.3 |
| 35.4 | -6.0 | 371.0 | -11.2 |
| 51.5 | -5.0 | 500.3 | -11.1 |
| 68.0 | -4.0 | 626.3 | -11.0 |
| 86.1 | -3.0 | 747.5 | -10.9 |
| 103.8 | -2.0 | 879.1 | -10.8 |

Table 0.5: Interface characterization readings of MMA sealed specimen.

| Debonded | | Sealed | |
|---|---|---|---|
| Time [sec] | Vacuum Pressure [psig] | Time [sec] | Vacuum Pressure [psig] |
| 0 | -9.0 | 0 | -11.3 |
| 22.1 | -8.0 | 204.3 | -11.2 |
| 46.5 | -7.0 | 412.2 | -11.1 |
| 72.4 | -6.0 | 621.1 | -11.0 |
| 101.8 | -5.0 | 833.6 | -10.9 |
| 135.0 | -4.0 | 1049.7 | -10.8 |
| 178.2 | -3.0 | 1269.4 | -10.7 |
| 229.1 | -2.0 | 1492.7 | -10.6 |

Table 0.6: Interface characterization readings of NM-MMA sealed specimen.

| Debonded | | Sealed | |
|---|---|---|---|
| Time [sec] | Vacuum Pressure [psig] | Time [sec] | Vacuum Pressure [psig] |
| 0 | -11.0 | 0 | -11.4 |
| 14.2 | -10.0 | 334.7 | -11.3 |
| 27.4 | -9.0 | 565.8 | -11.2 |
| 40.2 | -8.0 | 847.6 | -11.1 |
| 52.7 | -7.0 | 1299.0 | -11.0 |
| 64.8 | -6.0 | 1541.9 | -10.9 |
| 77.0 | -5.0 | 1815.0 | -10.8 |
| 89.3 | -4.0 | 2076.1 | -10.7 |